David Veit BSc

A Feasibility Study of Novel Applications in Automotive UWB Radar Systems

MASTERARBEIT

zur Erlangung des akademischen Grades

Diplom-Ingenieur

Masterstudium Elektrotechnik

eingereicht an der

Technischen Universität Graz

Betreuer

Ao. Univ.-Prof. Dipl.-Ing. Dr.techn. Erich Leitgeb

Institut für Hochfrequenztechnik

Mitbetreuer: Ass.Prof. Dipl.-Ing. Dr.techn. Franz Teschl, IKS
Dr. Thomas Gigl, Maxim Integrated

Graz, Dezember 2016

A Feasibility Study of Novel Applications in Automotive UWB Radar Systems

Master Thesis

David Veit

Institute of Microwave and Photonic Engineering,
Graz University of Technology

in cooperation with:
Maxim Integrated

Supervisors: Ao.Univ.-Prof. Dipl.-Ing. Dr.techn.Erich Leitgeb
Ass.Prof. Dipl.-Ing. Dr.techn. Franz Teschl
Dr. Thomas Gigl, Maxim Integrated

Graz, 14. Dezember 2016

EIDESSTATTLICHE ERKLÄRUNG

AFFIDAVIT

Ich erkläre an Eides statt, dass ich die vorliegende Arbeit selbstständig verfasst, andere als die angegebenen Quellen/Hilfsmittel nicht benutzt, und die den benutzten Quellen wörtlich und inhaltlich entnommenen Stellen als solche kenntlich gemacht habe. Das in TUGRAZonline hochgeladene Textdokument ist mit der vorliegenden Masterarbeit identisch.

I declare that I have authored this thesis independently, that I have not used other than the declared sources/resources, and that I have explicitly indicated all material which has been quoted either literally or by content from the sources used. The text document uploaded to TUGRAZonline is identical to the present master‘s thesis.

Datum / Date

Unterschrift / Signature

Kurzfassung

In dieser Arbeit wurde untersucht, ob es möglich ist, mittels Patchantennen mit geringer Direktivität eine Parkhilfe oder Alarmanlage für Autos zu realisieren. Alle Messungen wurden mit einem Vektor Netzwerkanalysator im Frequenzbereich von 3 GHz bis 8 GHz getätigt. Der erste Teil dieser Arbeit beschäftigt sich mit Parkhilfen und ob es möglich ist eine solche mit diesen Antennen zu realisieren. Beginnend mit einfachen Testmessungen, mit einzelnen Objekten auf ebenem Untergrund, bis hin zu komplexeren Anordnungen, bei denen die Antennen an einem echten Auto montiert wurden und verschiedenste Situationen nachgestellt wurden, denen man auch im realen Straßenverkehr begegnen kann. Es konnte gezeigt werden, dass sich die Antennen nicht dafür eignen eine Parkhilfe zu realisieren, da verschiedene Objekte nicht eindeutig voneinander unterschieden werden konnten.

Der zweite Teil der Arbeit beschäftigte sich damit, eine Alarmanlage für Autos zu realisieren. Dabei sollte erkannt werden, ob jemand in den Innenraum des Autos eindringt. Es wurden 2 verschiedene Methoden getestet. Die erste Methode verwendet 2 Antennen in der Mitte des Autos. Durch kontinuierliches Messen überprüft man ob innerhalb einer gewissen Entfernung Änderungen in der Impulsantwort detektiert werden. Detektiert man Änderungen innerhalb dieser Entfernung wird der Alarm ausgelöst.

Die komplexere Methode war einen Lokalisierungsalgorithmus zu verwenden. Zu diesem Zweck wurden Antennen an verschiedenen Positionen im und am Auto montiert und die Anordnung mit den besten Ergebnissen gesucht. Zur Lokalisierung wurde ein “weighted least squares” Algorithmus und ein Partikelfilter verwendet. Um den Messaufwand möglichst gering zu halten und eine größere Anzahl von Antennen in einem Setup untersuchen zu können, wurden die Ergebnisse aus verschiedenen Messaufbauten virtuell miteinander kombiniert. Dieser Ansatz erlaubte eine grobe Lokalisierung von Eindringlingen. Die Genauigkeit dieses Systems war zu gering, um in Grenzfällen sichere Entscheidungen treffen zu können. Die ungenaue Lokalisierung ließ sich dadurch erklären, dass der Lokalisierungsalgorithmus nach einem Punktziel sucht, eine Person jedoch nicht auf einen Punkt reduziert werden kann.

Abstract

In this master thesis, it was investigated, if it is possible to realize a parking aid or interior surveillance system for cars with low directivity patch antennas. All measurements were performed with a vector network analyser in a frequency range of 3 GHz to 8 GHz. The first part of this thesis is about parking aids. Starting with simple test measurements of single objects on flat surfaces, to more complex setups with antennas mounted on a real car and different situations, which may be encountered in real life. It could be shown, that the antennas are not suited for a parking aid, because different objects could sometimes not be distinguished from each other.

The second part of this thesis dealt with the realization of an interior surveillance system for cars. Experiments were conducted with two different approaches. One approach was to position two antennas in the middle section of the car. Then they measure continuously and check if something has changes within a given distance. The distance threshold is then chosen such, that the alarm is only raised if a change is detected inside the car.

The more sophisticated approach was to use a localization algorithm. For localization, a weighted least squares algorithm and a particle filter were used. To keep the measurement effort to a minimum and to combine a higher number of antennas in one setup, results from different measurements were combined virtually. This allowed a rough localization of intruders. The accuracy of this system was too low to allow correct decisions in border cases. The low localization accuracy could be explained by the fact that the algorithm is looking for point targets, but the simplification of a person by a point introduces too large errors.

Index

1. Introduction

Radar systems are used more and more often for automotive applications. These are safety applications like pre-crash detection, collision warning or avoidance systems as well as parking aids, adaptive cruise control and other comfort applications. Also the future of autonomous cars depends heavily on the reliability of radar systems. For security applications also interior surveillance systems based on radar technology are already in use. Compared to the mostly used ultra-sonic systems they are less susceptible to vibrations and false alarms due to open windows [1].

Because many passive radio telescopes use the frequency range around 24 GHz the EU is going to limit the use of automotive radar to frequencies around 77 GHz. Because 77 GHz technology is still very expensive many manufacturers are looking for alternatives.

One alternative for UWB (Ultra-Wide Band) systems could be the frequency range around 6 – 7 GHz. For many practical setups antennas are mounted at the edges of the front and rear bumper, as well as at the side mirrors. The first part of this master thesis is a feasibility study for a radar system which uses antennas at these locations.

In the second part of this thesis it was tried to realize an interior surveillance system with the same setup and if needed additional modules inside the car.

Interior surveillance is often used in modern cars to prevent theft. For detection of movement inside the car the two most commonly used systems are ultrasonic systems and radar systems.

Most ultrasonic systems measure the impulse response of the interior, and if the impulse response changes something in the car has moved. This only works because windows block ultrasonic, therefore, movement outside the car does not affect the system. But if a window is slightly opened, these systems react very sensitive and false alarms are common.

Radar systems can detect also through the windows of a car and need to be adjusted such that they can distinguish between movement outside and inside

the car. The easiest way is to place the antennas in the middle of the car. This way most parts of the car can be covered and easily distinguished from areas outside the car.

Problems arise when it is not possible to install enough antennas on the right positions and if a monostatic radar is not possible on this hardware. In this thesis it was tried to find ways to overcome those problems without the need to use different antennas or mount the antennas on different locations.

2. Fundamentals of Automotive Radar System

In order to know what results had to be expected, extensive research about already existing systems and their properties was conducted. This chapter includes results from research about existing driving assistance systems.

2.1 Comparison of different sensing technologies

Not all sensors and systems, which are available on the market, are discussed in the following document. Especially camera systems are not mentioned further in this document, despite the fact that they are an important part of most manoeuvring aids.

The ISO norm 17386 (MALSO – Manoeuvring Aids for Low Speed Operation) deals with the topic of driving aids for low speeds, such as parking aids, stop-and-go aids and so on. This norm defines which obstacles have to be detected and how the system has to react.

2.2 Measurement due to ISO 17386

The ISO 17386 is a norm which deals with low speed manoeuvring aids. A manoeuvring aid should be able to achieve at least the performance described in this norm. All the information and graphics in this sub chapter are taken from [2].

2.2.1 Monitoring ranges

The ISO 17386 classifies different monitoring ranges. In order to these ranges, a manoeuvring aid is classified by its capability to cover theses ranges. Figure 1 shows a plan of how the ranges are arranged horizontally.

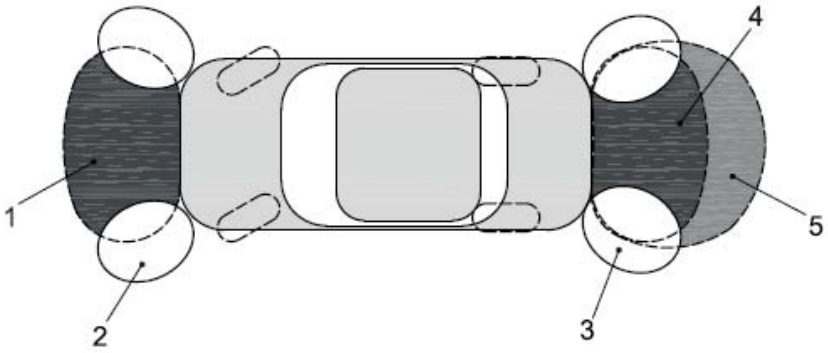

Key
1 front
2 front corner
3 rear corner
4 rear-1
5 rear-2

Figure 1: range plan [2]

Table 1 shows the dimensions of the different ranges visualized in Figure 1.

Table 1: ranges of ISO 17386 [2]

Monitoring range	Abbreviation	Detection distance m	Maximum driving speed m/s
Rear-1	R1	0,6	0,3
Rear-2	R2	1,0	0,5
Rear corner driver side	Rcd	0,5	0,3
Rear corner passenger side	Rcp	0,5	0,3
Front	F	0,6	0,3
Front corner driver side	Fcd	0,5	0,3
Front corner passenger side	Fcp	0,5	0,3

2.2.2 Requirements

In order to get certified by this ISO norm a system needs to meet different requirements. A short comparison of these requirements can be found in this chapter.

Range and coverage

The manoeuvring aids for low-speed operation (MALSO) are classified according to their capability of covering the different monitoring ranges described in Figure 1 and Table 1.

Because state-of-the-art ultrasonic sensing technology is not able to detect obstacles in a proximity closer than 20 cm, areas closer than this shall not be tested.

The minimum required coverage of the different areas of relevance are as follows:

- Front and rear-1 in A1 (25 cm to 60 cm): 90%
- Rear-2 in A2 (60 cm to 10 cm): 87%
- Corners: 100%

Within the whole monitoring range, there shall be no more than two continuous detection holes in a straight line, either horizontally, vertically or diagonally in the horizontal plane. This does not apply to the vertical plane.

Dynamic performance of object detection

For area rear-1, the system shall be able to detect stationary objects while the vehicle itself is either stationary or moving at a speed up to 0.3 m/s. For area rear-2, the same applies with velocities up to 0.5 m/s.

Start-up detection delay

The start-up detection delay is the time interval between the activation of the MALSO system and the moment the MALSO system presents to the driver the correct information about a relevant obstacle already present in the monitoring range under consideration. If the MALSO system does not provide a readiness-for-service indication, the start-up detection delay is measured from the moment the ignition is set to ON and the engine is running. The engine is defined as running after the battery voltage has reached 90% of the typical battery voltage after starting the engine.

The start-up detection delay shall not exceed 1.5 seconds, including internal system and sensor tests. If the MALSO system provides a readiness-for-service indication, the start-up detection delay is measured from the moment the readiness-for-service indication ends. The average start up detection shall not exceed 600 ms.

Detection latency

As long as the system is active, the time delay between appearance of a relevant obstacle and presentation of the correct information to the driver shall not exceed 500 ms in all monitoring ranges. The delay is calculated as the arithmetic mean of the least 10 tests. No single value of the tests shall exceed 600 ms.

2.2.3 Coverage measurement

For parking aids especially the rear and rear-corner areas of a car are of special interest. For measurement procedure of the front area please have a look at ISO 17386. How the detection of an object is done is not part of the standard. For our purpose, we will need to try out different arrangements of sensors.

Horizontal coverage measurement of rear area 1 and 2

Steps for measurement of the horizontal coverage in rear-1 and rear-2

- Position the car on a concrete ground with no walls or other obstacles in the near environment
- Define a rectangular area in the rear area of the car as shown in Figure 2.
- The area from 20 to 60 cm is rear-1, from 60 to 100 cm is rear-2. The width is rounded up to the next 10 cm step.
- Define a grid in the 2 areas. The length of one cell in the grid is defined as 10 cm.

- Position the test object on every place of the grid (in the middle of each square) and do a detection measurement. The test object for radar application is defined as follows:

    A metal pole (e.g. copper pipe) with a diameter of 25 mm and a length of 1 m for horizontal areas.

- The result of these measurements should be a coverage diagram like shown in Figure 3.
- The coverage ratio calculates as the percentage of correctly detected cells.

EXAMPLE: For a total area of relevance of 96 cells with a covered area of 88 cells, the coverage ratio is 91.7%.

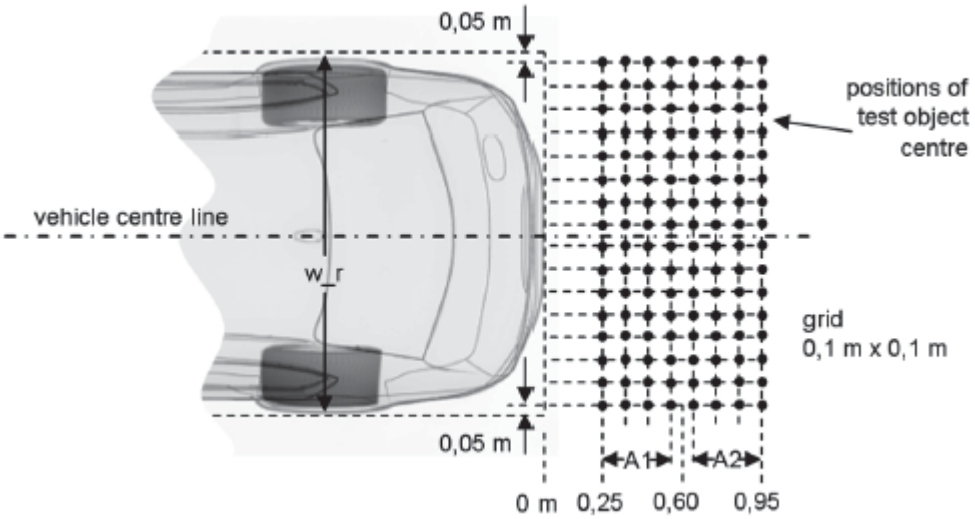

Figure 2: test grid for rear-1 and rear-2 area [2]

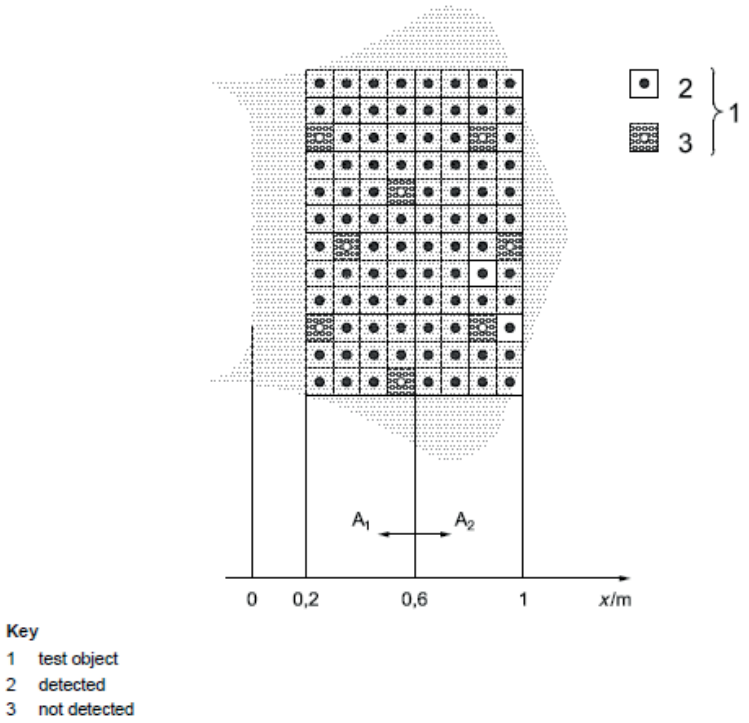

Figure 3: Determination of the rear horizontal coverage ratio in the sub-areas A1 and A2 [2]

Vertical coverage measurement of rear area 1 and 2

For testing the vertical coverage, it is sufficient to use a grid of 20 cm. The height of the surrounding rectangles is 60 cm. The centre of the lowest line shall be 30 cm above ground. At least one cell in column A (nearest to the bumper) shall be covered. To measure vertical coverage follow the next steps:

- Position the car on a concrete ground with no walls or other obstacles in the near environment
- Define a grid in the rectangular areas as described above and shown in Figure 4.
- Position the test object on every place of the grid (in the middle of each square) and do a detection measurement. The test object for radar application is defined as follows:

  A metal pole (e.g. copper pipe) with a diameter of 25 mm and length equal to the width of the test vehicle bumper plus 20% to 40%.

- The minimum coverage shall be as defined in table 2. The numbers define how many positions in each area have to be detected. At distance

A only 1 of the three test cases needs to be detected correctly. For Rear-2 and Rear-1, at least two correct detections are needed.

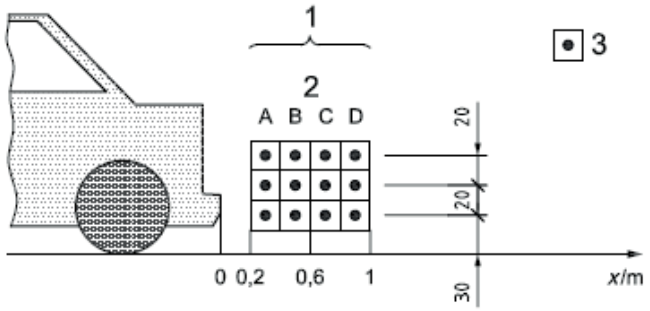

Key
1 rear vertical area of relevance
2 column
3 test object grid position

Figure 4: Vertical coverage measurement [2]

Table 2: Minimum vertical coverage [2]

Monitoring ranges	Column			
	A	B	C	D
Rear-2	1	2	2	1
Rear-1 and front	1	2	0	0
Rear and front corner	1	1	0	0

Horizontal coverage measurement of corner area

The following steps describe the definition of the horizontal areas of relevance for corner areas. Corner areas have not been considered in this thesis.

- Draw a rectangular box close around the vehicle outline.
- Draw lines from each box corner to the vehicle at an angle of 45°.
- The intersection of these lines and the vehicle boundary are the vehicle corners. Define seven squares with a length of 10 cm like shown in Figure 5.
- Be careful to use the correct angles for front (45° inclination) and rear corners (30° inclination).

- Position the test object on every place of the grid (in the middle of each square) and do a detection measurement. The test object for radar application is defined as follows:

  A metal pole (e.g. copper pipe) with a diameter of 25 mm and 1 m length.

- The minimum coverage of corner areas is defined as 100 %.

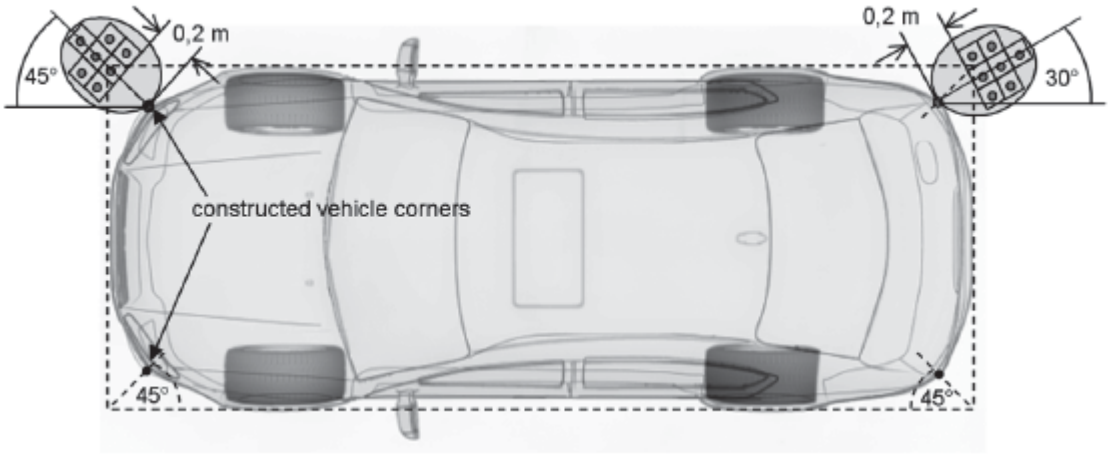

Figure 5: Corner areas of relevance [2]

2.2.4 Detection latency measurement

The ISO 17386 does not specify the test method for the evaluation of the system reaction time, but a sufficient measuring accuracy of one-tenth of the measured time shall be guaranteed.

A method using a camera for measuring is described in the annex of the ISO 17386.

2.3 Ultrasonic system

Typical ranges for ultrasonic systems are in the range from 0.2 m to 1.5 m, although there are already systems with ranges up to 4.5 m. The target of

developers is to develop systems with ranges up to 5 meters and the same accuracy as today's systems for shorter ranges. [3].

Bosch guarantees a detection range of 20 – 450 cm for their ultrasonic sensors for automotive applications [4].

In many other scientific papers and datasheets, similar values can be found for automotive ultrasonic systems. Furthermore, the maximum distance is also heavily affected by the type of obstacle, which has to be detected. For ultrasonic sensors, especially the shape of an obstacle is very important. As long as the material is not sound absorbing it does not affect detection range.

A flat plane reflects the ultrasonic waves better back to the receiver than a curved one. Sound absorbing materials like rubber foam drastically reduce detection range. Also human clothing approximately cuts detection range by one third. [5].

In general ultrasonic sensors are heavily depending on the temperature as well as on the humidity as these factors affect the wave propagation of the ultrasonic wave in the air.

Depending on the used signal processing and number of sensors, accuracy of ultrasonic systems can vary widely. Currently used systems have a radial accuracy of some mm up to a few cm. In [5] especially the basics of ultra-sonic sensors are described. [6] [7] show examples and measurement data of ultra-sonic systems. [8] and [9] contain data sheets of different ultra-sonic sensors.

Ultrasonic sensors are in general very robust against external influences. At high velocities, the noise level due to the wind becomes so big, that approximately above 140km/h no detection with ultrasonic sensors is possible. Furthermore, the system can be disturbed by strong external ultrasonic emitters like pneumatic brakes of trucks and the sound trains produce when they are braking. These events are typically of short duration and can be coped with by appropriate signal processing.

To prevent unwanted interference due to a coupling of the sensor with the chassis of the vehicle, the sensor has to be clean of ice and dirt [5].

Ultrasonic sensors need to be mounted such, that they have direct contact with the surrounding air. Due to that they are mostly mounted on the surface of the

bumper bar and can be seen from outside. They may have the same colour as the vehicle but cannot be hidden, which sometimes disturbs the design of the car.

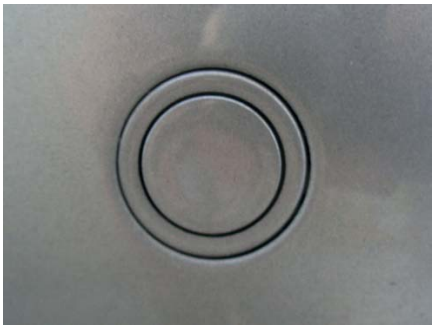

Figure 6: Audi A4 ultrasonic sensor [10]

Summary of described properties of an ultrasonic system:

- Range: 0.1…0.2 – 4.5 m
- Resolution: 2…3 cm down to millimetres
- Robustness: very robust at low to medium velocities
- Integration: Sensor needs to be on the surface in order to operate properly.

2.4 Radar

In contrast to ultrasonic sensors, radar is subject of frequency regulations. This is a problem because radar shares the spectrum with many other systems (communication systems, radio astronomy …). Due to this and the fact that transmit power is strictly regulated and cannot be chosen randomly, especially in the frequency range of 24 GHz, which is heavily used for automotive radar applications, strict regulations of the EU exist. It is planned that after 2018 no more new automotive radar applications in the 24 GHz range are allowed in Europe. The future frequency range of automotive radars is going to be around 79 GHz [11] [12].

Today most of the 24 GHz automotive radar systems are used for short and medium ranges (SRR and MRR) from 0.2…0.3 m up to 20…30 m. 79 GHz radar systems are mostly used for long ranges (LRR) from 20 m up to 150 m. Automatic

Cruise Control (ACC) is the most common application for Long Range Radars In [12] mostly general information about automotive radar systems can be found. [13] is about ultra-wideband short-range radars and [14] also contains information about long-range radars.

In general the radial resolution is indirectly proportional to the used bandwidth. Therefore, more bandwidth means better resolution. At the same time the pulses of pulsed radars have to be shorter and shorter. If the pulses are not short enough, different echoes overlap in such a way that they cannot be distinguished any more [15].

The UWB SRR (Ultra-Wide Band Short Range Radar) which is built in the S-Class of Mercedes (2006) is being built by Tyco Electronics M/A. Com and has the following specifications for radial and lateral resolution.

In a range of 0.2 to 30 m an object can be detected with a resolution of 15 cm and a radial accuracy of 7.5 cm. The System can track up to 10 different targets and identify them with their range and velocity vector [14].

A big advantage of the radar is that, due to the Doppler Effect, the relative velocity of the detected object can be measured directly from the frequency shift of the received signal [12].

Similar to ultrasonic sensors radar is very robust against external influences. Frequency regulations limit the maximum transmit power to be lower than specific thresholds. A maximum detecting range which can be calculated by the radar equation could not be determined for a 7.5 cm PVC pipe, because no values for the RCS (Radar Cross Section) of a PVC cylinder were available.

For a very far away perfectly conducting metal cylinder, the RCS calculates with the following equation [16].

$$\sigma = \frac{2\pi L^2 a}{\lambda}$$ *Equation 2.1*

a … radius of the cylinder
L … height of the cylinder
λ … wavelength of the electromagnetic wave
σ … radar cross section

This equation is only correct if we assume that the electromagnetic wave, which hits the object, is a plane wave and the wavelength is much shorter than the size of the object [16].

With the radar cross section the maximum range of a radar can be calculated with the radar equation [15].

$$R = \sqrt[4]{\frac{P_{TX} G^2 \lambda^2 \sigma}{P_{RX} (4\pi)^3}} \qquad \textit{Equation 2.2}$$

P_{TX} … Transmitted Power
P_{RX} … Received Power

The advantage of a radar compared to an ultrasonic system in terms of integration is, that the antennas can be mounted behind a plastic bumper bar, because the electromagnetic waves are able to pass through it. Reflections from the own bumper bar can easily be distinguished from other reflections due to the short travel time.

Summary of described properties of a radar system:

- Range: SRR and MRR have a range of 0.2…0.3 m to 20…30 m, while LRR have a typical range of 20 m to 150 m.
- Resolution: depending on the bandwidth/pulse duration some cm
- Robustness: Very robust, but strictly regulated spectrum.
- Integration: Antenna can be hidden behind the bumper bar.

2.5 Lidar (Light Detection and Ranging)

A LIDAR uses the same principle as a radar, with the difference that the wavelength of the electromagnetic wave is in the infrared range. Lidar does not use frequency modulation like some radars, instead, intensity modulation is used. Most commonly PM (Pulse Modulation) with pulse durations of a few nanoseconds is used [12].

Lidar is not used for parking aids, therefore, this chapter only gives a brief overview of the main properties of a LIDAR.

At night LIDAR systems can achieve a range of up to 150m. At day time the range is heavily reduced due to the strong scattered light. In general LIDAR is not suitable for any automotive safety system if used alone, because the range is strongly depending on the environment, especially fog and spray [12].

Radial resolution of a LIDAR is very good and with appropriate signal processing resolutions of a few cm are possible. The determination of the relative velocity happens by calculation from different range values measured over time. The lateral resolution of a LIDAR depends on the type of system. Scanning systems with adjustable mirrors achieve a much higher resolution than multi – beam systems. A scanning system is able to achieve resolutions of cm to mm depending on the range [12].

Lidar systems are very prone to environmental interference. Bad weather conditions like fog and spray drastically limit LIDAR in its function. Also dirt in the optical path of the LIDAR is a problem. Due to this a LIDAR cannot be used for automotive security systems alone [12].

Lidar sensors have to be mounted such, that they have vision of the object which they want to detect. Best places to mount a LIDAR would be the windscreen or the headlights. Each of this places has its own advantages and disadvantages.

Summary of described properties of a LIDAR system:

- Range: Depending on environment and light conditions (day/night) up to 150 m.
- Resolution: A few cm to mm
- Robustness: very prone to bad weather and dirt
- Integration: Best places behind windscreen or within the headlights.

2.6 Comparison of different technologies

Table 3 contains an overview over the previously described sensing technologies used in automotive applications.

Table 3: Comparison of different sensing technologies

	Range	Accuracy	Robustness	Integration	Specific
Ultrasonic	0.2 m to 4.5 m	a few cm to mm	no high velocities	needs to be mounted on surface	
Radar	0.2 m to 150 m	depends on bandwidth	very robust	can be hidden	subject to frequency regulations
LIDAR	up to 150 m	a few cm to mm	Heavily affected by bad weather and dirt	Behind windscreen or in lights.	May not be used alone for safety applications

2.7 Calculation of RCS and radar equation

In order to predict the strength of the reflections from our test objects, the radar equation was used.

2.7.1 Basics about radar cross sections

The RCS can be described as ratio to the ideal reference reflector. The reference reflector is an equivalent isotropic reflector, which reflects incoming waves equally to all directions. In practice this is only achieved by a spherical reflector with perfectly conducting surface. From some distance the sphere cannot be recognized any more, just a circle, the so called projection can be seen. For the reference reflector this projection has the size of 1 m^2. Which means the sphere has a radius of about 1.33 m. If a target has a RCS of 3 m^2, this means, that the target reflects the same amount to a given direction as an equivalent isotropic reflector with a projected area of 3 m^2.

2.7.2 RCS calculation

The RCS of the used objects was calculated like in Equation 2.3 for the copper pipe and Equation 2.4 for the aluminium foil [15]. Additionally the RCS of an aluminium plate was simulated and compared to the theoretical result. A comparison of the measured and calculated results was shown in Table 4. For

the copper pipe simulation results of the RCS were not possible, because the number of elements available was too low to model the round shape correctly.

$$\sigma_{cylinder} = \frac{2\pi\, r\, h^2}{\lambda}$$ *Equation 2.3*

r … Radius of cylinder
h … Length of cylinder

$$\sigma_{plate} = \frac{4\pi\, b^2 h^2}{\lambda^2}$$ *Equation 2.4*

b … Width of plate
h … Length of plate

Table 4: Calculated and simulated RCSs

Object	Calculated RCS	Simulated RCS
Cylinder: r = 28 mm, h = 1m	4.69 m^2	not available
Plate: b = 26 cm, h = 28 cm	47.36 m^2	23.44 m^2

2.7.3 Estimation with radar equation

In order to estimate the strength of the reflections from our test objects, the radar equation was used, using the results from Table 4 and antenna parameters shown in chapter 3.1.5. If we rewrite Equation 2.2 we can derive the following equation.

$$\frac{P_{RX}}{P_{TX}} = \frac{G_{RX} G_{TX}\, \lambda^2\, \sigma}{(4\pi)^3\, R^4}$$ *Equation 2.5*

This ratio of received to transmitted power is exactly what we measure with the network analyser. However, the radar equation is only valid for the far field. Also most simple RCS (Radar Cross Section) formulas are only valid for the far field [15]. If the biggest dimension L of an antenna is smaller than the wavelength λ, the border distance of radiating near field and far field can be calculated like in Equation 2.6. The used patch antennas had a diameter of 5 cm, which was

already bigger than the minimum used wavelength of 3.75 cm for 8 GHz. In addition to that, the sizes of the test objects needed to be considered. For antennas bigger than the minimum wavelength, the region for the reactive nearfield can be calculated like in Equation 2.7. The region for the radiating near field like in Equation 2.8. Everything farther away can be considered as the far field. A summary of different boundaries for test objects and antennas was shown in Table 5. The minimum distance to achieve far field conditions for our test objects would have been 4 m for the aluminium foil and 53 m for the copper pipe. However, the measurements were done up to a distance of only 2 m to 4 m. Because of this, the calculated results were expected to differ from the measurements. Nevertheless, it was tried to compare the calculated results with the measurements to show how big the difference was. This comparison can be seen in chapter 3.2.4, Figure 34 and Figure 35. In this figures it could be seen that the estimated results from the radar equation were higher than the results from the measurement, especially for small distances.

The reason why the measured results were lower than the calculated results probably was that the RCS of an object is not constant with respect to distance. The trend is that the RCS becomes smaller and smaller with shorter distances. This behaviour was described in [17] for a cylinder and in [18] for a square plate and disk. Especially in [18] it could be seen that the RCS was not declining monotonically. Especially for the disc shape large dips occurred at specific distances. Because of this shape dependent not generally predictable behaviour, no simple formula for the near field region could be derived. This is also the reason why the biggest dimension of the target also has to be considered when defining the near field to far field boundary. Nevertheless, the radar equation and theoretical RCS values for simple shapes may be used to provide an upper bound.

$$d_{far} = \frac{\lambda}{2\,\pi}$$ *Equation 2.6*

$$d_{reactive} < 0.62\sqrt{L^3/\lambda}$$ *Equation 2.7*

$$0.62\sqrt{L^3/\lambda} < d_{radiating} < 2\,L^2/\lambda$$ *Equation 2.8*

Table 5: Borders of reactive and radiating near field for different antenna sizes

L [m]	$d_{reactive}$ [m]	$d_{radiating}$ [m]
0,05	0,036	0,133
0,28	0,474	4,181
1	3,202	53,33

3. Measurements and analysis

In this chapter all measurements and calculations performed for the radar section of this thesis are summarized. The first measurement was performed to get familiar with the use of a network analyser and how to use it for channel measurements.

The second measurement was carried out to get more detailed information about the radio channel and how different test objects change the impulse response of the channel. Then a grid measurement as described in chapter 2.2 and measurements with disturbing obstacles were conducted.

3.1 First test measurement

The task of this measurement was to get familiar with the use of a network analyser for channel measurements.

3.1.1 Task

The goal was to measure different S - parameters with 4 antennas and different obstacles at different distances. The S - parameters of interest were S12, S13 and S14, corresponding to the measurement setup described in 3.1.2.

3.1.2 Measurement setup

The positioning of the antennas was done as shown in Figure 7 below. The Antennas were mounted on tripods for cameras. The side antennas were placed approximately 1 meter away from the centre antennas. All antennas were mounted at the minimum height of 65 cm. The side antennas were also rotated towards the centre by approximately 45° as shown in Figure 8. The object which had to be detected is placed in a variable distance x away from the centre antennas. The distance x was changed in a range from 20 cm up to 300 cm

depending on the object. A photo of the actual measurement setup can be found in Figure 9.

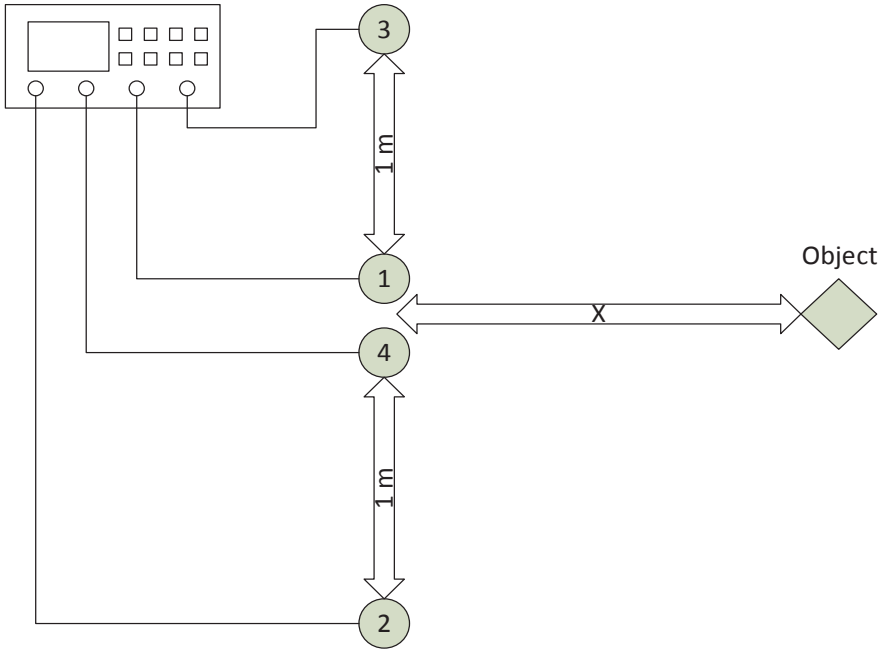

Figure 7: Measurement setup of first measurement

Figure 8: photo of 45° rotation of side antennas

Figure 9: Photo of measurement setup of first measurement

The antennas were positioned such, that the area behind the obstacle was flat concrete followed by a flat grass area. As shown in Figure 10 there were no bushes or trees in close distance to the measurement area. After the initial positioning of the antennas, the antenna setup was not altered anymore.

Figure 10: Measurement location in Lebring

28 mm copper pipe

The first object to test was a copper pipe with an outer diameter of 28 mm. There were no 25 mm pipes available at the hardware store. Only 22 mm and 28 mm pipes were available. For first tests the 28 mm copper pipe looked more suitable.

As a stand for the copper pipe a weight from a barbell was used. The weight was made of a plastic hull filled with sand. The copper pipe exactly fitted into the hole of the weight and can be positioned like shown in Figure 8 and Figure 9.

Carton wrapped in aluminium foil

The second test object was a piece of carton wrapped in 3 layers of aluminium foil. The size of the area covered with aluminium foil was 26 cm x 28 cm. The size of the whole carton was 26 cm x 36 cm. The carton itself was attached to the 28 mm copper pipe as shown in Figure 11. This object was chosen to have an object with a larger RCS than the copper pipe available for measurements.

Figure 11: Photo of carton wrapped in aluminium foil

Bicycle

The last object tested during the first measurement was a bicycle. The front-gear wheel was the reference point where the distance to the centre antennas was measured from. How the bicycle was positioned can be seen in Figure 12 and Figure 13.

Figure 12: Reference point of bicycle

Figure 13: Positioning of bicycle

Settings of the network analyser ZVB 8

For this measurement the following settings were used for the network analyser.

- Channel Base Power: 0 dBm
- Measurement Bandwidth: 1kHz
- Sweep: linear, 1 MHz step size (5001 samples), 3 to 8 GHz

3.1.3 Measurement procedure

The measurement procedure was split into three parts. First part was the calibration of the network analyser. After calibration the measurements could be conducted. At the end the attained results needed to be analysed in Matlab.

Calibration of the network analyser

The first step was to calibrate the network analyser. For calibration a box with defined endings was used. Calibration was done following these steps:

- Attach the whole setup to the network analyser, except the antennas.
- Press “Cal” button on the network analyser.
- Choose TOSM (Through Open Short Match) from the list.
- Choose your calibration kit from the drop down menu and press next.
- Follow the instructions displayed on the screen and attach the corresponding endings to the ports.
- Once all calibration measurements are done press “finish”.
- The network analyser is now calibrated for this measurement setup.

Measurement

After calibration, the antennas were attached to the cables and the measurement was performed like described below:

- Place the object of interest at a defined position along x.

- Let the network analyser perform a sweep for the S – parameters of interest.
- Save the measured values to a USB – stick.
- Place the object at the next position to measure.
- Repeat these steps with all objects and distances.

Due to the fact, that it is not possible to read much information directly out of the spectrum, further signal analysis with Matlab was performed.

Analysis of measured values with Matlab

To see if a reflection could be detected, the impulse response was of interest. To get the impulse response out of a given spectrum an Inverse Fourier Transform (IFFT) had to be performed.

3.1.4 Results

It was very difficult to align the antennas at correct angles and same heights. In addition, the minimum height of the used tripods was rather high with 65 cm. Due to the tripods and the weight used as stand for the pipe, it was also not possible to get closer than 30 cm to the antennas.

Results for 28 mm copper pipe

The vertical red and green lines in the following figures show the calculated time at which the reflection of the pole is expected. It can be seen, that there are always peaks close behind the calculated values. The other peaks more or less stay at the same time. This means that the moving peaks correspond to the reflection of the copper pole. The first high peaks correspond to the LOS (Line of Sight) component, which travels directly from one antenna to the other without being reflected.

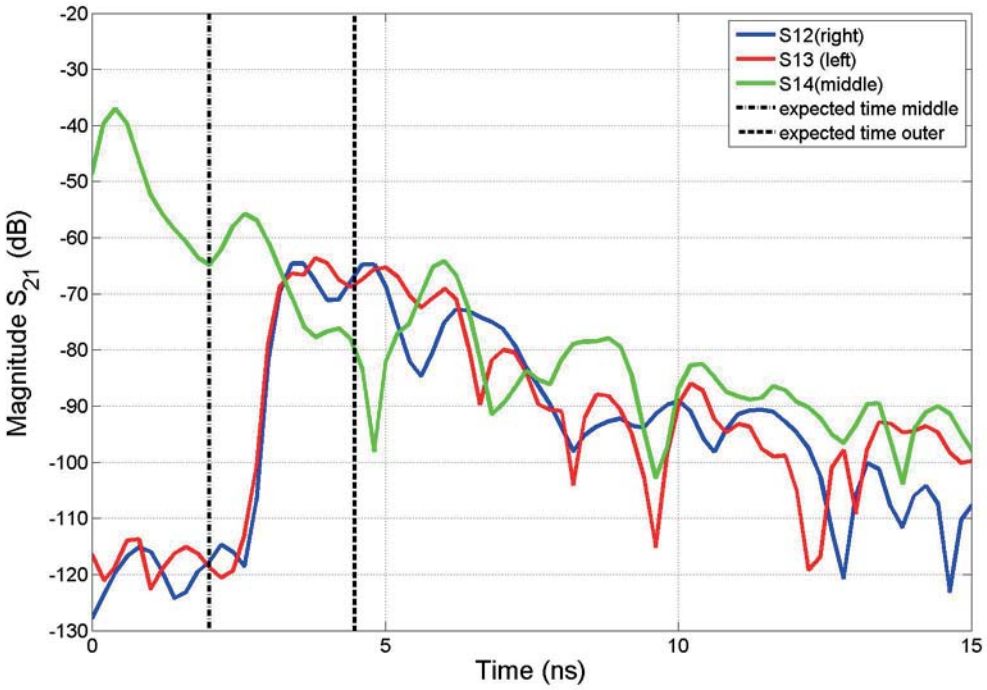

Figure 14: Measurement 1, 28 mm Cu, 30 cm

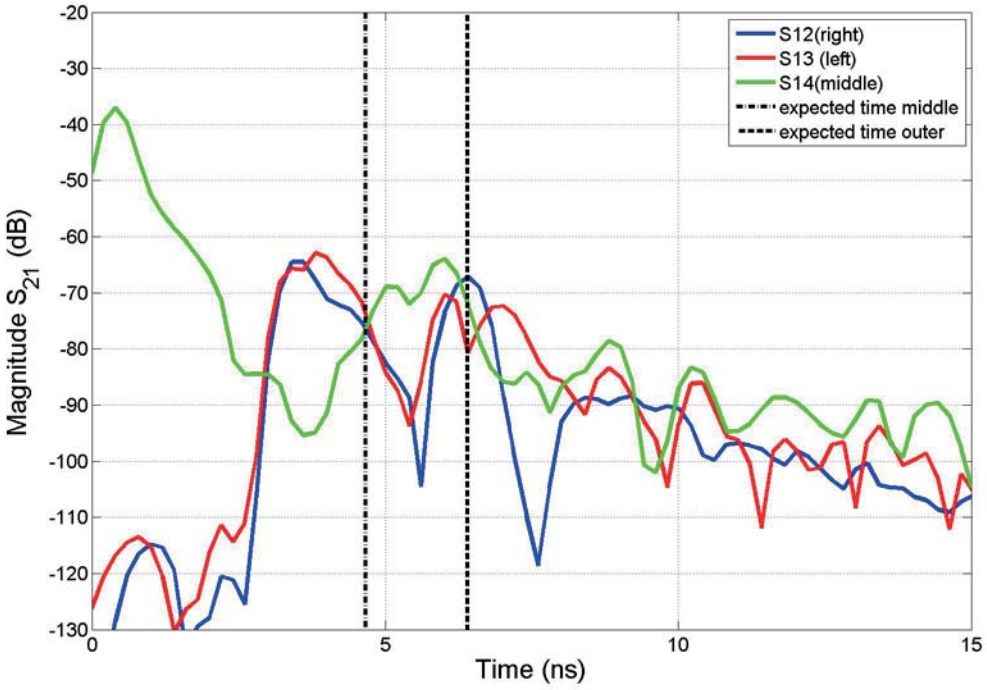

Figure 15: Measurement 1, 28 mm Cu, 70 cm

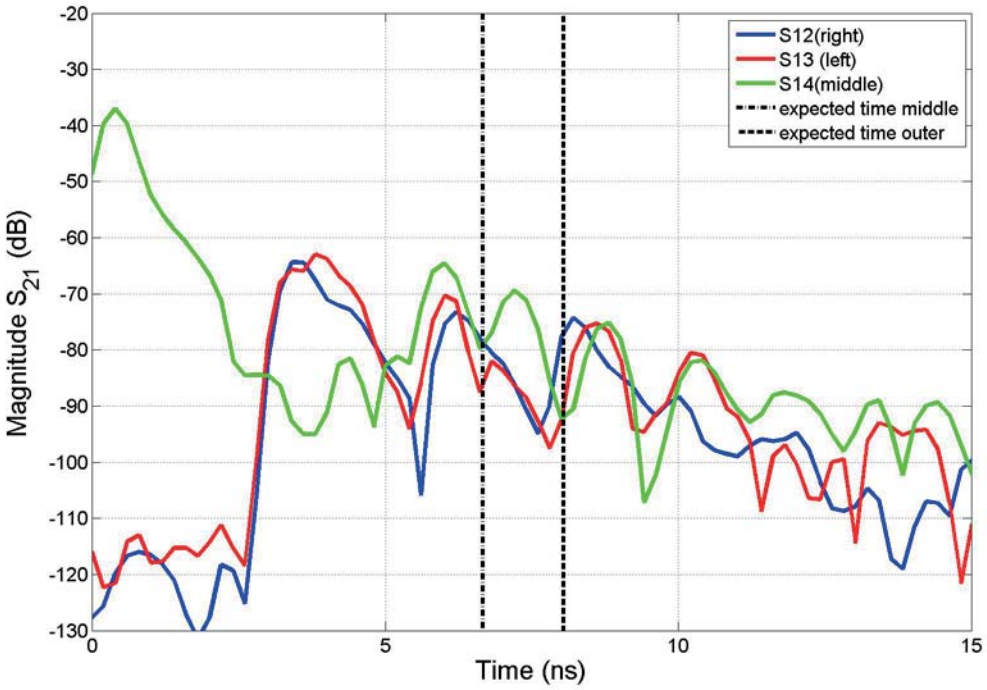

Figure 16: Measurement 1, 28 mm Cu, 100 cm

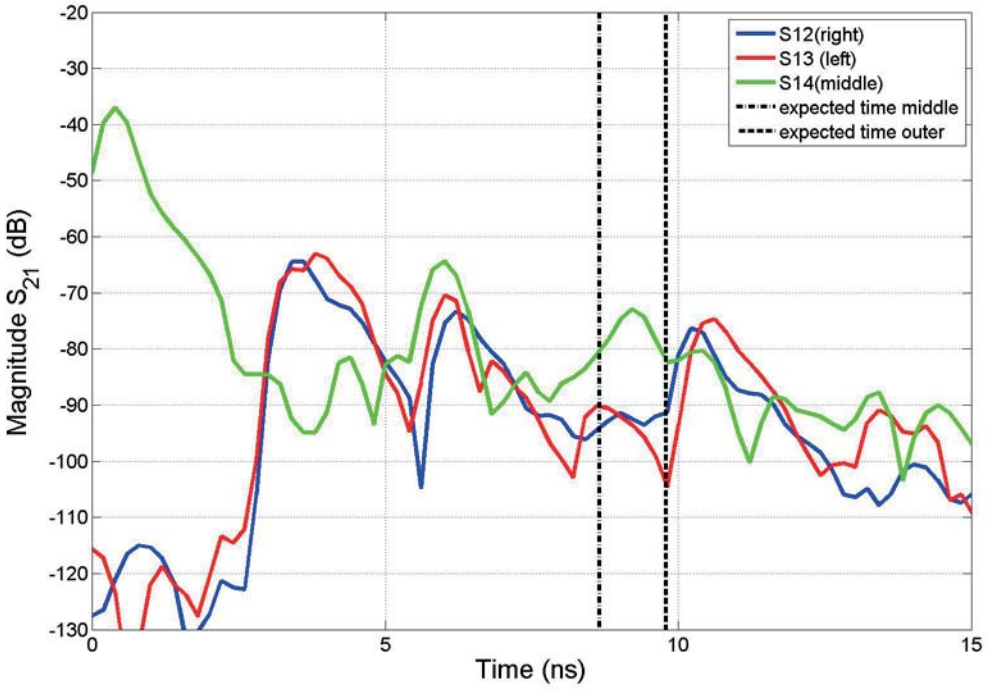

Figure 17: Measurement 1, 28 mm Cu, 130 cm

Although there is a reflection corresponding to the obstacle we tried to detect, the amplitude of the reflection had about the same size as other reflections. A better

way to visualize the different reflections was plotting the impulse response of the same antennas but with different object distances into one plot. This is shown in Figure 18.

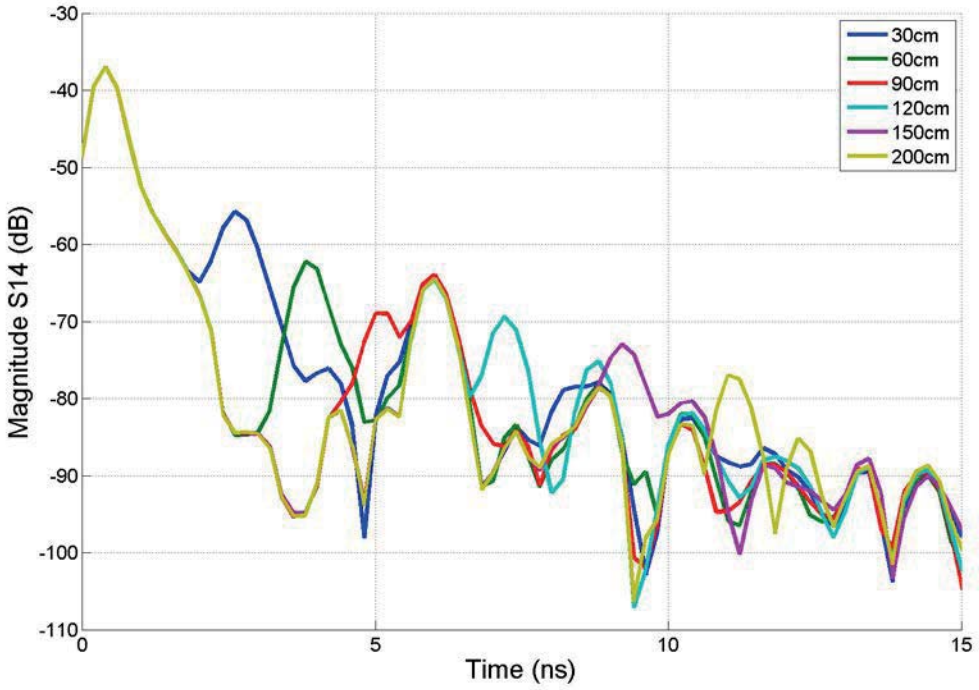

Figure 18: Measurement 1, 28 mm Cu, S14

S14 was used to visualize the change of the impulse response with changing distance to the object. Figure 18 clearly shows the reflections corresponding to the object. The time until the reflection arrived was easy to calculate for S14, because the distance the wave had to travel was twice the distance x. The speed of light is approximately 30 cm per nanosecond.

Results for carton wrapped in aluminium foil

The carton wrapped in aluminium foil showed significantly stronger reflections. This was expected because the reflecting surface of the aluminium was much larger than the small copper pipe. Furthermore, the copper pipe was round and reflected the wave in many directions. As it can be seen in Figure 19 and Figure 20 the reflection of the aluminium foil was stronger than the background reflections, even at distances of 1.5 m. Figure 21 shows again S14 with different

distances for the object. The corresponding reflections were clearly visible in the diagram. Only for 120 cm the reflection was relatively small. This was most probably because of a misalignment of the test object.

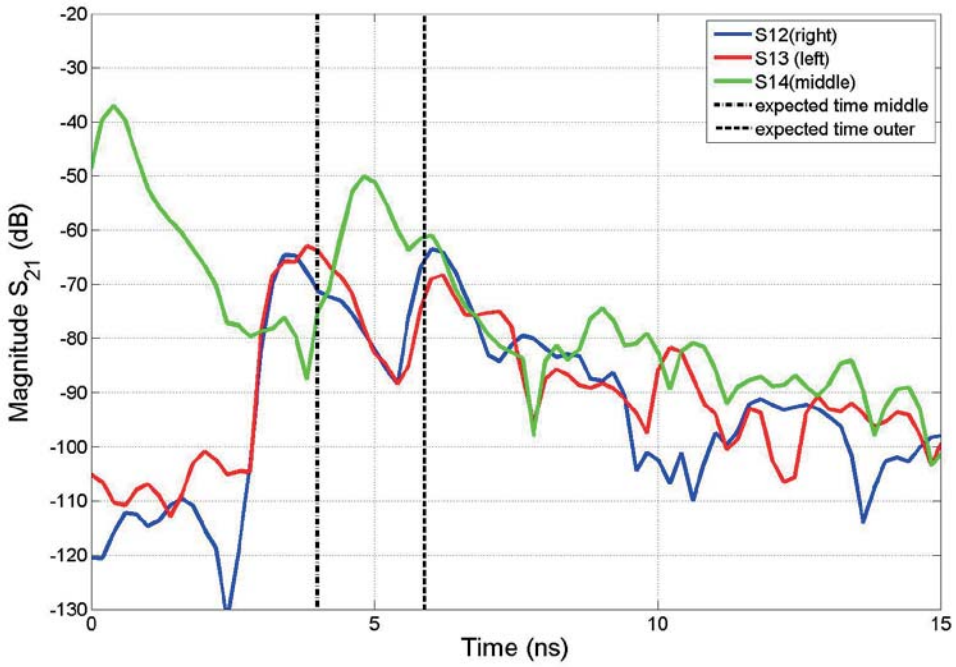

Figure 19: Measurement 1, carton with Al - foil, 60 cm

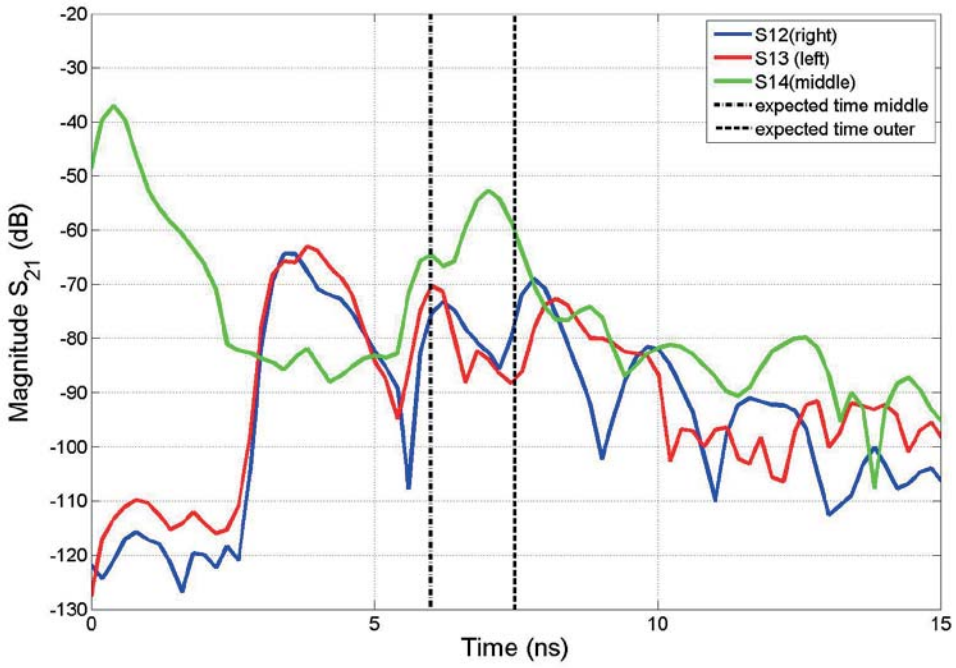

Figure 20: Measurement 1, carton with Al - foil, 90 cm

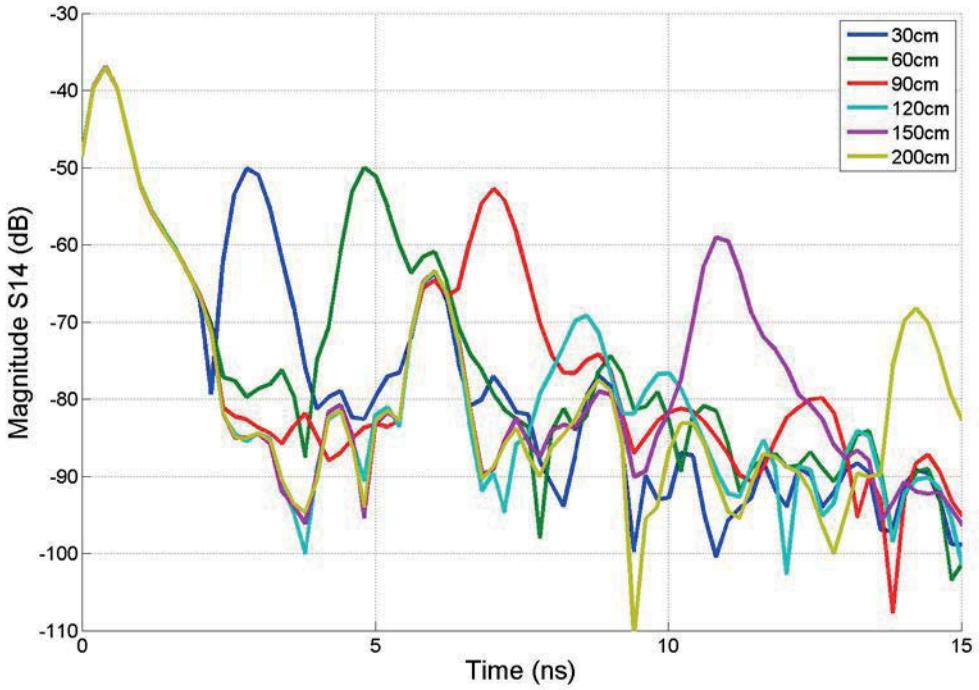

Figure 21: Measurement 1, carton with Al - foil, S14

Results for bicycle

It was very hard to detect any corresponding reflections of the bicycle in Figure 22 and Figure 23. Again, if S14 is plotted with different distances to the test object, the corresponding reflections were clearly visible. Because of the bicycles shape the reflection was not one pulse, but rather consisted of multiple overlapping pulses.

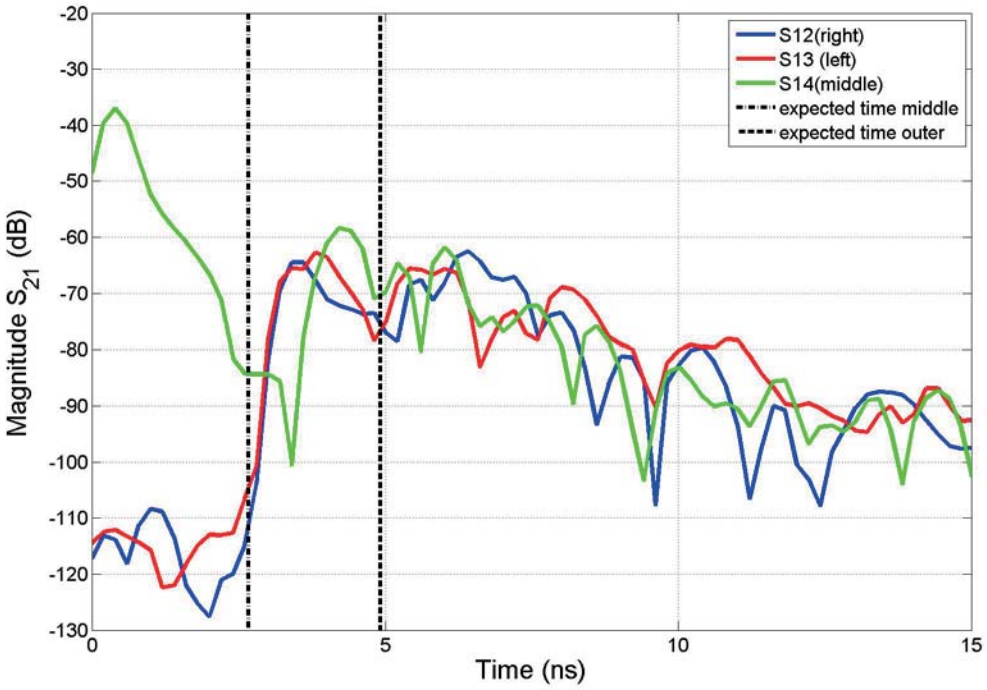

Figure 22: Measurement 1, bicycle, 40 cm

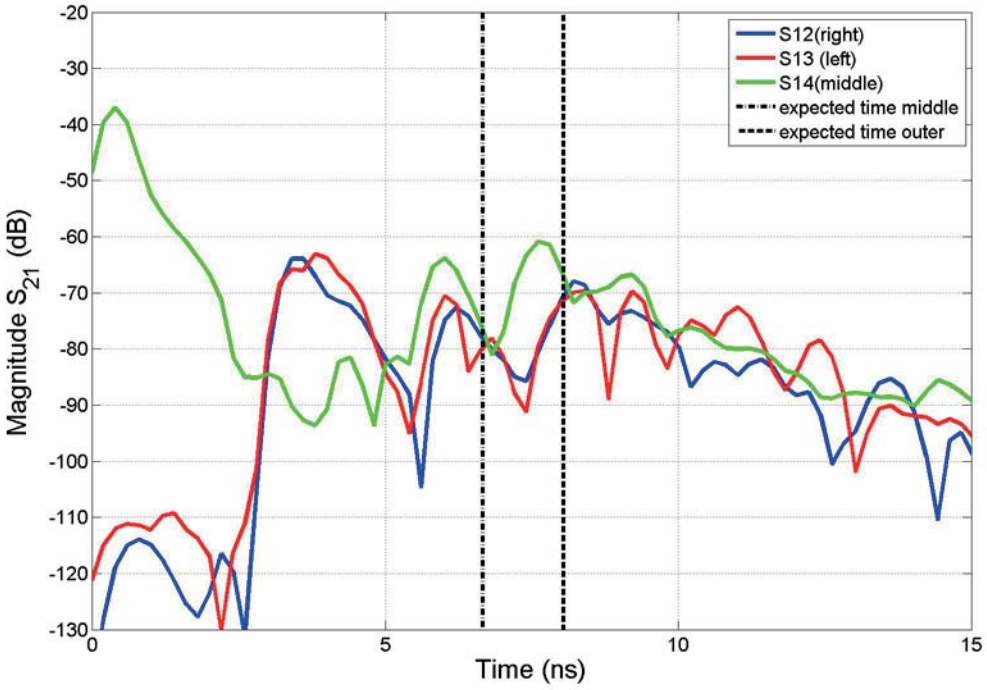

Figure 23: Measurement 1, bicycle, 100 cm

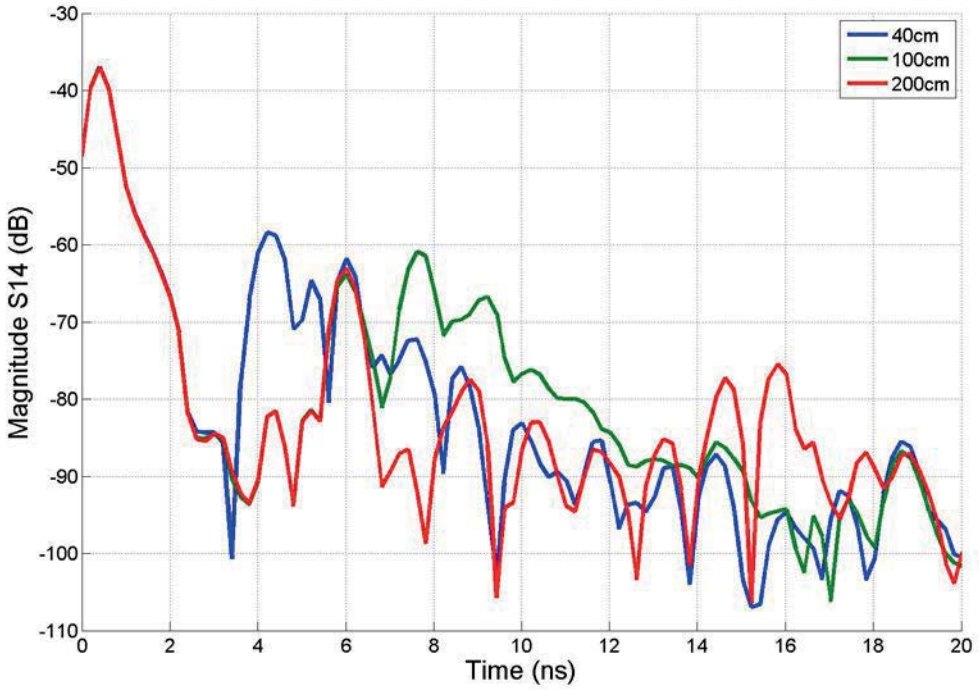

Figure 24: Measurement 1, bicycle, S14

3.1.5 Used devices

The following devices were used to perform the above described measurements. The antennas mentioned below were also used for any further measurements.

- Rohde & Schwarz Vector Network Analyser, 4 ports, 300 kHz – 8 GHz
- 4 x UWB patch antennas
- 4 x antenna cables
- Test objects like described at 3.1.2
- PC, Windows 7
- Matlab 2013

Antennas

The 4 UWB patch antennas were circularly polarized. The directional pattern of one antenna is described in Figure 25 and Figure 26. As shown in these figures the antenna pattern for right hand circularly polarization and left hand circularly

polarization differed very much. For a radar application this is a big problem, because for circular polarization the polarization direction changes when the wave gets reflected. This means that the receive pattern has a big lobe at the back of the antenna, and reflections from the backside of the antenna are not dampened much by the receive antenna.

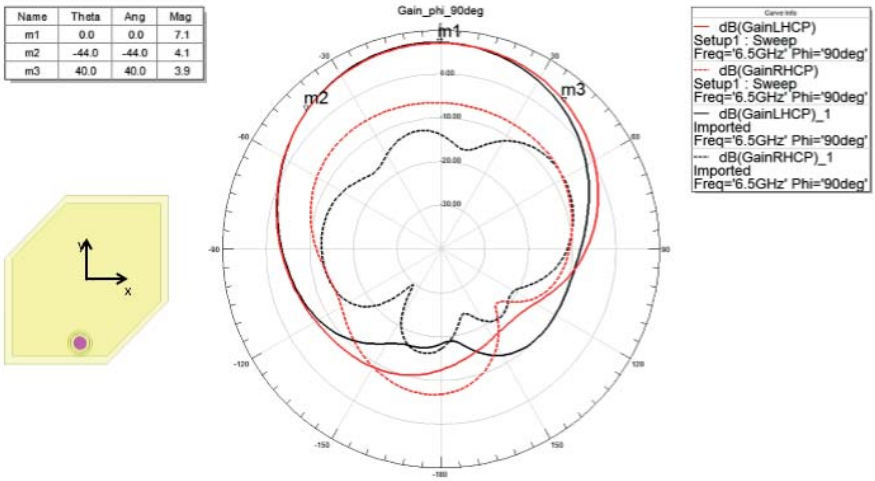

Figure 25: YZ - plane of UWB antenna pattern [19]

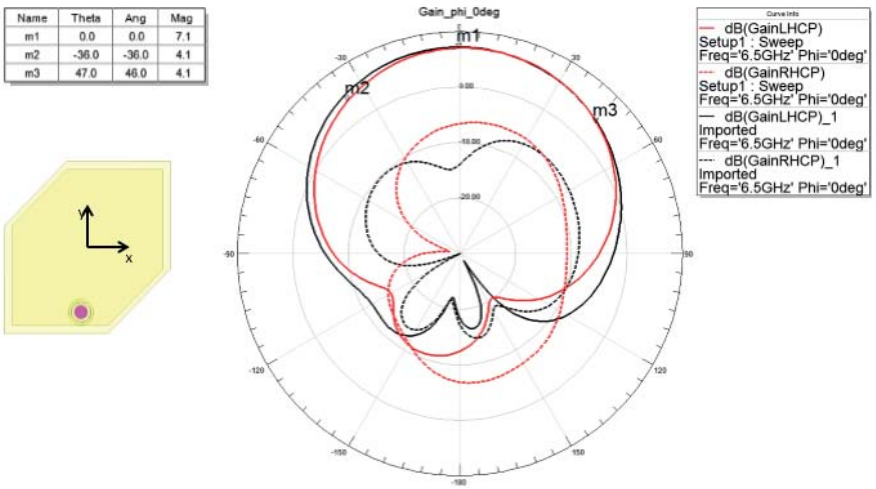

Figure 26: XZ - plane of UWB antenna pattern [19]

3.1.6 Conclusion for first test measurement

The strength of a reflection heavily depended on the shape and size of the object it came from. Objects like poles and flat surfaces reflected single short pulses. More complex objects like a bicycle reflected many overlapping pulses.

Furthermore, all reflections had an amplitude around -60 to -80 dB.

It would have been good to measure the reflection factors S11, S22 and S33 to see if any useful information could be gathered out of them. Also S23 would have been of interest, because it was not guaranteed that the central antennas would exist in the final system. Therefore, it was of interest to find out if the system could only work with the outer antennas.

3.2 Measurement 2 – concrete ground

During and after the first measurement I discovered many things, which needed verification or should be done better with the second measurement. The second measurement was split into two parts. The first one was the measurement on concrete ground. The second was the measurement on grass.

3.2.1 Task

The task of the second measurement was similar to the task of the first one. This time more S – parameters had to be measured and the distances were uniform for all objects. Also the file names of the measured data followed uniform rules. The following parameters had to be measured corresponding to the measurement setup described in 3.2.2.

- Reflection coefficients: S11, S22 and S44
- Transmission coefficients: S12, S23 and S44

The following distances had to be measured:

- 20, 40, 60, 80, 100, 120, 140, 160, 180, 200 cm
- 250, 300, 350, 400 cm

In addition to the 28 mm copper pipe and the carton wrapped in aluminium foil a 75 mm plastic pipe (polokal) was used as test object. The bicycle was not used again.

The common rule for file names were:

sxx_yyy.csv

sxx … parameter measured

yyy … distance to object measured in cm

The raw measurement data can be found as described in the appendix at D.

3.2.2 Measurement setup

This time the distance between the antennas was defined more accurate because the antennas were not mounted onto tripods like in measurement 1. Instead, the antennas were placed onto small carton boxes which were mounted onto an ale-bench with sticky tape. This allowed to align the antennas more accurate. The antenna centre lay in a height of 53 cm above the ground. Examples can be seen in Figure 27 and Figure 28. The distances between the antennas are shown in Figure 29. The values for x were chosen as mentioned above.

Figure 27: Backside of antenna mount

Figure 28: Front side of antenna mount + height of antenna

The copper pipe and the carton wrapped in aluminium foil were the same as described in 3.1.2.

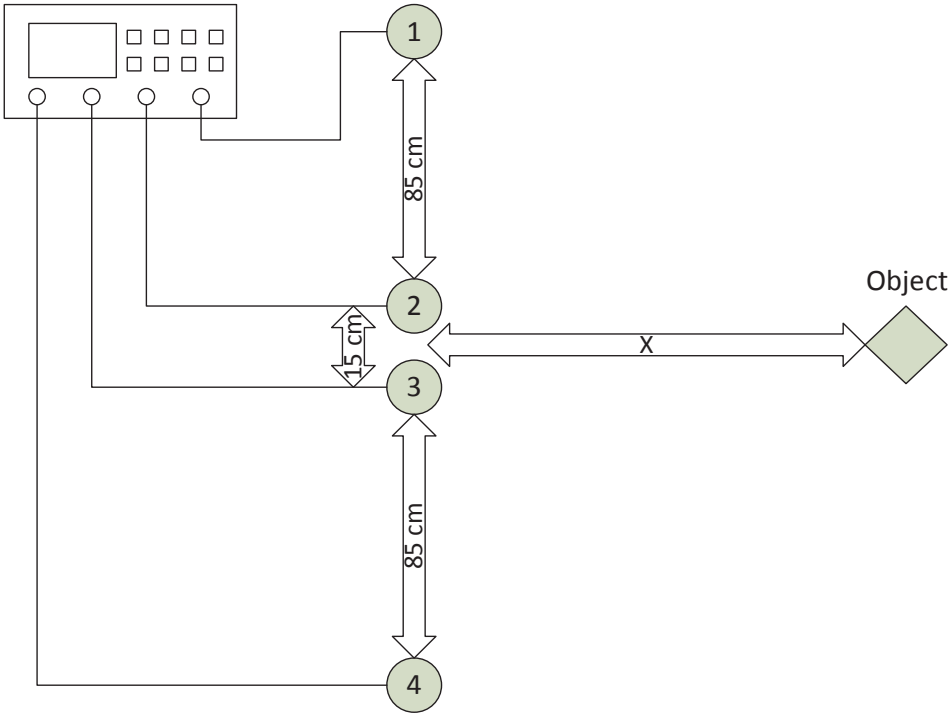

Figure 29: Measurement setup of second measurement

75 mm plastic pipe

A 75 mm plastic pipe is the standard test object for MALSO systems using ultrasonic sensors. That is why we decided to use it as test object, although we were using radar instead of ultrasonic. As stand for this pipe a bucket with street chalk as weight was used. The pipe was a Polokal Pipe as it can be bought at any hardware store. The wall of the pipe was 1.9 mm thick.

Figure 30: 75 mm plastic pipe stand

Settings of the network analyser ZVB 8

This time a “Channel Base Power” of 20 dBm was used. Therefore, the “Measurement Bandwidth” increased from 1 kHz to 10 kHz which allowed faster measuring because of reduced settling time of the filter.

- Channel Base Power: 20 dBm
- Measurement Bandwidth: 10kHz
- Sweep: linear, 1 MHz step size (5001 samples), 3 to 8 GHz

3.2.3 Measurement procedure

The measurement procedure is exactly the same as mentioned in 3.1.3. The common rule for file names and distances allowed for the use of a Matlab script to improve efficiency of data evaluation.

3.2.4 Results

The results for the second measurement looked similar to the results of the first measurement, but more data had been acquired and the measurement setup was more accurate.

Results for 28 mm copper pipe

In this measurement the results for the copper pipe looked more promising, because the reflections could be distinguished from each other much better. Only at a distance of 20 cm the reflections of the LOS component and the reflection from the object could barely be separated.

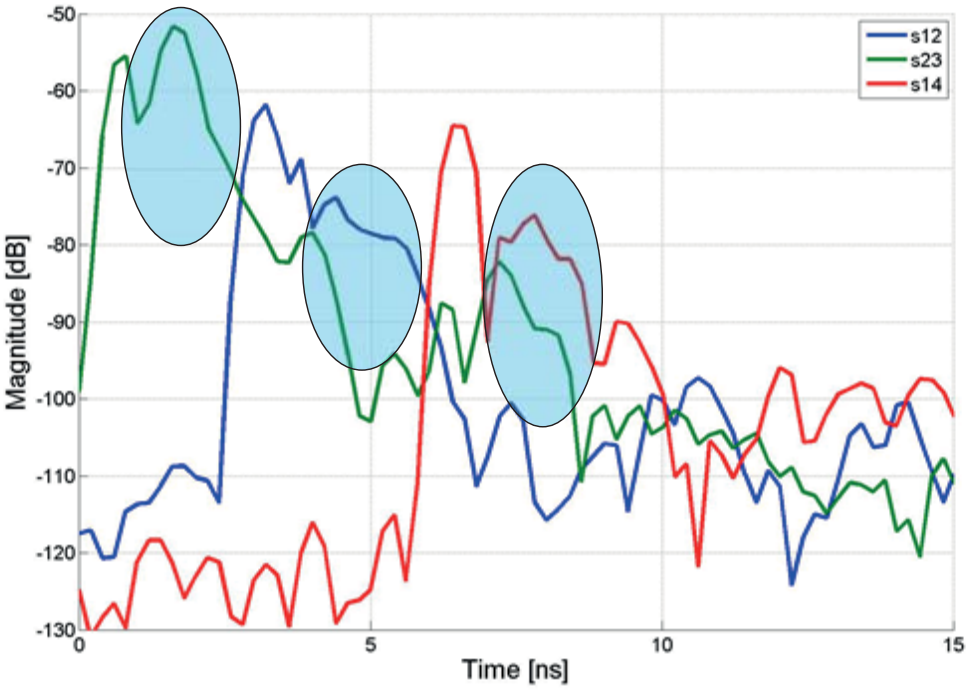

Figure 31: Measurement 2, 28 mm Cu, 20 cm

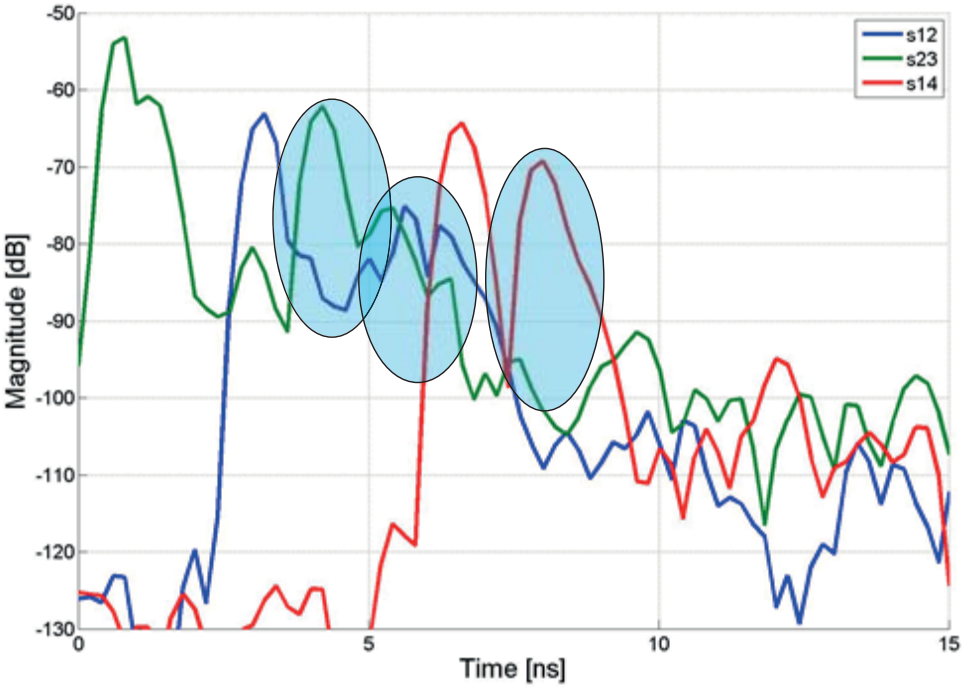

Figure 32: Measurement 2, 28 mm Cu, 60 cm

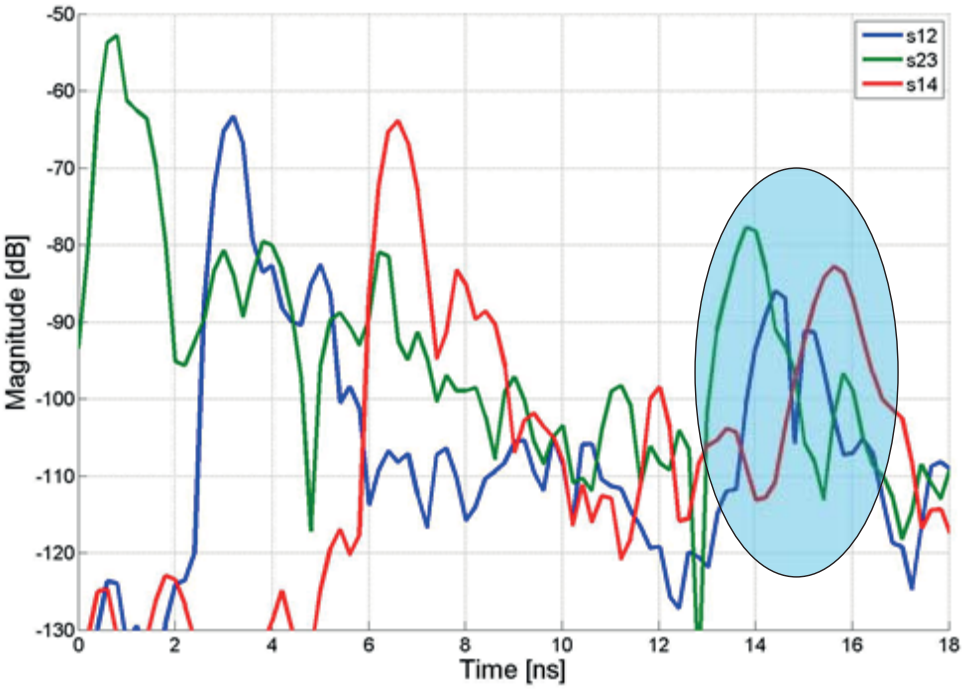

Figure 33: Measurement 2, 28 mm Cu, 200 cm

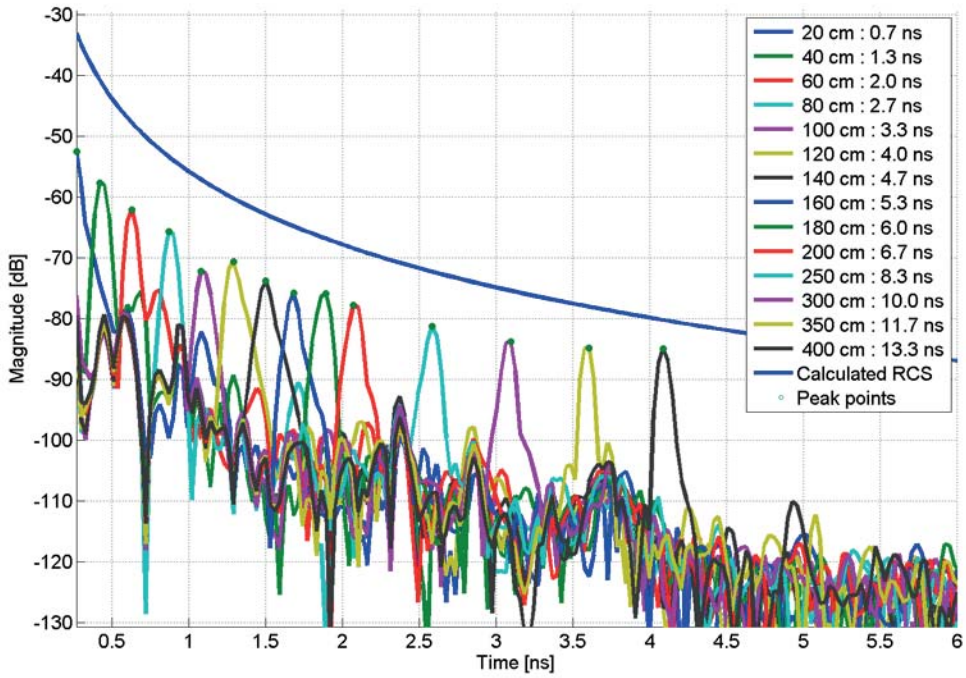

Figure 34: Measurement 2, 28 mm Cu, S23, with comparison to calculation

In Figure 34 the reflections for the corresponding distances can be clearly seen with a difference of 15 dB to 20 dB to other reflections. The estimation with the calculated RCS is higher than the measurement results. For bigger distances the difference between calculation and measurement becomes smaller and smaller.

Results for carton wrapped in aluminium foil

The results for aluminium foil of the second measurement were similar to the results for the 28 mm copper pipe. Only the amplitude difference between the reflections of the object and other reflections was between 20 dB and 30 dB which was significantly higher. The estimation with the calculated RCS is again higher than the measurement results, where estimation with the simulated RCS matches the measurement results quite good.

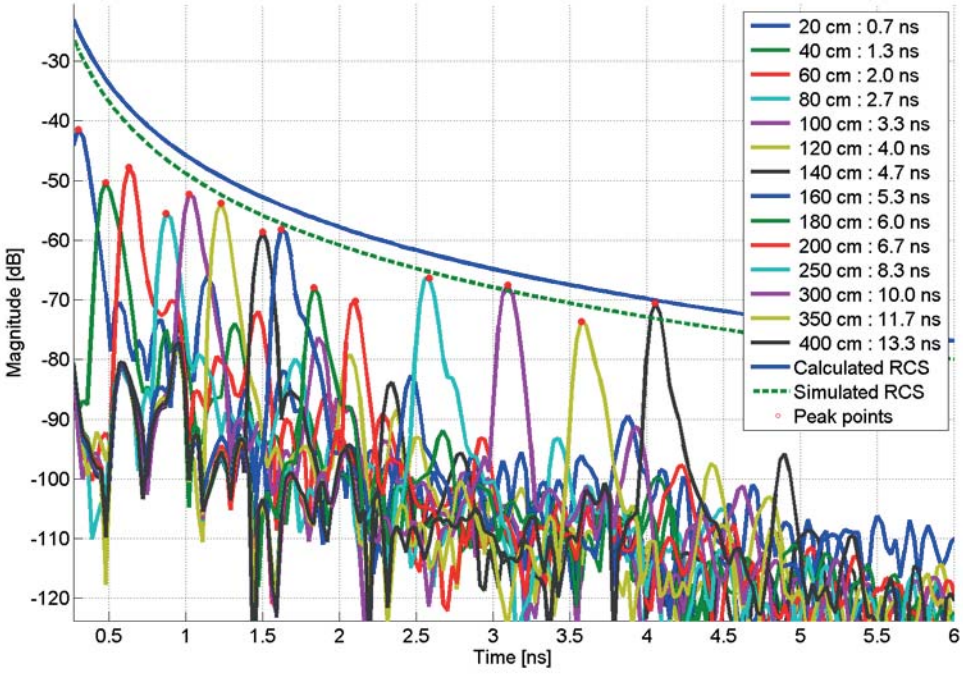

Figure 35: Measurement 2, aluminium foil, S23, with comparison to calculation

Results for 75 mm plastic pipe

The measurement for the plastic pipe showed, that the amplitudes of the reflections of the plastic pipe were significantly lower than the ones from metal

objects. It is very hard to see any reflections in Figure 36, only in Figure 37 the reflections can be distinguished from clutter.

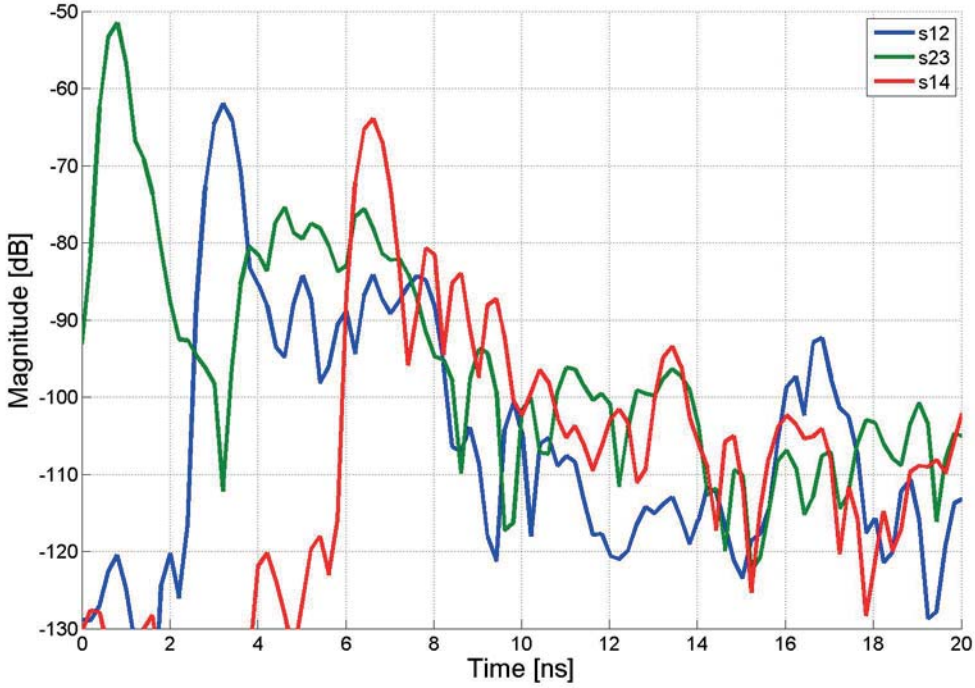

Figure 36: Measurement 2, 75 mm plastic pipe, 60 cm

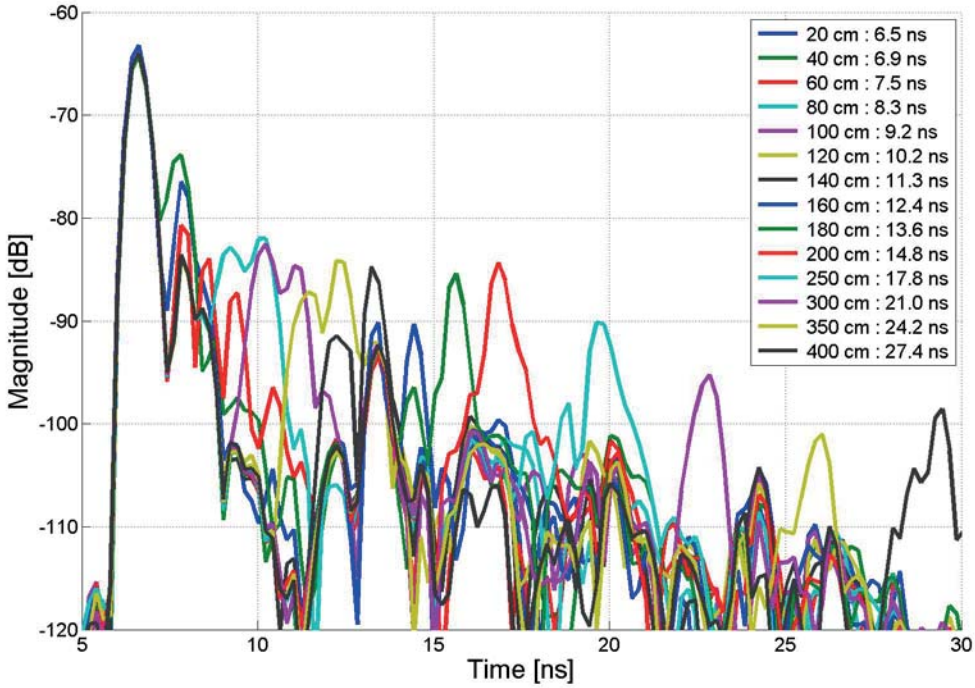

Figure 37: Measurement 2, 75 mm plastic pipe, S14

3.2.5 Used devices

The following devices were used to perform the above described measurements. The used antennas were the same as described in 3.1.5.

- Rohde & Schwarz Vector Network Analyser, 4 ports, 300 kHz – 8 GHz
- 4 x UWB patch antennas
- 4 x antenna cables
- Test objects like described at 3.2.2
- PC, Windows 7
- Matlab 2013

3.2.6 Conclusion for measurement on concrete

This measurement had shown that it would be hard to detect objects made of plastic. For development of a path loss model for different grounds another measurement on grass had been be conducted.

3.3 Measurement 2 – grass ground

Measurement 2 – grass ground was exactly the same measurement as described at 3.2. Every point not described here was done like the measurement on concrete.

3.3.1 Measurement setup

It was tried to rebuild the measurement setup described at 3.2.2 as exactly as possible. Figure 38 and Figure 39 show how the setup looked like.

Figure 38: Measurement 2 - grass setup front view

Figure 39: Measurement 2 - grass setup back view

3.3.2 Results

The results look similar to the results from the measurement on concrete. A more detailed comparison of the results was done at 3.4.

3.3.3 Conclusion for measurement on grass

Because of the very similar results to the measurement on concrete, no significant differences could be observed.

3.4 Calculation of path loss model

In order to find a suitable threshold for detection, a path loss model was needed. For this purpose, the results of the previous measurements were used. The peak points of the reflections were used in a least squares approach to calculate a polynomial of first order. With this fitted line the path loss could be determined. Figure 40 summarizes different path losses for different test objects and undergrounds. The measured path losses lay approximately at -28 dB/decade.

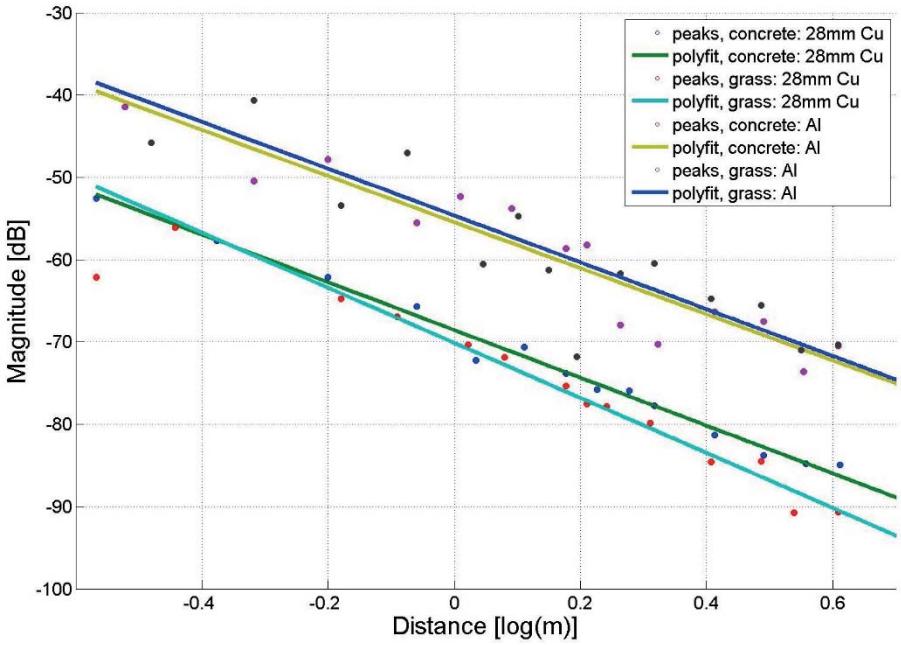

Figure 40: Comparison of path losses for different test objects and undergrounds with double log scale

3.5 Grid Measurement

In this measurement the test object was positioned along a grid with 10 cm distance steps. This measurement was intended to deliver a coverage diagram like the one described in 2.2.3.

3.5.1 Measurement setup

Because it was not possible to use the same antenna for transmission and reception, 2 antennas were mounted next to each other.

Figure 41: Antenna positioning of grid measurement

The measurement setup looks like shown in Figure 42 and Figure 43.

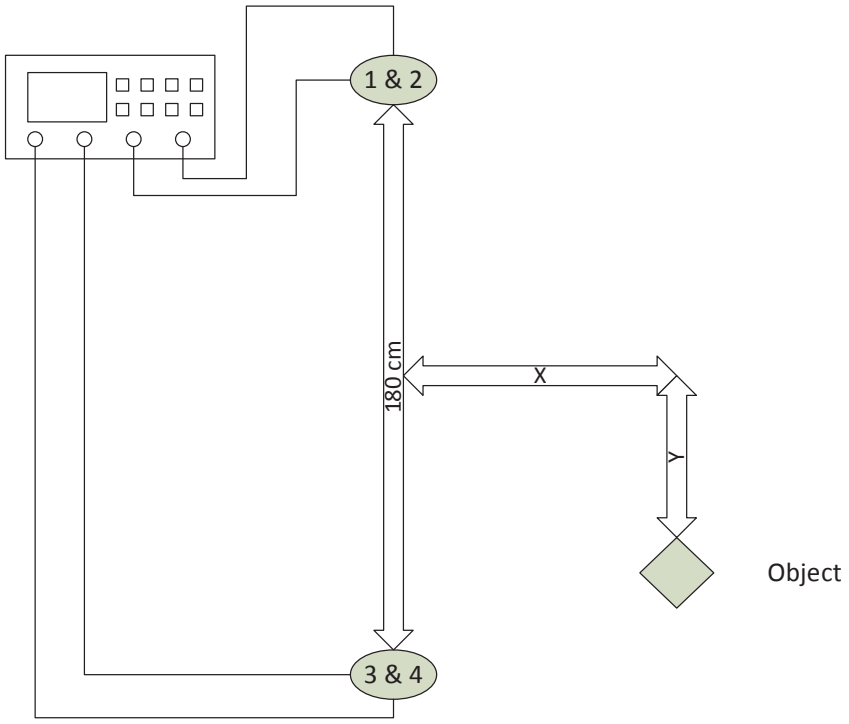

Figure 42: Measurement setup for grid measurement

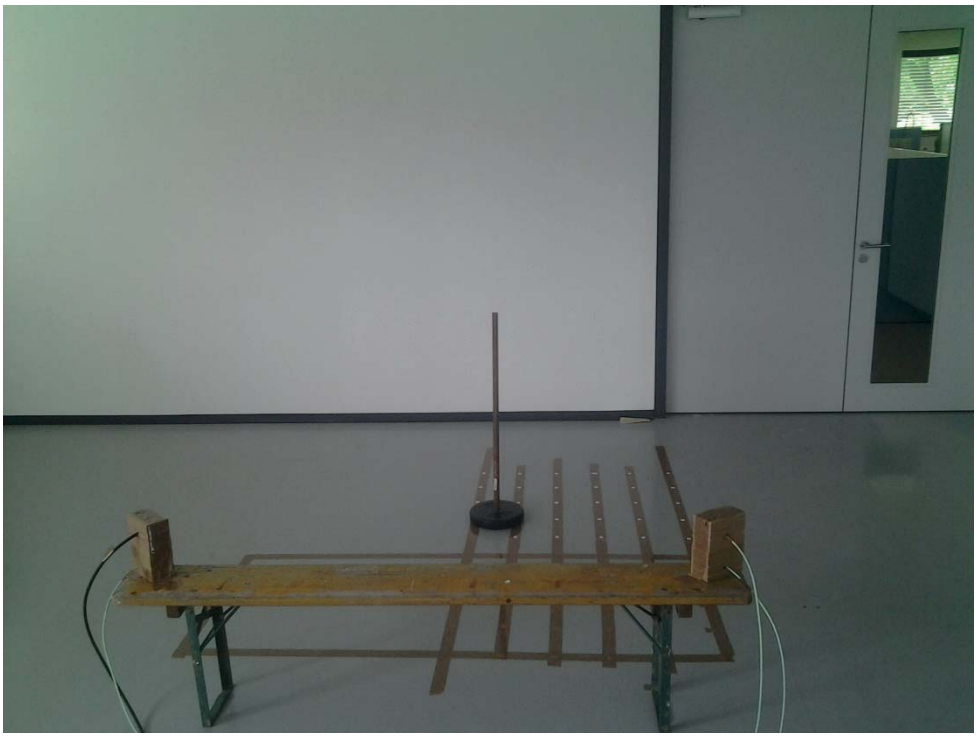

Figure 43: Measurement setup of grid measurement – photo

Test objects

For this measurement again a 28 mm copper pipe and a 75 mm polokal plastic pipe were used as targets.

3.5.2 Measurement procedure

Because of the large number of positions which had to be measured, a Matlab script was automatically measuring all the S – parameters for one position and saved the results with a common rule for file names to the destination folder.

The performed measurement steps were as follows:

- Calibrate the network analyser.
- Configure Matlab script to use correct calibration file.
- Configure other parameters of the script. (S-parameters to be measured, distances, power, number of samples …)
- Start the Matlab script.
- Place target on first position which is indicated by the Matlab script
- Press “c” to perform the measurement for this position
- When the measurement for this position has been finished, the Matlab script informs the user via “text-to-voice” and console to reposition the target to the next position.
- If a measurement was somehow disturbed, the last measurement can be repeated by pressing “r” instead of “c”.
- After all measurements have been performed, the script automatically closes the connection to the network analyser.

3.5.3 Analysis of measurement data

Again the impulse response for each measurement was computed. A threshold for each S-parameter was manually fitted such, that it lay close above the reflections from the background and started right after the LOS component.

Threshold

The threshold was computed like shown in Equation 3.1, adjusting the parameters manually to stay close above the clutter level.

$$threshold = P_{RX}(d_{LOS}) - 10 \cdot n \cdot log\left({}^{x}/_{d_{LOS}}\right) \qquad \textit{Equation 3.1}$$

$P_{RX}(d_{LOS})$ … manually adjusted start value for the threshold

Needed to be adjusted such that the threshold lay above the ground reflection. If this value was chosen to large, the threshold was too high and smaller reflections would not be detected. If it somewhere lay below the background reflection level, a false detection would happen.

n … manually adjusted path loss exponent

The path loss exponent for these measurements lay between 2.8 and 6. It was tuned to keep the threshold slightly above the background reflection level up to a distance of 4 meters.

d_{LOS}… Line of sight distance between 2 antennas

x … distance travelled by the signal

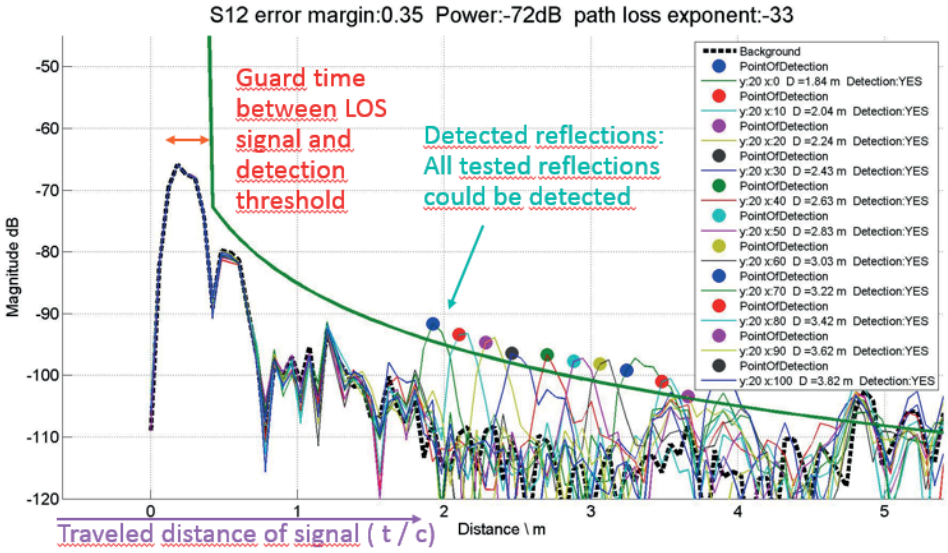

Figure 44: Detection of reflections with threshold – S12

As shown in Figure 44 the threshold started after a given guard time after the LOS component. A reflection was then considered to be detected if the signal level was higher than the threshold. Also the time at which the signal exceeded the threshold needed to be close to the expected time. How close it needed to be was defined by the error margin. In the figure above an error margin of 0.35 means that a signal level higher than the threshold was considered as detection, if it was in an area of +/- 35 cm around the expected time. The “path loss exponent” above the following figures needs to be divided by -10 to get the correct path loss exponent n. For Figure 44 this results in a $n = -33/(-10) = 3.3$.

Coverage diagram

As shown in 2.2.3 this information can be shown in form of a coverage diagram. Therefore, a table filled with “1” and “0” was exported to an Excel file. “1” stands for detection and “0” for no detection. The row and column of the table indicate the position in the measurement grid.

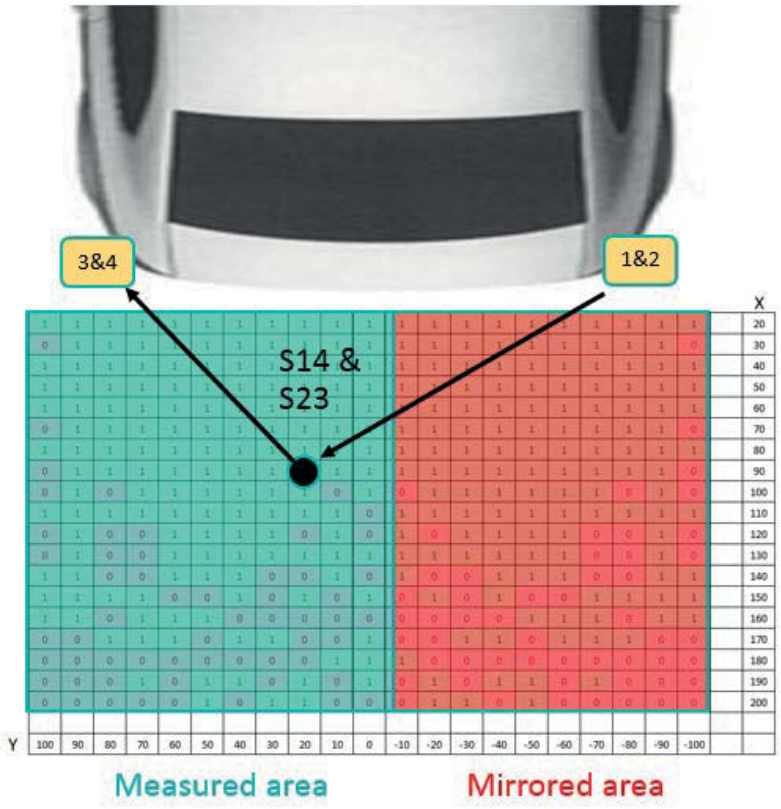

Figure 45: Explanation of the coverage diagram

As shown in Figure 45 only one side of the coverage diagram had been measured and was displayed. The other half was considered to be symmetric.

3.5.4 Results

The following figures show the results for the different grid measurements. First the results for copper pipe are shown, then for the plastic pipe.

Results for copper pipe

The results of the copper pipe, which worked quite well in this measurement, are shown on the following pages. Only reflections that coincided with ground reflections and reflections which came very close to the LOS component could not be detected well.

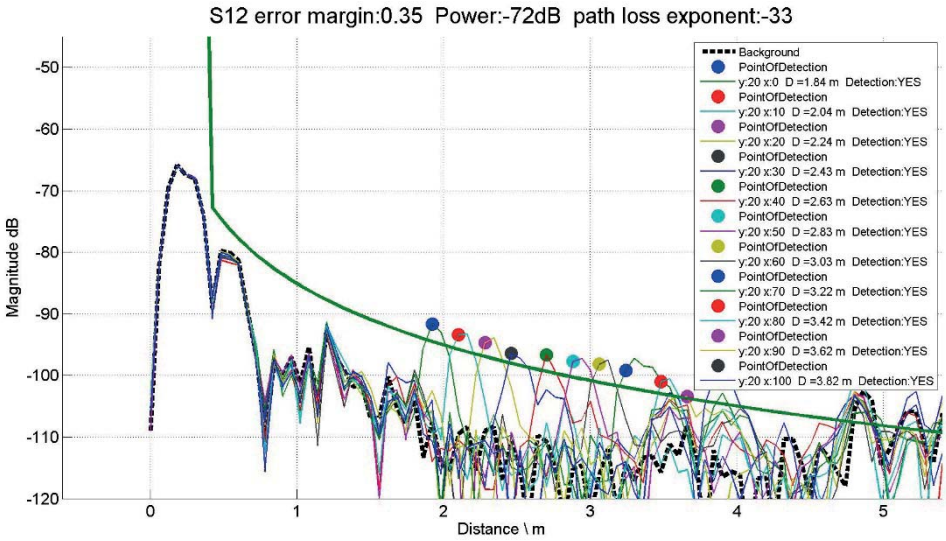

Figure 46: Grid measurement 28 mm copper pipe - S12

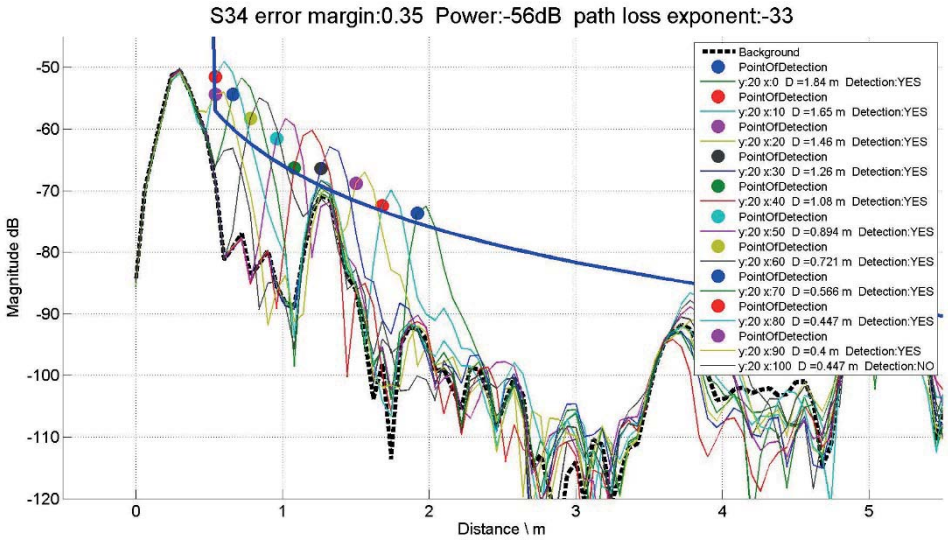

Figure 47: Grid measurement 28 mm copper pipe - S34

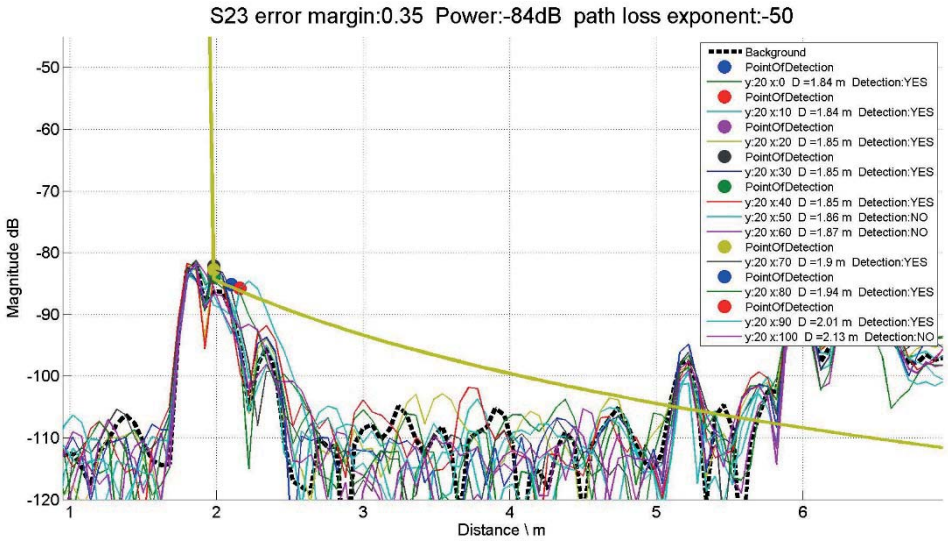

Figure 48: Grid measurement 28 mm copper pipe - S23

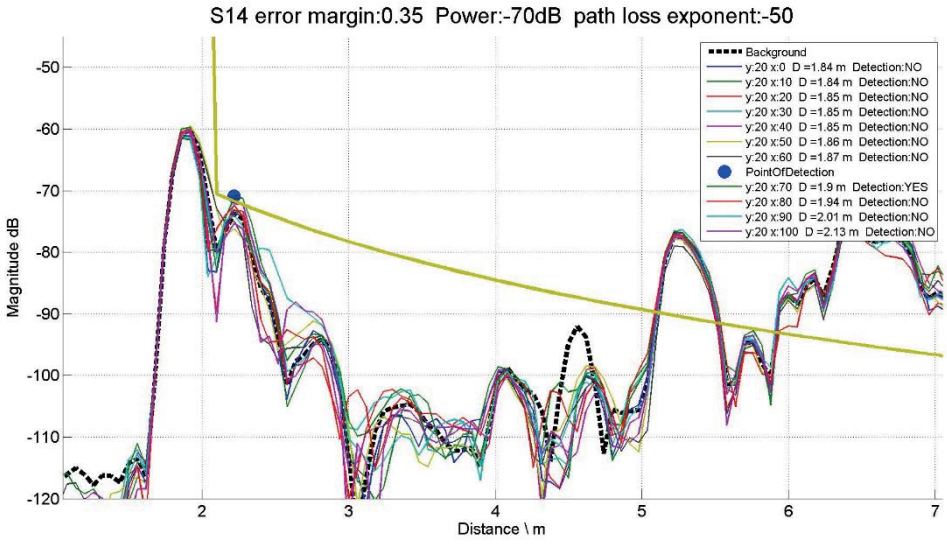

Figure 49: Grid measurement 28 mm copper pipe - S14

The figures above show only a few positions, a coverage diagram is better suited to represent all the measured data in one plot.

													X
	1	1	1	1	1	1	1	1	1	1	1		20
	0	1	1	1	1	1	1	1	1	1	1		30
	1	1	1	1	1	1	1	1	1	1	1		40
	1	1	1	1	1	1	1	1	1	1	1		50
	1	1	1	1	1	1	1	1	1	1	1		60
	0	1	1	1	1	1	1	1	1	1	1		70
	1	1	1	1	1	1	1	1	1	1	1		80
	0	1	1	1	1	1	1	1	1	1	1		90
	0	1	0	1	1	1	1	1	1	0	1		100
	1	1	1	1	1	1	1	1	1	1	0		110
	0	1	0	0	1	1	1	1	0	1	0		120
	0	1	0	0	1	1	1	1	1	1	1		130
	1	1	0	0	1	1	1	0	0	1	0		140
	1	1	1	1	0	0	1	0	1	0	1		150
	1	1	0	1	1	1	0	0	0	0	0		160
	0	0	1	1	1	0	1	1	0	0	1		170
	0	0	0	0	0	0	0	0	0	1	1		180
	0	0	0	1	0	1	1	0	1	0	1		190
	0	0	0	0	0	1	0	1	1	0	0		200
Y	100	90	80	70	60	50	40	30	20	10	0		

Figure 50: Coverage diagram, copper pipe, S12

													X
	0	0	1	1	1	1	1	1	1	1	1		20
	0	1	1	1	1	1	1	1	1	1	1		30
	0	1	1	1	1	1	1	1	1	1	1		40
	1	1	1	1	1	1	1	1	1	1	1		50
	1	1	1	1	1	1	1	1	1	1	1		60
	1	1	1	1	1	1	1	1	1	1	1		70
	1	1	1	1	1	1	1	1	1	1	1		80
	1	1	1	1	1	1	1	1	1	1	1		90
	1	1	1	1	1	1	1	1	1	1	1		100
	1	1	1	1	1	1	1	1	1	1	1		110
	1	1	1	1	1	1	1	1	1	1	1		120
	1	1	1	1	1	1	1	1	1	1	1		130
	1	1	1	1	1	1	1	1	1	1	1		140
	1	1	1	1	1	1	1	1	1	1	1		150
	1	1	1	1	1	1	1	1	1	1	1		160
	1	1	1	1	1	1	1	1	1	1	1		170
	1	1	1	1	1	1	1	1	1	1	1		180
	1	1	1	1	1	1	1	1	1	1	1		190
	1	1	1	1	1	1	1	1	1	1	1		200
Y	100	90	80	70	60	50	40	30	20	10	0		

Figure 51: Coverage diagram, copper pipe, S34

													X
	0	1	1	1	0	0	1	1	1	1	1		20
	0	1	1	1	1	1	0	1	0	0	0		30
	1	1	1	1	1	0	1	1	1	0	0		40
	1	1	1	1	1	0	1	0	0	0	0		50
	1	1	1	1	1	0	0	1	1	0	0		60
	1	1	1	1	1	1	1	1	1	1	1		70
	1	0	1	1	1	1	1	1	1	1	1		80
	1	1	1	1	1	1	1	1	1	1	1		90
	1	1	1	1	1	1	1	1	1	1	1		100
	1	1	1	1	1	1	1	1	1	1	1		110
	1	1	1	1	1	1	1	1	1	1	1		120
	1	1	1	1	1	1	1	1	1	1	1		130
	1	1	1	1	1	1	1	1	1	1	1		140
	1	1	1	1	1	1	1	1	1	1	1		150
	1	1	1	1	1	1	1	1	1	1	1		160
	1	1	1	1	1	1	1	1	1	1	1		170
	1	1	1	1	1	1	1	1	1	1	1		180
	1	1	1	1	1	1	1	1	1	1	1		190
	0	1	1	1	1	1	1	1	1	1	1		200
Y	100	90	80	70	60	50	40	30	20	10	0		

Figure 52: Coverage diagram, copper pipe, S23

													X
0	0	0	0	0	0	0	0	0	0	0		20
0	0	0	0	0	0	0	0	0	0	0		30
0	0	1	1	0	0	0	0	1	0	1		40
0	0	0	0	1	0	1	0	1	1	1		50
0	0	0	0	0	1	0	1	1	0	1		60
0	0	0	0	0	0	1	0	0	0	0		70
0	0	0	0	0	0	0	1	1	0	1		80
0	0	0	0	0	1	0	0	1	1	0		90
0	0	0	0	0	0	0	1	0	0	1		100
0	0	0	0	0	0	0	0	0	1	0		110
0	0	0	0	0	1	0	0	0	1	1		120
0	0	0	0	0	0	0	1	0	1	1		130
0	0	0	0	0	0	0	0	1	1	0		140
0	0	0	0	0	0	1	0	1	1	1		150
0	0	0	0	0	0	1	1	0	1	1		160
0	0	0	0	1	0	1	1	0	0	0		170
1	1	1	0	1	1	0	0	0	0	0		180
0	1	0	1	1	0	0	0	1	0	1		190
0	0	0	0	0	1	1	1	1	1	1		200
Y	100	90	80	70	60	50	40	30	20	10	0		

Figure 53: Coverage diagram, copper pipe, S14

Results for plastic pipe

The results for a plastic pipe are very bad. Nearly no reflections could be distinguished from clutter.

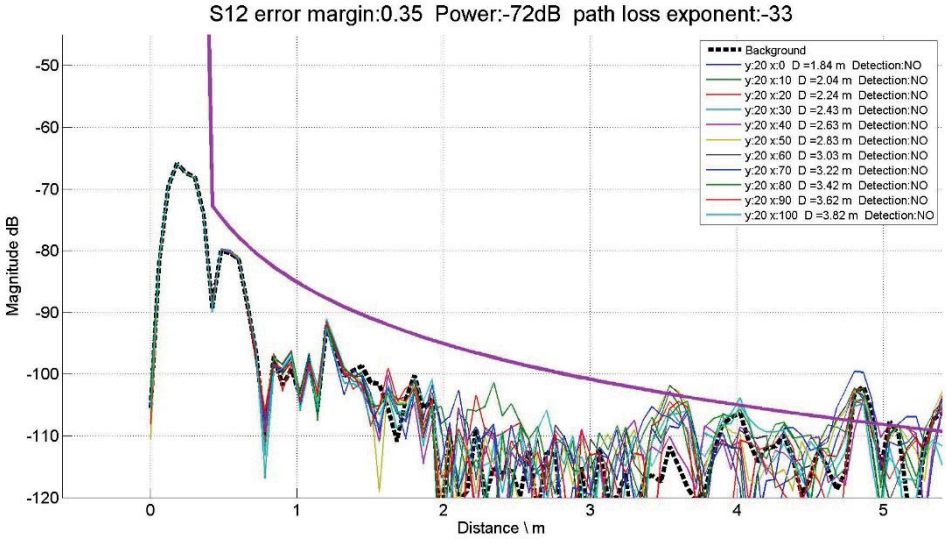

Figure 54: Grid measurement 75 mm plastic pipe - S12

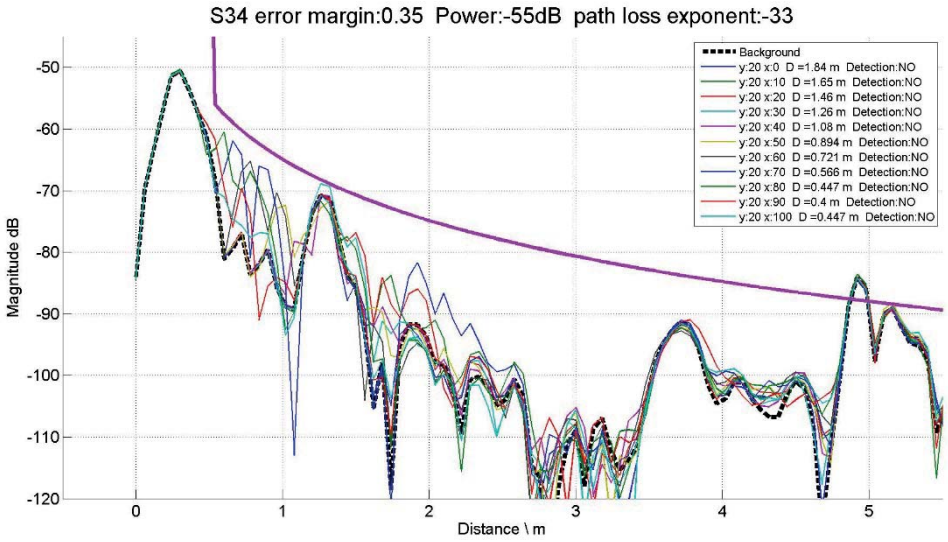

Figure 55: Grid measurement 75 mm plastic pipe - S34

												X
1	1	0	0	0	0	0	0	0	0	0		20
1	1	0	0	0	0	0	0	0	0	0		30
0	0	1	0	0	0	0	0	0	0	0		40
1	1	1	0	0	0	0	0	0	0	0		50
1	0	0	0	0	0	0	0	0	0	0		60
0	1	1	0	0	0	0	0	0	0	0		70
0	0	0	1	1	0	0	0	0	0	0		80
0	0	0	1	0	0	0	0	0	0	0		90
0	0	0	0	0	0	0	0	0	0	0		100
0	0	0	0	0	1	1	0	0	0	0		110
0	0	0	0	1	0	0	1	0	0	0		120
1	0	0	1	0	1	0	1	0	0	0		130
1	0	0	0	0	0	1	0	0	0	0		140
1	1	0	0	0	0	0	0	0	0	1		150
0	0	1	0	0	0	0	0	1	0	0		160
0	0	1	0	0	0	0	0	0	0	0		170
0	0	1	1	1	1	0	0	1	0	0		180
0	0	0	0	0	1	1	0	0	0	1		190
0	0	0	0	0	0	0	0	0	0	0		200
Y	100	90	80	70	60	50	40	30	20	10	0	

Figure 56: Coverage diagram, 75 mm plastic pipe, S12

													X
	0	0	0	0	0	0	0	0	0	0	0		20
	0	0	0	0	0	0	1	0	0	0	0		30
	0	0	0	0	0	0	0	0	0	0	0		40
	0	0	0	0	0	1	0	0	0	0	0		50
	0	1	0	1	0	0	0	0	0	0	0		60
	0	0	0	0	0	0	0	0	0	0	0		70
	0	0	0	0	0	0	0	0	0	0	0		80
	0	0	0	0	0	0	0	0	0	0	0		90
	0	0	0	0	0	0	0	0	0	0	0		100
	0	0	0	0	0	0	0	0	0	0	0		110
	0	0	0	0	0	0	0	0	0	0	0		120
	0	0	0	0	0	0	0	0	0	0	0		130
	0	0	0	0	0	0	0	0	0	0	0		140
	0	0	0	0	0	0	0	0	0	0	0		150
	0	0	0	0	0	0	0	0	0	0	1		160
	0	0	0	0	0	0	0	0	1	0	0		170
	0	0	0	0	0	0	0	0	0	0	0		180
	0	0	0	0	0	0	0	0	0	0	0		190
	0	0	0	0	0	0	0	0	0	0	1		200
Y	100	90	80	70	60	50	40	30	20	10	0		

Figure 57: coverage diagram, 75 mm plastic pipe, S34

3.5.5 Conclusion for grid measurement

Under ideal conditions the copper pipe could be detected, the plastic pipe could not be detected at all.

It had to be considered that the clutter level for this measurement was very low. The clutter level could increase significantly if the antennas were mounted on a car. Therefore, a measurement was carried out, to find out how much higher the clutter level would be if the antennas were mounted on a car.

An object could not be located in 3 - dimensional space if only two S-parameters were detecting the object. At least 3 S-parameters were needed to locate an object in 3-D space. At least one more antenna at the middle of the car would be needed to assure this.

S23 and S14 delivered diverse results. When looking at Figure 48 and Figure 49 it can be observed that there was only a small difference between the clutter and signal level. This means that small differences between the antennas and slightly

different alignment of the antennas may have caused the big difference between S23 and S14 which can be observed in their coverage diagrams.

3.5.6 Measurement with antennas mounted on a car

The purpose of this measurement was to find out how high the clutter level would be if the antennas were mounted on a car and how different positions for antennas affect the measurement results.

Measurement setup

For this measurement only the 28 mm copper pipe was used as a test object, because the last measurement showed that even under ideal conditions the plastic pipe could not be detected at all.

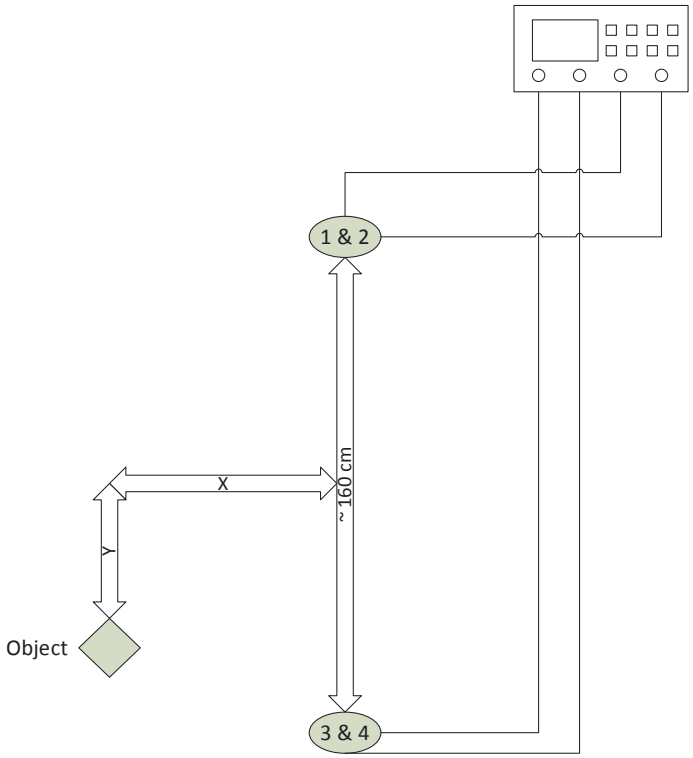

Figure 58: Measurement setup with antennas mounted on a car

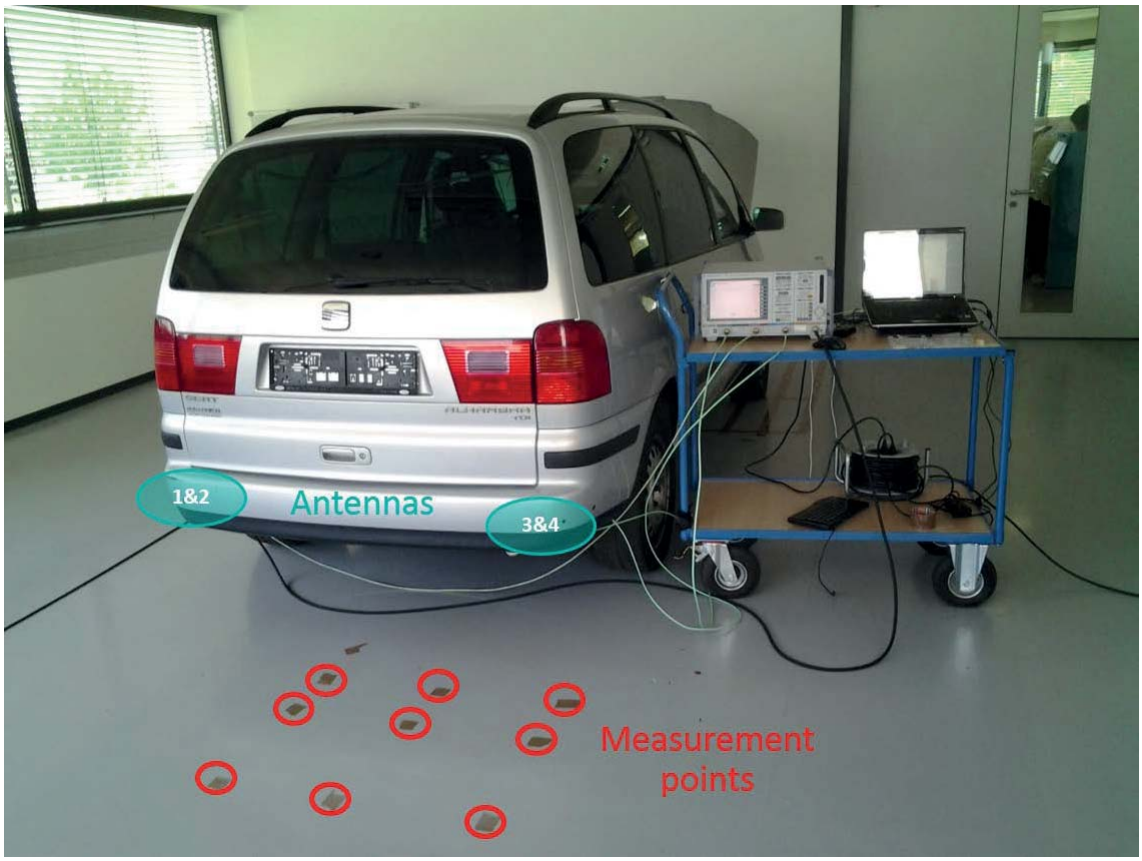

Figure 59: Photo of measurement setup with antennas on a car

As indicated by the red circles in Figure 59 only 9 points had been measured. These points delivered reference values, which could be compared with the results from previous measurements. The positions of the points were as follows:

X: 20, 40, 80 cm

Y: 0, 40, 80 cm

Also the positions where the antennas were mounted are indicated by the blue circles.

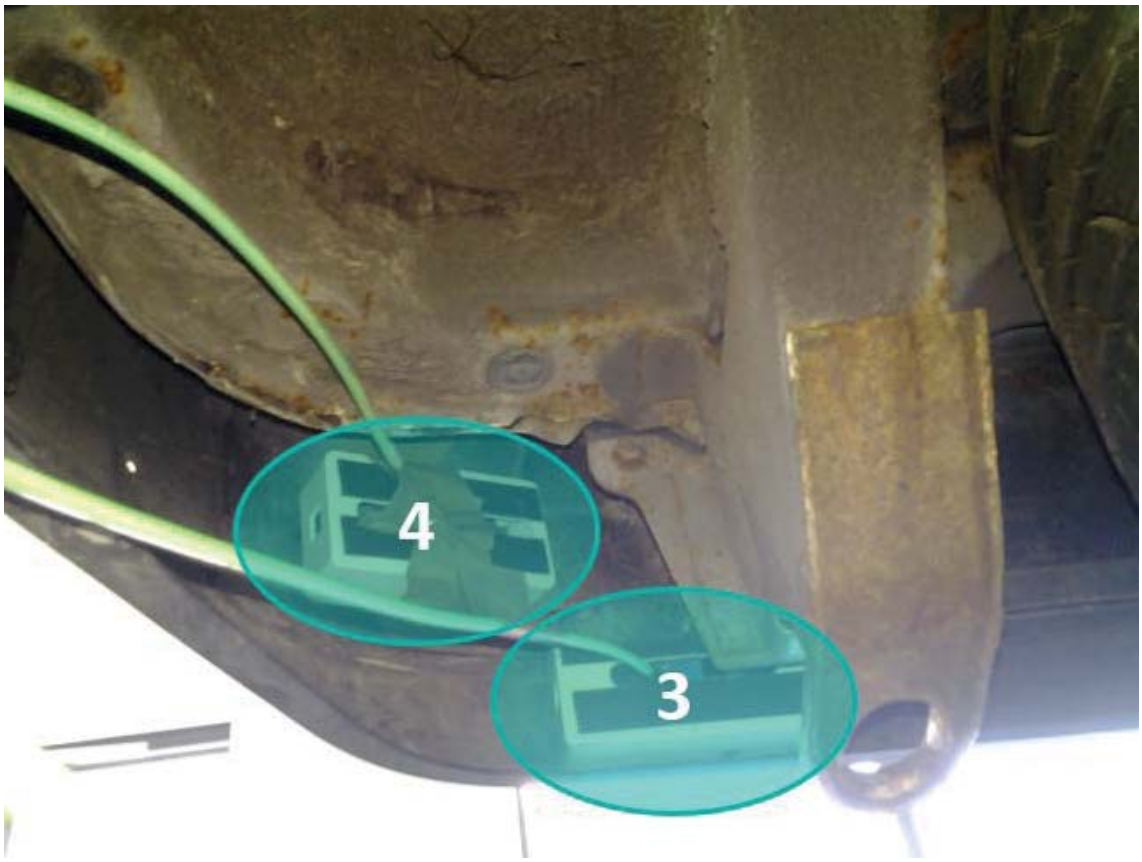

Figure 60: Antennas mounted beneath the rear bumper

Measurement procedure

The measurement was performed as described in chapter 3.5.2, therefore the steps were not repeatedly shown here.

Results

The following figures show the results when the antennas were mounted directly on the car.

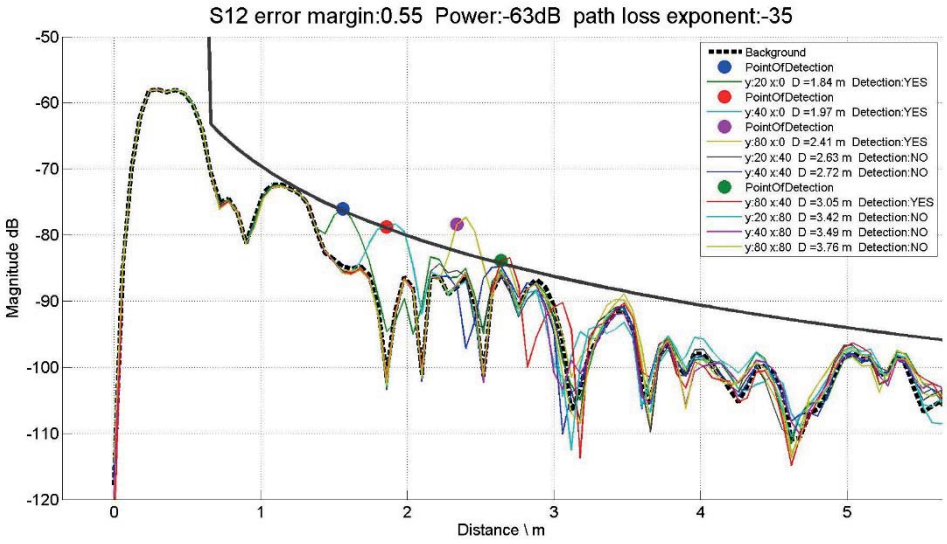

Figure 61: Antenna on car, 28 mm copper pipe, S12. 4 of 9 reflections were detected.

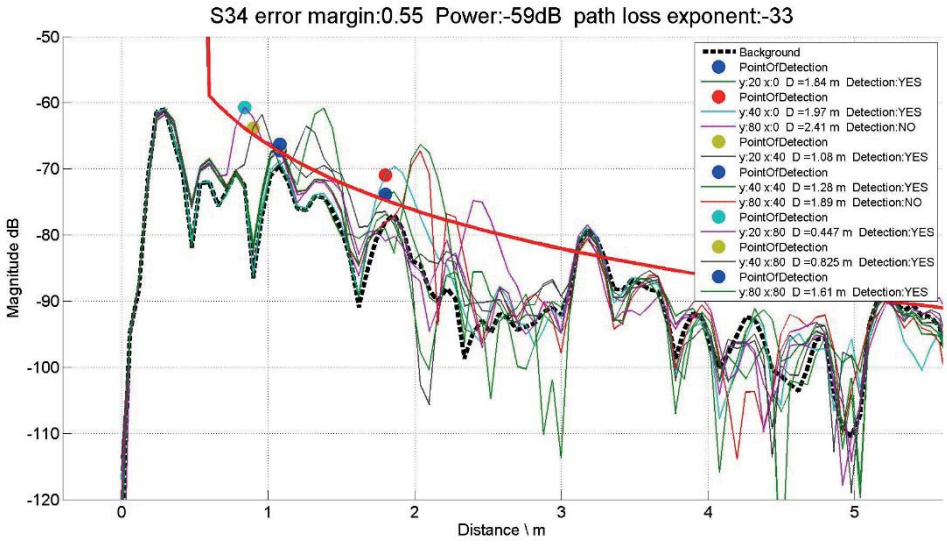

Figure 62: Antenna on car, 28 mm copper pipe, S34. 7 of 9 reflections were detected

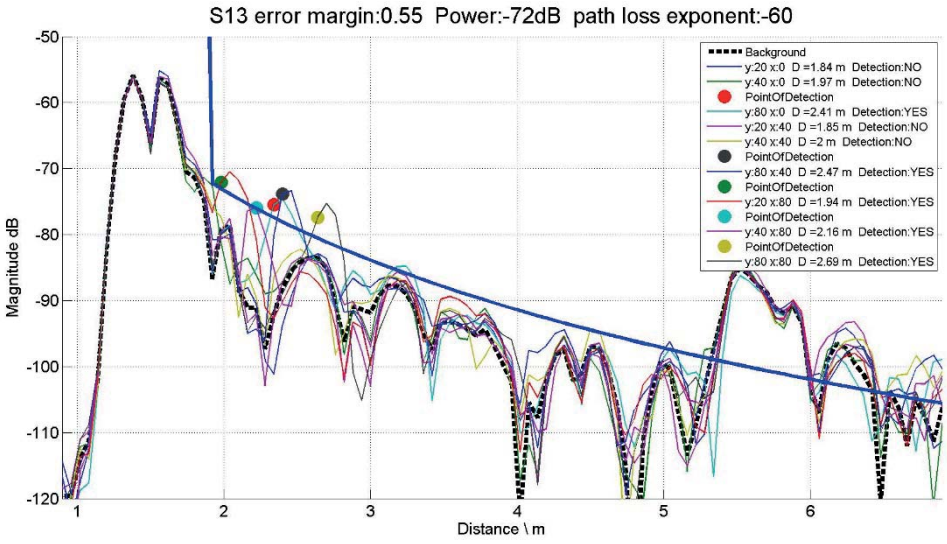

Figure 63: Antenna on car, 28 mm copper pipe, S13. 5 of 9 reflections were detected.

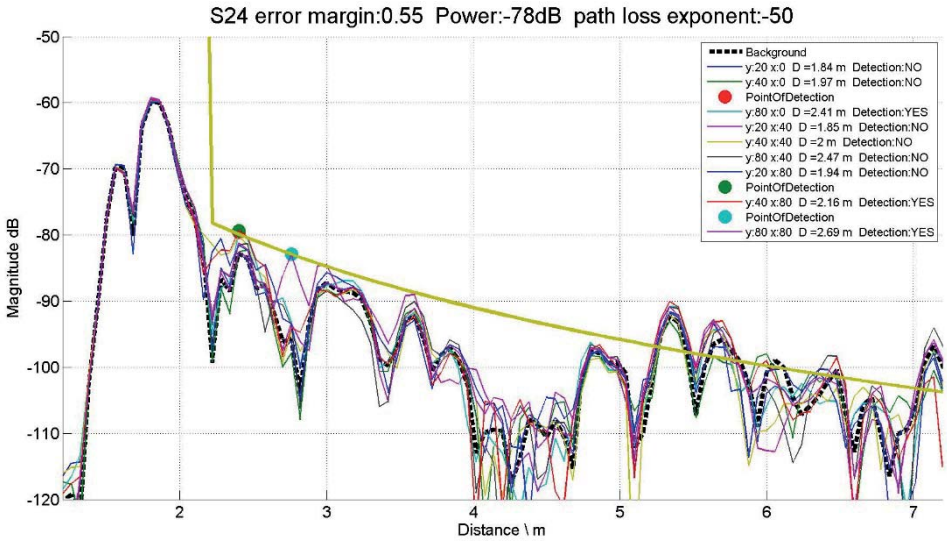

Figure 64: Antenna on car, 28 mm copper pipe, S24. 3 of 9 reflections were detected.

Conclusion for antennas on a car

The clutter level was significantly higher. Many reflections could not be detected any more. With results like that a technical realization in this way was not possible. If antennas with a better directivity would have been used, the clutter level would be significantly lower and detection might be possible.

In addition to this measurement more measurements, with disturbing objects outside the main lobe of the antenna, had been performed.

3.5.7 Measurement with large disturbing objects

The goal of this measurement was to verify the effect of objects with a large RCS which lie outside the main lobe of the antenna. This introduced additional problems to the already bad results from the previous measurement.

Measurement setup

The object used was a car door on a stand. The door was aligned in 3 different ways to rebuild situations which could appear in real life.

In the first situation the car door was positioned parallel to the car with 30-40 cm distance.

Figure 65: Setup with parallel car door at 30 - 40 cm distance

During the second situation the car door was positioned 45° inclined with approximately 50 cm distance to the right corner of the rear bumper.

Figure 66: Setup with 45° inclined car door at 50 cm distance

In the last situation the car door was positioned parallel to the car with only 20 cm distance.

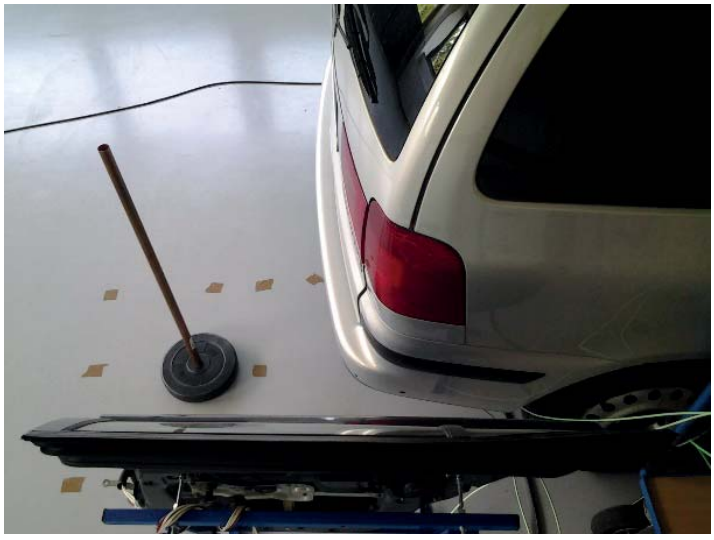

Figure 67: Setup with parallel car door at 20 cm distance

The rest of the measurement setup was the same as described at 3.5.6. The measurement procedure is also the same as described during the previous measurement.

Parallel door at 30 – 40 cm distance

These are the results for the situation described above.

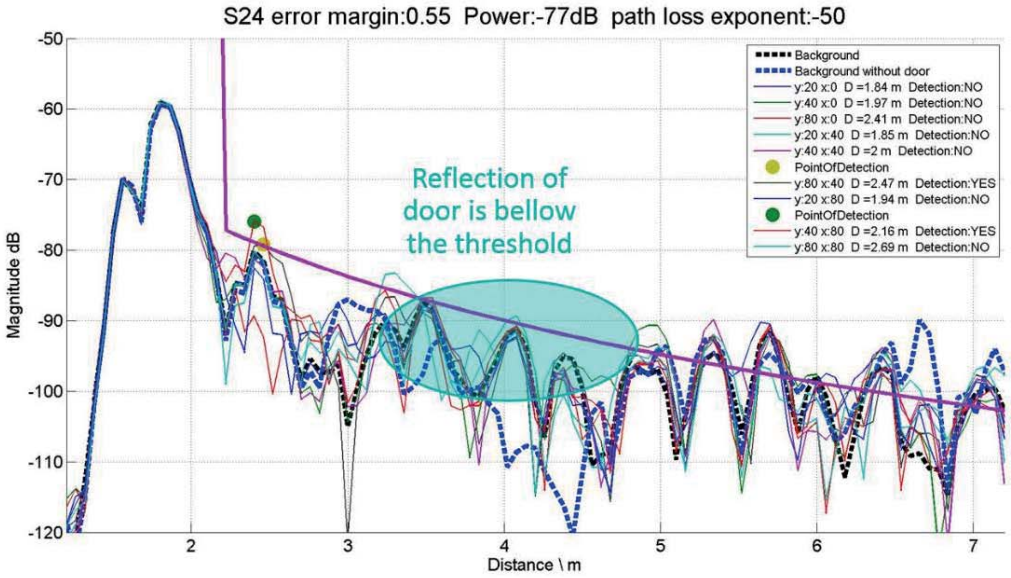

Figure 68: Parallel door at 30 - 40 cm distance, S24

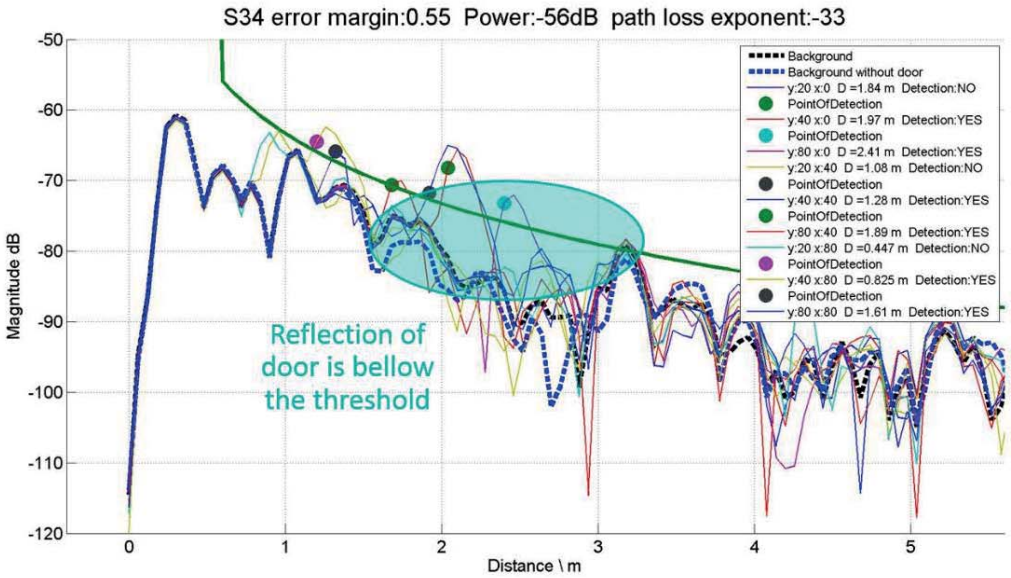

Figure 69: Parallel door at 30 - 40 cm distance, S34

The other S - parameters looked very similar to these, thus they are not shown here.

45° inclined door at 50 cm distance

The figures below show the results for the second situation described above.

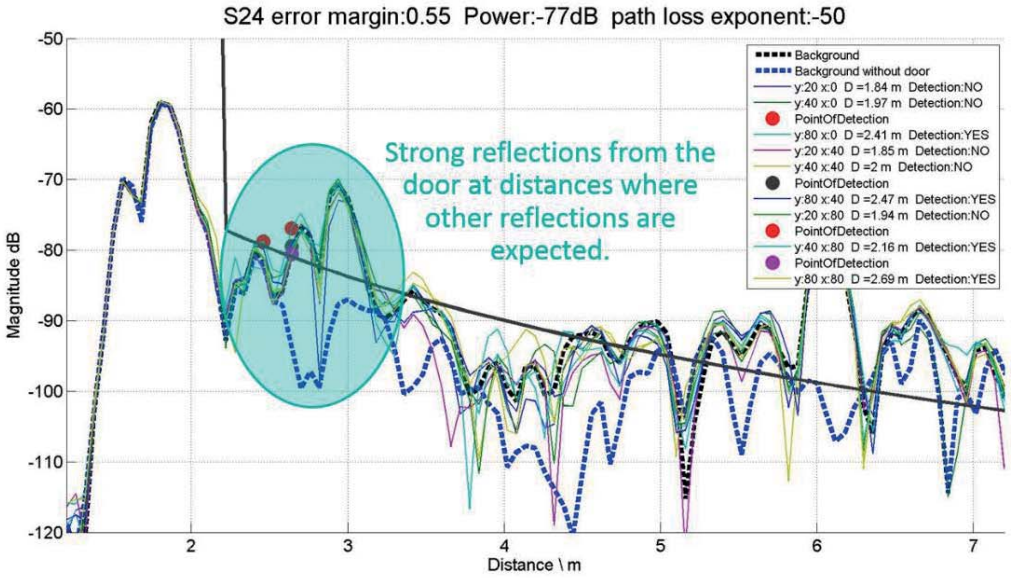

Figure 70: 45° inclined door at 50 cm distance, S24

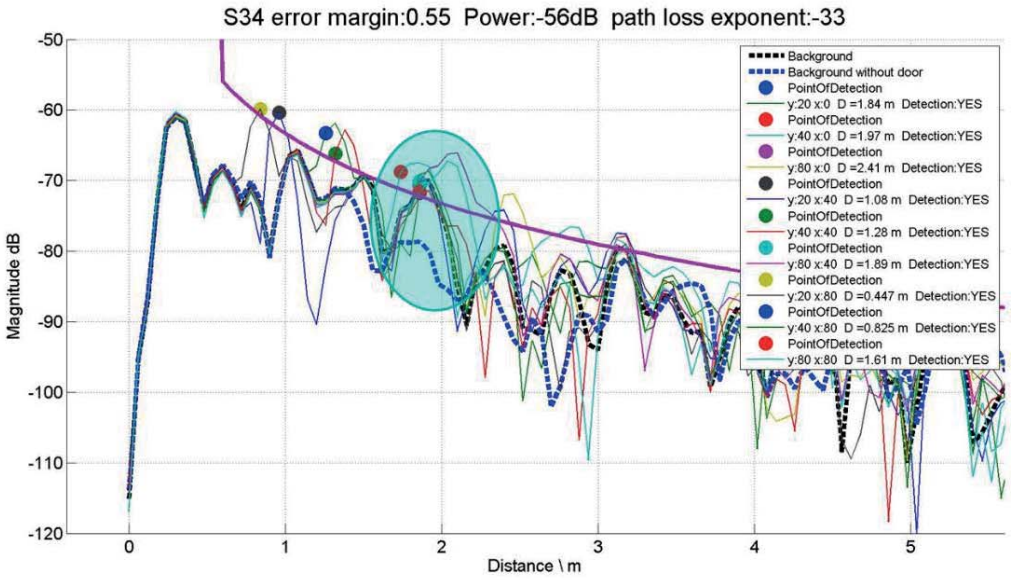

Figure 71: 45° inclined door at 50 cm distance, S34

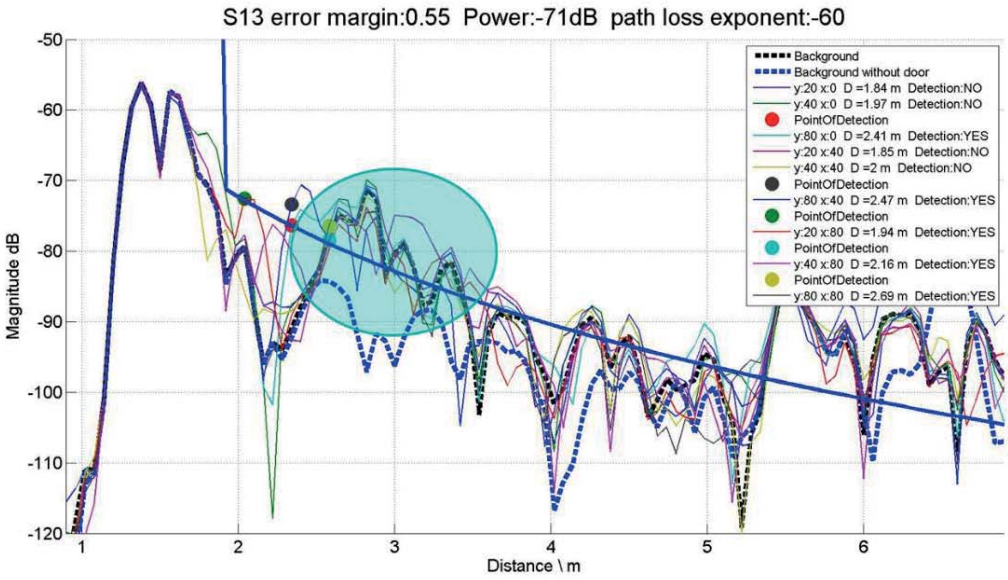

Figure 72: 45° inclined door at 50 cm distance, S13

Parallel door at 20 cm distance

Here the results for the third and last situation described above can be seen.

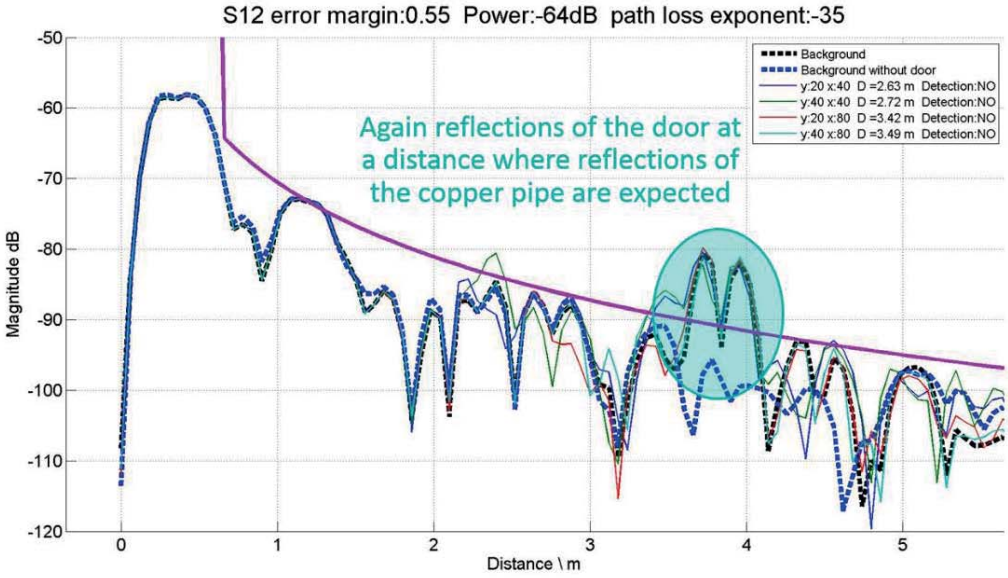

Figure 73: Parallel door at 20 cm distance, S12

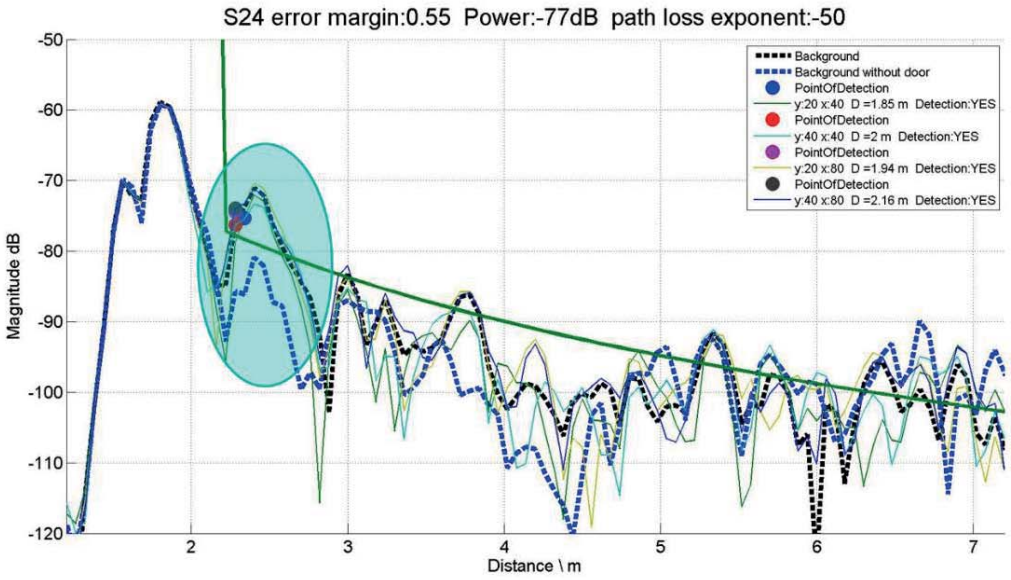

Figure 74: Parallel door at 20 cm distance, S24

Conclusion for disturbing objects

The Parallel door at 30 – 40 cm did not disturb the measurement because the reflections where below the threshold. But the inclined door and the parallel door at 20 cm distance heavily interfered with the reflections from our test object. A detection of the test object was impossible under these conditions.

3.6 Summarized results for parking aid

The first measurements showed that there was no significant difference between a concrete floor and grass. The magnitude of background reflections was approximately the same for grass and concrete.

Reflections from the test object mostly depended on distance to and size, shape and material of the target. The estimations made in chapter 2.7 proofed to be not accurate enough to calculate a link budget. They could only be used as an upper bound. This was because the RCS of objects declines for smaller distances if the object is in the near field region.

After a path loss model had been developed from the first measurements, grid measurements as described in 2.2.3 were carried out with different antenna

setups and test objects. The setup in which the antennas were not mounted onto the car worked quite well for the copper pipe, but could not detect the plastic pipe. Big problems arose once the antennas were mounted directly onto the car. The clutter level significantly increased due to the bad directivity of the antennas.

A second problem caused by the bad directivity of the antennas was demonstrated in 3.5.7. This time a car door has been placed beside the car at the same distance to the antennas as the test object. Despite the fact that the car door was positioned outside the main lobe of the antennas, reflections from it were much stronger than reflections from the test object, because its radar cross section was significantly higher. The only way to work around this problem, would have been to place more antennas spread over the rear bumper of the car, or use antennas with a better directivity.

The final conclusion of this part of this thesis is, that the used antennas were not suitable for a parking assistance system. UWB signals are also not suitable for detection of non-conducting materials like plastic. Another possible application was discussed in chapter 4 of this thesis.

4. Interior Surveillance

In this part of this master thesis, it was tried to implement a radar interior surveillance system for cars with antennas mounted on specific positions. Available positions were restricted because car manufacturers do not allow positioning of antennas at random locations because of cost reasons. Many different setups had been measured and the best performing setups were compared and discussed more deeply.

4.1 Simple solution – Intrusion detection

Most already used radar systems use 1 or two antennas which lie in the middle of the passenger cabin. Then they measure continuously and check if something has changes within a given distance. The distance threshold is then chosen such, that the alarm is only raised if a change is detected inside the car. A setup like this was also tested with 3 antennas at

- The gear leaver
- Under the rear passenger seats
- At the middle mirror

and it worked quite good, except some blind spots at the edges and rear section of the car. This can be seen in Figure 75. The big advantage of this setup was, that the distance threshold could be chosen such that all ellipsoids which formed the Fresnel Zones of the antenna pairs, lay inside the car. Therefore, no false alarms where produced with this setup. Why the covered volume had the form of ellipsoids is described more detailed in chapter 4.2. The downside of this setup was that the used antenna positions are very impractical for antenna mounting. Furthermore, it was not possible to exactly determine where the intrusion had happened. To solve these problems a more sophisticated approach had to be considered. An approach where the intrusion could be located and more practical antenna positions could be used.

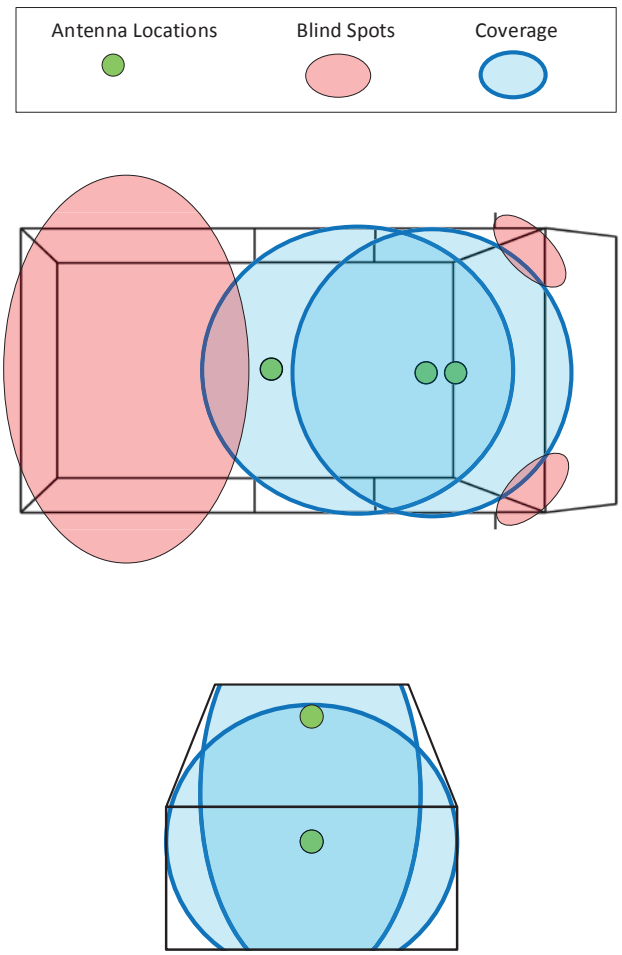

Figure 75: Simple solution coverage

4.2 Intrusion localization

In order to overcome the disadvantages described in 4.1 an algorithm for the localization of an intruder was developed. How this algorithm worked is described in this section.

First the impulse responses of all antennas and between all antennas were measured. This was done like discussed in chapter 0. After this the test object or person entered the measurement setup. Then again all impulse responses were measured. Now we had the background impulse response and the test case impulse response.

In the next step the difference of each impulse response pair was calculated. If the difference of the impulse responses exceeded a certain threshold, the first

time at which the threshold was exceeded, was the detection time for this impulse response. The reason why only the first time was considered, was the heavy multipath propagation inside a car. Each S-parameter corresponded to one or a pair of antennas.

To model the maximum sensitivity of our receiver all values of the impulse response below -88 dB were set to -88 dB.

Which different values for the threshold could be chosen and how they affect the performance of the system was discussed later in chapter 4.5.1.

In the example shown in Figure 76 the detected distance of this parameter would be 3.6 m. This distance d was used below to calculate an ellipsoid of possible points.

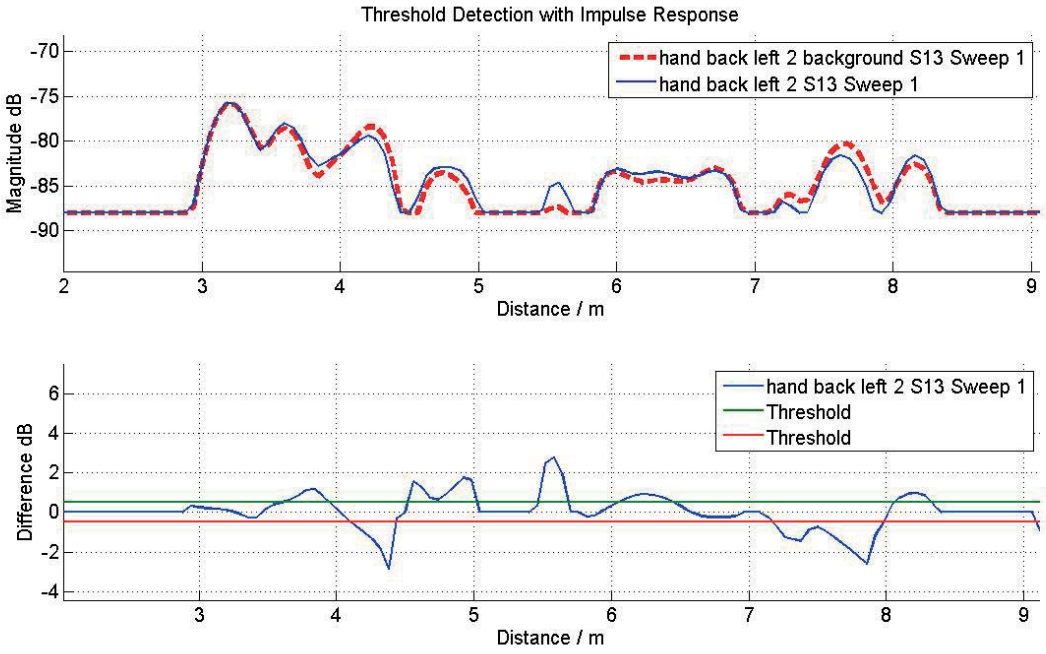

Figure 76: Threshold detection with impulse response

In order to calculate an ellipsoid its 2 focal points were needed. Its focal points were exactly at the antenna positions. Therefore, a global coordinate system and coordinates of each antenna were needed.

Like known from the Fresnel zones, each reflecting point with the same time delay from one antenna to the other, lies on an ellipsoid. If you multiply the detection

time with the speed of light, you get the distance d, which this specific reflection had travelled from one antenna to the other.

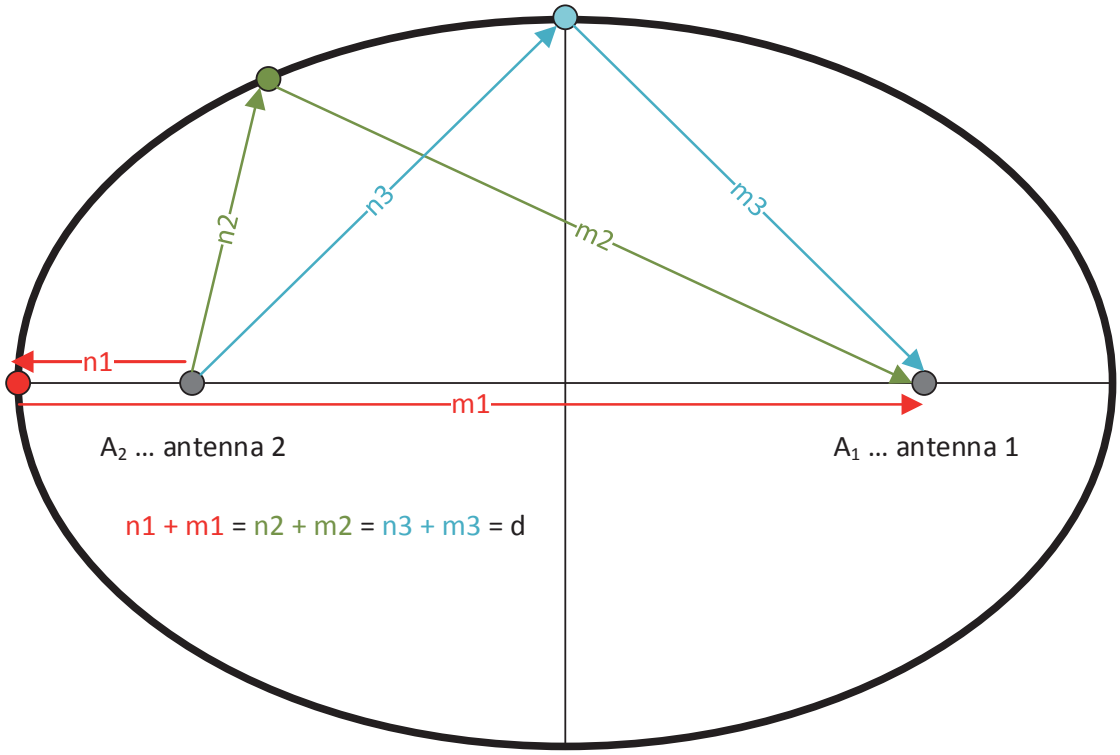

Figure 77: Possible paths between two focal points in an ellipsoid

Because the equations of an ellipsoid assume that the origin of the coordinate system lies in the centre of the ellipsoid and the long half axis lies in direction of the z-axis, a transformation matrix was needed to transform a point in the global coordinate system E to the local coordinate system B of each ellipsoid.

The following steps had to be performed to create a transformation matrix for each ellipsoid.

Determine the base vectors of the global coordinate system.

$$E = \begin{pmatrix} 1 & 0 & 0 \\ 0 & 1 & 0 \\ 0 & 0 & 1 \end{pmatrix}$$

Equation 4.1

The z-axis of the local coordinate system B had to lie in direction between the two focal points of the ellipsoid. Equation 4.2 and Figure 78 show how the first vector of B could be obtained.

$$\overrightarrow{z_0} = \vec{A}_1 - \vec{A}_2$$

Equation 4.2

$$\vec{b}_3 = \frac{\vec{z}_0}{\|\vec{z}_0\|}$$

Equation 4.3

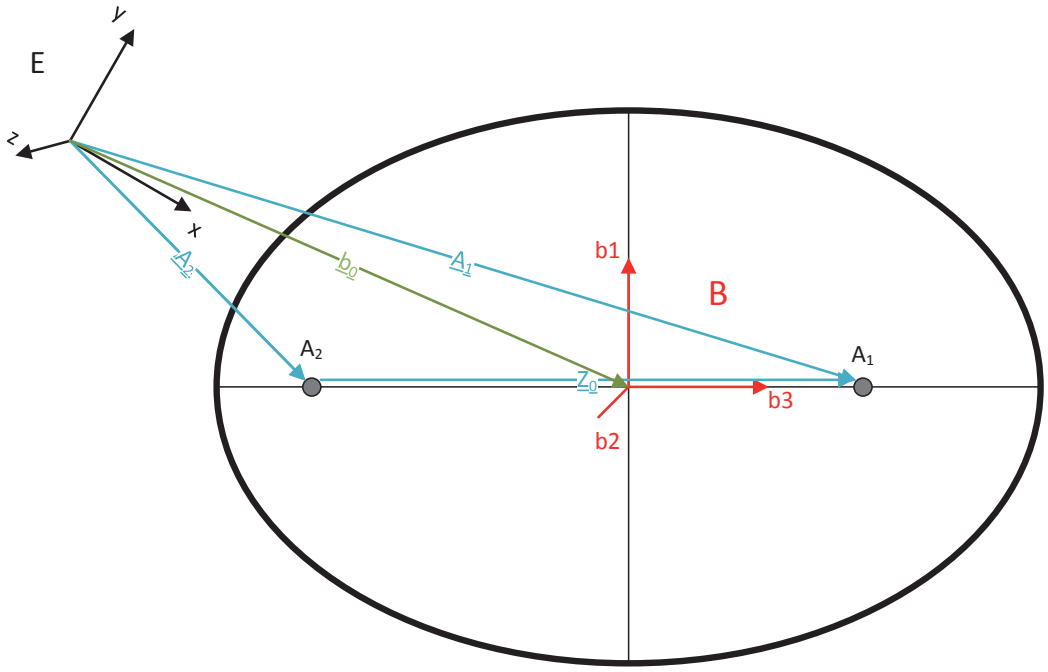

Figure 78: Obtaining first vector of local coordinate system B

With Gramschidt orthogonalization, the 3 base vectors of the local coordinate system could then be determined using the first one. Because the ellipsoid was rotationally symmetrical, the directions of the remaining 2 base vectors were not important, as long as all 3 base vectors were orthogonal to each other. With these

3 base vectors the base of the local coordinate system could then be written as described in Equation 4.4.

$$B = [\vec{b}_1 \quad \vec{b}_2 \quad \vec{b}_3] \qquad \textit{Equation 4.4}$$

For additional information about the use of Gramschmidt orthogonalization please have a look at the appendix at chapter A.

The transformation matrix for the rotation of the coordinate system then looked like:

$$T = B * E \qquad \textit{Equation 4.5}$$

For a complete transformation of the coordinate system, rotation was not enough. As shown in Figure 78, also the origin of the coordinate system needed to be moved to the origin of the ellipsoid. The origin of the ellipsoid was in the middle between the two focal points. The vector for movement of the origin could be calculated like this:

$$\vec{b}_0 = \vec{A}_2 + \frac{\vec{z}_0}{2} \qquad \textit{Equation 4.6}$$

With the detection time d and coordinates of the two focal points, the geometrical values of an ellipsoid could be determined as shown below.

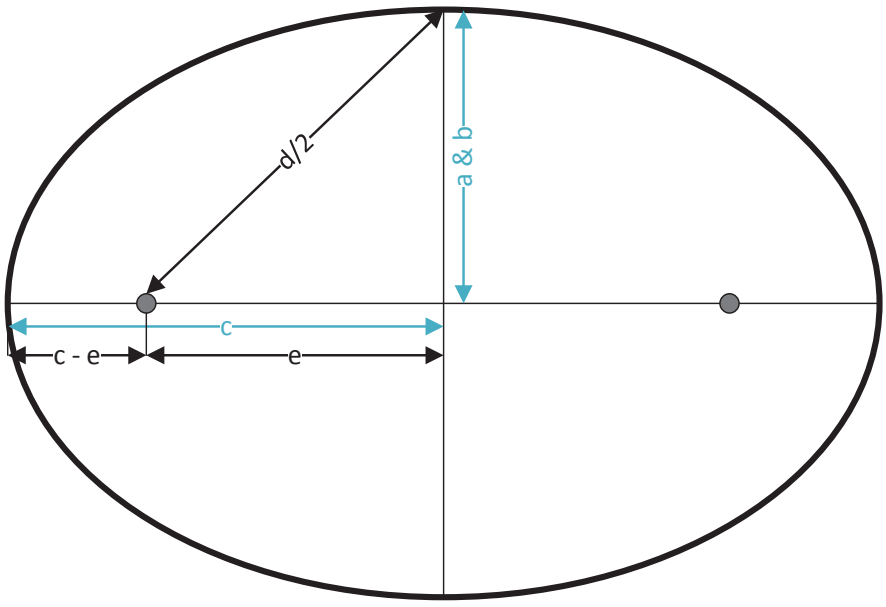

Figure 79: Geometrical relations of a rotationally symmetrical ellipsoid

$$e = \frac{norm(\vec{z}_0)}{2}$$ *Equation 4.7*

$$a = b = \sqrt{({}^{d}/_{2})^2 - e^2}$$ *Equation 4.8*

$$c = {}^{d}/_{2}$$ *Equation 4.9*

4.2.1 Cost function

The cost function J(x) which had to be optimized was a 3 - dimensional function. The arguments of this function were the Cartesian coordinates of the global coordinate system.

$$\vec{x} = \begin{bmatrix} x \\ y \\ z \end{bmatrix}$$ *Equation 4.10*

The values of the function for each $\vec{x}$ was calculated as follows:

$$\vec{x}_{local} = T\ (\vec{x} - \vec{b}_0)$$ *Equation 4.11*

For finding the point on an ellipsoid which was closest to a given other point, a self-written iterative algorithm was used. The algorithm worked like described below. N denotes the number of iterations performed and i denotes the index of the current iteration.

$$\Delta\varphi = \frac{{}^{\pi}/_{2}}{2^N}$$

$$u = {}^{\pi}/_{2}$$

$$\varphi_i = \frac{\pi}{4\ i}$$

$$v = arc\ \tan(\frac{y_{local}}{x_{local}})$$ *Equation 4.12*

The first point on the ellipsoid was calculated with the formulas for an ellipsoid and the values mentioned above in Equation 4.12.

$$\hat{x} = a\ \sin(u)\ \cos(v)$$

$$\hat{y} = b\ \sin(u)\ \cos(v)$$

$$\hat{z} = c\ \cos(u)$$

$$\vec{q} = \begin{bmatrix} \hat{x} \\ \hat{y} \\ \hat{z} \end{bmatrix}$$ *Equation 4.13*

Then the distance from this point to the point provided by the optimization algorithm was calculated:

$$d = norm(\vec{x}_{local} - \vec{q})$$ *Equation 4.14*

The same steps were repeated for a slightly larger and smaller value of u.

$$\hat{x}_{plus} = a\ \sin(u + \Delta\varphi)\ \cos(v)$$

$$\hat{y}_{plus} = b\ \sin(u + \Delta\varphi)\ \cos(v)$$

$$\hat{z}_{plus} = c\ \cos(u + \Delta\varphi)$$

$$d_{plus} = norm(\vec{x}_{local} - \vec{q}_{plus})$$ *Equation 4.15*

$$\hat{x}_{minus} = a\ \sin(u - \Delta\varphi)\ \cos(v)$$

$$\hat{y}_{minus} = b\ \sin(u - \Delta\varphi)\ \cos(v)$$

$$\hat{z}_{minus} = c\ \cos(u - \Delta\varphi)$$

$$d_{minus} = norm(\vec{x}_{local} - \vec{q}_{minus})$$ *Equation 4.16*

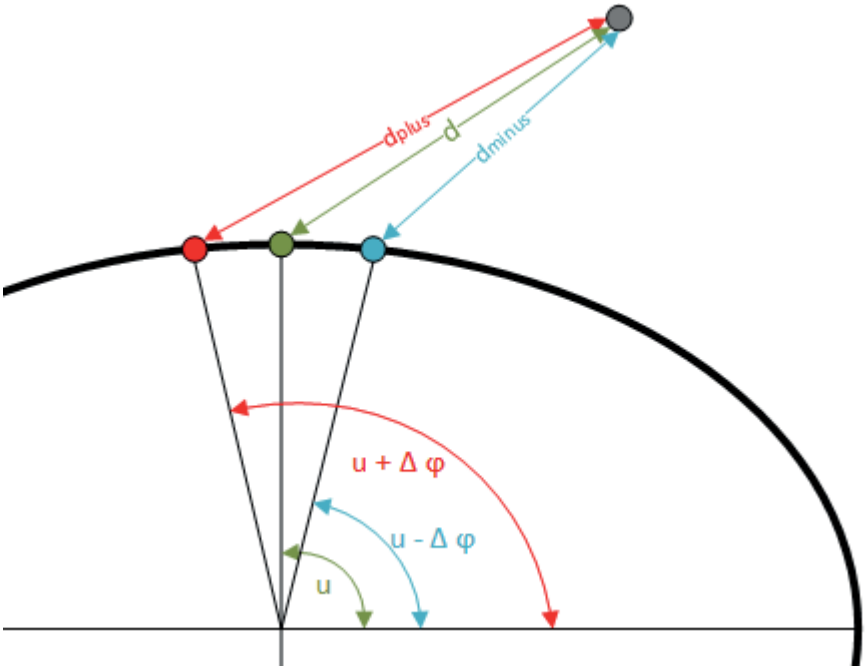

Figure 80: Explanation of iterative algorithm for point detection on an ellipsoid

If $d_{minus} < d_{plus}$ then u is changed by $u = u - \varphi_i$

If $d_{minus} > d_{plus}$ then u is changed by $u = u + \varphi_i$

But if $d < d_{minus}$ & $d < d_{plus}$ the iteration algorithm was aborted, because the best possible result had already been found. The coordinates which corresponded to the smallest remaining d, were the coordinates of the point on the ellipsoid with the smallest distance to the analysed point. These steps had to be performed for all ellipsoids and for every ellipsoid one smallest distance remained. To get one value as a result, all distances were combined with a weighting matrix like shown in Equation 4.17. This matrix was a diagonal matrix. How the values of this matrix were chosen was discussed later in chapter 4.5.2. Figure 81 summarizes the previously described steps.

$$D(x,y,z) = [d_1(x,y,z) \quad d_2(x,y,z) \quad \cdots \quad d_n(x,y,z)]$$

$$J(x,y,z) = (D * W * D^T) \Big/ \sum_i w_i \qquad \textit{Equation 4.17}$$

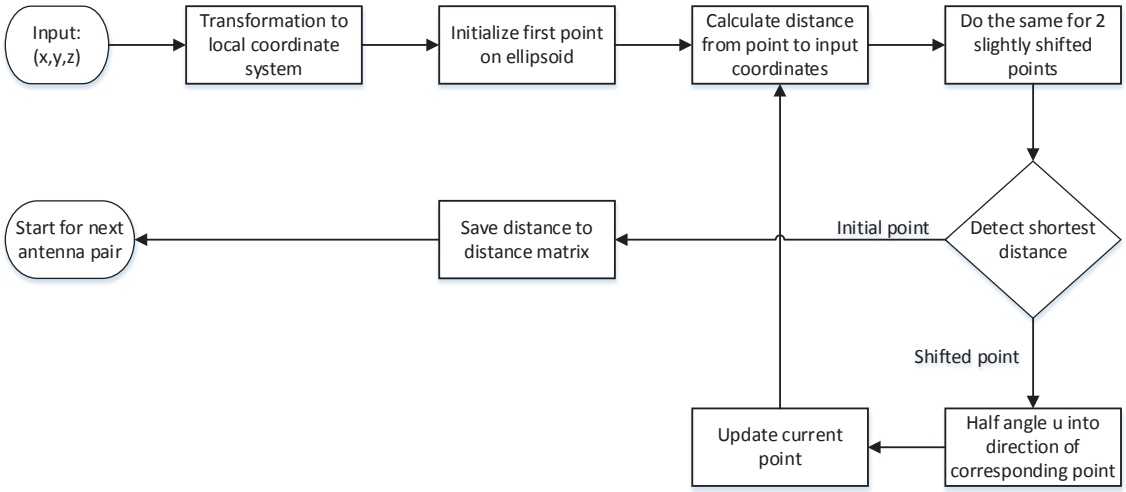

Figure 81: Steps for finding shortest distance from an ellipsoid to any point.

4.2.2 Estimation with fmincon (Matlab)

The goal was to find the minimum of the cost function J(x,y,z). For this purpose the optimization function fmincon of Matlab was used to find the coordinates, which resulted in the smallest weighted distance to all analysed ellipsoids. For equal weighting the detected point was the point with the least squared error. Fmincon was configured to use an interior point optimization algorithm for this task. A possible outcome could look like the figure below.

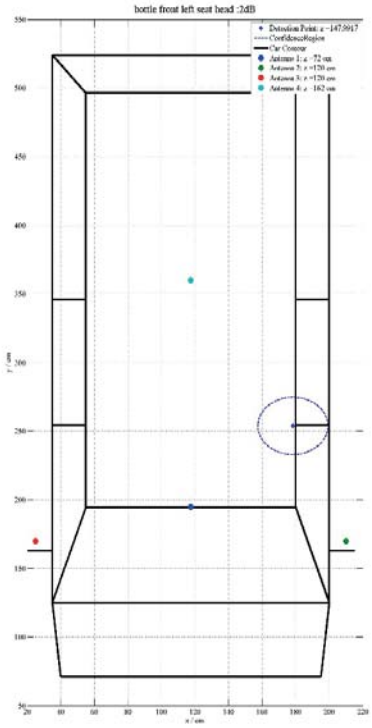

Figure 82: Possible outcome of position estimation

The radius of the circle marked as confidence region, was calculated by the square root of the return value of J(x,y,z). A larger circle means larger average error distances on ellipsoids. The circle was not an area where the real test object had to be, it just visualized how good all the ellipsoids met at one point. All steps needed to find a point are summarized below in Figure 83.

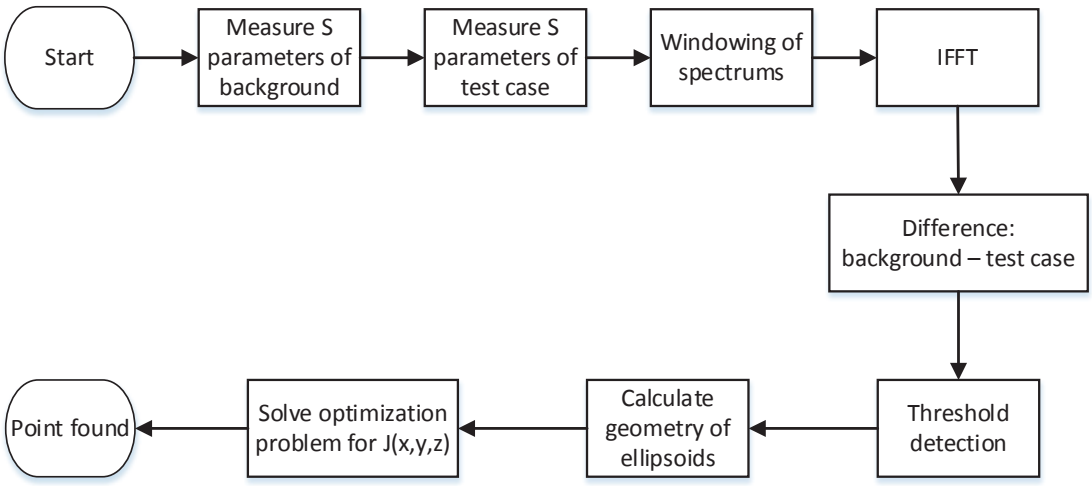

Figure 83: Working steps performed to localize an intruder

4.2.3 Estimation with a Particle Filter

Because the interior point optimization algorithm, used with the fmincon optimization function of Matlab, was rather complex, a self-written particle filter was also used to solve this optimization problem.

A particle filter was used because it could not be assumed that the probability distribution of the cost function was Gaussian. Therefore a Kalman Filter was not appropriate. A particle filter might also be scaled easily in terms of computational complexity, by increasing or decreasing the number of used particles. Also the implementation in C / C++ would have been very straight forward.

Furthermore, a particle filter provides information about the shape of the probability density function and therefore its variance. This additional information might be used to reduce the falls alarm rate.

Implementation of Particle Filter

The implementation of a Particle Filter can generally be described in the following steps.

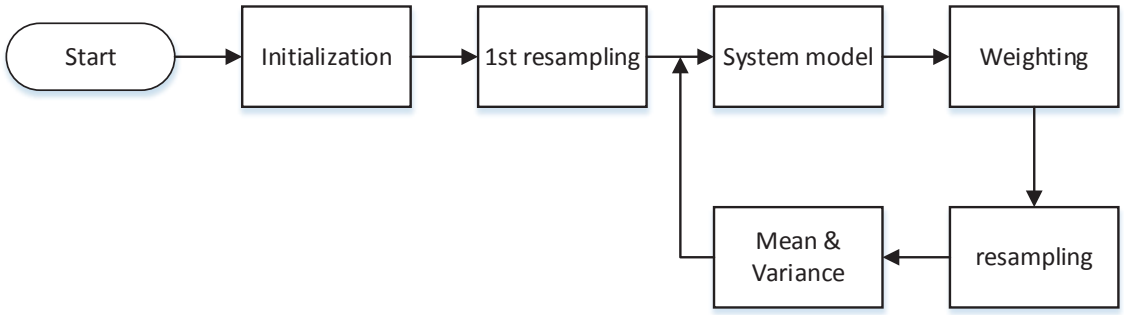

Figure 84: Steps of a particle filter

Information about design of particle filters was taken from [20], [21] and [22].

Initialization of particles equally distributed based on prior knowledge

In our case this meant that we put particles equally spaced inside the car and some region around the car. The size of the volume and space between each initial particle determined the number of particles, and therefore the computational complexity. A compromise between accurate approximation of the probability density function and computational complexity needed to be found.

During initialization the particles were also weighted for the first time. For weighting the same cost function J(x) was used as it was described in 4.2.1. But for further use the output of this cost function needed to be scaled somehow to a region of $w(i) \in [0, \dots, 1]$. Why this needed to be done can be seen during the resampling step. For scaling the output of the cost function was used in an exponential function as shown in Equation 4.18 below. It is obvious that a higher squared error means a lower weight of the particle. It also has to be noticed that by the use of this nonlinear function the type of the probability density function (PDF) is changed. This means that the PDF of w has a different type as the PDF of the cost function. However, if the values of the cost function do not differ much from each other, this nonlinearity should not be too big.

$$w(i) = e^{-\alpha J(\vec{x}_i)} \qquad \textit{Equation 4.18}$$

$J(\vec{x}_i)$ … Cost function output for given input vector $\vec{x}_i$
α … Exponential scaling factor used to tune rejection rate of particles
$\vec{x}_i$ … Parameter vector with coordinates of a particle
$w(i)$ … Weight of a particle
i … Index of a particle. $i \in [1, \dots, N]$ if N denotes the total number of particles.

Resampling of particles

In a particle filter the weight of a particle needs to be multiplied with the new weight of this particle in each iteration. This results in numerical problems for very low weights. Therefore a resampling of particles needs to be done. In this way the probability distribution is not given by different weighted equally spaced particles, but by equally weighted particles.

The important thing about resampling is that particles with a low probability need to have a lower chance to survive than particles with a high probability. The deterministic approach to just remove the M particles with the lowest probability shall not be used, instead a probabilistic approach shall be used. In this way also small particles have a chance to survive. The easiest way to do this, is to remove a particle if Equation 4.19 is fulfilled. Notice that for each w(i) a new realization of X is needed. To reduce computational complexity a lookup table might be used.

$$w(i) < X \quad for \;\; X \sim U(0 \ldots 1) \qquad \textit{Equation 4.19}$$

Now it is clear why all weights have been scaled to a range of 0…1. In this way a simple comparison with a uniformly distributed random variable can be applied to sort out particles with low weights by use of a probabilistic approach.

The only problem is that we are reducing the number of particles during each iteration. Therefore, we need another step during resampling where we “split” particles with a high weight to get again the original number of particles. There are many different methods to do this splitting. Either by again using a statistical approach or by a deterministic one. In this case, we decided to use a deterministic approach, by always splitting the largest particle into two particles with half the weight, but same coordinates. This has to be done in a loop until the number of particles matches the original number of particles N.

In order to reduce computational complexity again, the weight of each particle is assumed approximately the same. This simplifies the next weighting step by just using Equation 4.18 again, because old weights are assumed to be the same for all particles.

Applying System Model

In the next step of the particle filter the system model is incorporated. Because there is no information about how a detected object is supposed to move, just a random walk is used as system model.

$$\vec{x}_i[n+1] = \vec{x}_i[n] + \nu \qquad \textit{Equation 4.20}$$

v … process noise

The process noise describes the expectation of the uncertainty of the process. In our case it described how far a detected object could move between two measurements. For completeness it shall be noted that, because of the simple random walk model and the missing knowledge of the measurement noise, the measurement noise had already been incorporated into the process noise. Usually measurement and process noise have to be treated separately.

As shown in Figure 84 again a weighting and a resampling step are performed after this one.

Mean and variance calculation

The last step, before the iteration starts again with the system model step, is the calculation of mean value and variance. Because the weight of all particles is assumed to be the same after the resampling step, the mean value can easily be calculated with the Matlab function mean(), which behaves like shown in Equation 4.21. Also the variance can be calculated with the Matlab function var() which performs the calculation like shown in Equation 4.22 [23].

$$\underline{\hat{\mu}} = \frac{1}{N}\sum_{i=1}^{N}\vec{x}_i \qquad \textit{Equation 4.21}$$

$$\underline{\hat{\sigma}}^2 = \frac{1}{N-1}\sum_{i=1}^{N}\left|\vec{x}_i - \underline{\hat{\mu}}\right|^2 \qquad \textit{Equation 4.22}$$

$\underline{\hat{\mu}} = \begin{bmatrix}\hat{\mu}_x \\ \hat{\mu}_y \\ \hat{\mu}_z\end{bmatrix}$ … Vector with estimated mean values of x, y and z coordinates

$\underline{\hat{\sigma}}^2 = \begin{bmatrix}\hat{\sigma}_x{}^2 \\ \hat{\sigma}_y{}^2 \\ \hat{\sigma}_z{}^2\end{bmatrix}$ … Vector with estimated variances for x, y and z coordinates

The estimated mean value and variance were stored to a trace vector for each iteration. In a real system each iteration would correspond to a new measurement. Therefore, the value of the cost function would change after each iteration. If a static setup was measured the process was stopped after the

position of the estimated point did not change more than 2 cm in 2 successive iterations.

4.3 Test setup

In order to produce comparable results with each of the different test setups, 17 test cases had been chosen. 8 of these test cases should have triggered an alarm, the remaining 9 should not have triggered an alarm.

Because the front window of the test car could not be opened, tests at the front section were made with a half-filled 1.5 litre bottle of water.

- Test case 1 – 6 is a person leaning at the car. The back of the person is touching a window.
- 8 and 7 is a person standing next to the car. The hip of the person is approximately 15 – 20 cm away from the car.
- 9 – 11 is a person reaching out into the car through the open window. The elbow is 10 cm above the lower window frame. The arm is inclined approximately 20° downwards.
- 12 – 14 is a person reaching down along the door. The elbow is at the same height as the lower window frame.
- 15 – 17 is a water bottle at the door latch, steering wheel and head rest.

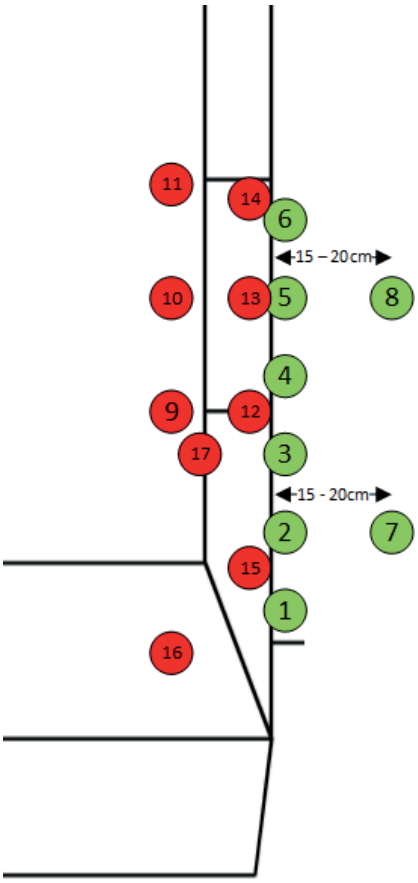

Figure 85: Test case positions

Figure 86: Photo of test case 15: door latch and 17: head rest

4.4 Antenna setups

Only 4 antennas could be used at the same time, because the network analyser only had 4 ports. This meant that a test setup could only have up to 4 antennas. 3 test setups with the best results, considering the restrictions from the communication systems, were analysed more detailed and compared to each other.

4.4.1 Antenna Setup 1

In this setup the antennas where mounted at the following positions.

- right side mirror
- left side mirror
- Where a shark – fin antenna would be mounted, in interior of the car.
- At position of the rear number plate, in interior of the car.

Figure 87: Antenna position - trunk middle

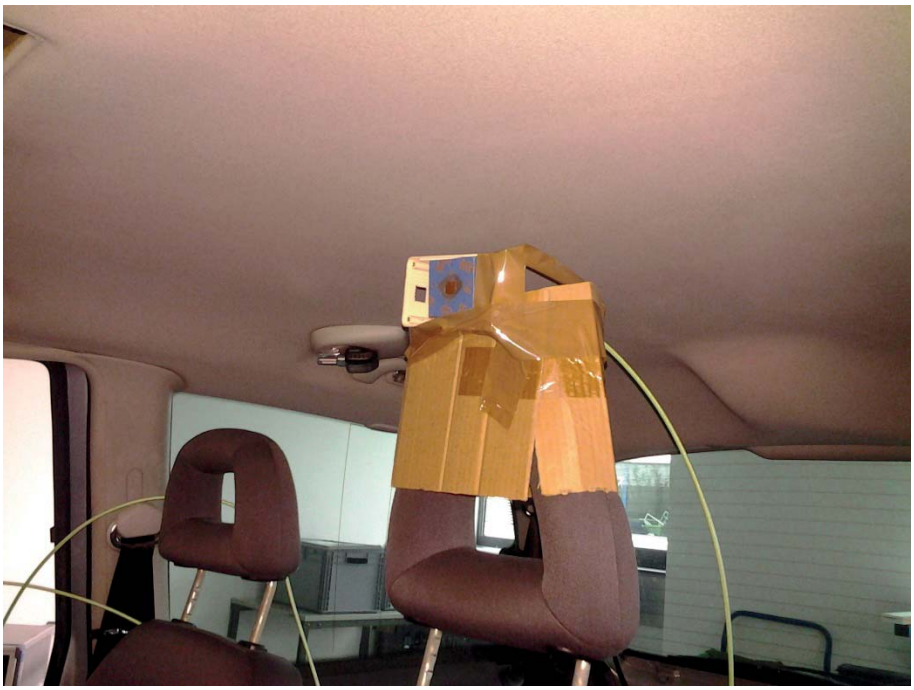

Figure 88: Antenna position - shark fin

Figure 89: Antenna position - left side mirror

4.4.2 Antenna Setup 2

In this setup the antennas where mounted at the following positions.

- in front of the gear stick
- at the rear view mirror
- Where a shark – fin antenna would be mounted, in interior of the car.
- At position of the rear number plate, in interior of the car.

Figure 90: Antenna position - in front of gear stick

Figure 91: Antenna position - at rear view mirror

4.4.3 Antenna Setup 3

In this setup the antennas where mounted at the following positions.

- right side mirror
- left side mirror
- Where a shark – fin antenna would be mounted, in interior of the car.
- in front of the gear stick

4.5 Parameters

Before results of different setups could be compared, the thresholds and weights needed to be determined. Therefore, different thresholds and weighting methods had been tested and compared. The bandwidth has been limited with a rectangular window in this chapter.

In chapter 5.5 a way to simulate many different setups was described. This allowed the use of a statistical approach to analyse the impact of different thresholds, weighting methods and bandwidths. Over 280 setups had been simulated and where then compared according to the corresponding parameter.

4.5.1 Threshold

The values which could be chosen as a threshold, were restricted by the minimum size of a quantization step of the used receiver. Thus, the minimum threshold for the used receiver was 2 – 3 dB. Tests showed that the threshold should be around 1 dB to deliver the best results.

Because of higher thresholds, weak reflections were not detected, therefore, detection accuracy was reduced. This can be clearly seen in Figure 93 below.

The x – axis of Figure 93 is the boundary offset. This denotes the position of the border for an alarm. If an object was detected within this border, the alarm was

triggered. An offset of 0 means that the boundary lay directly at the doors of the car.

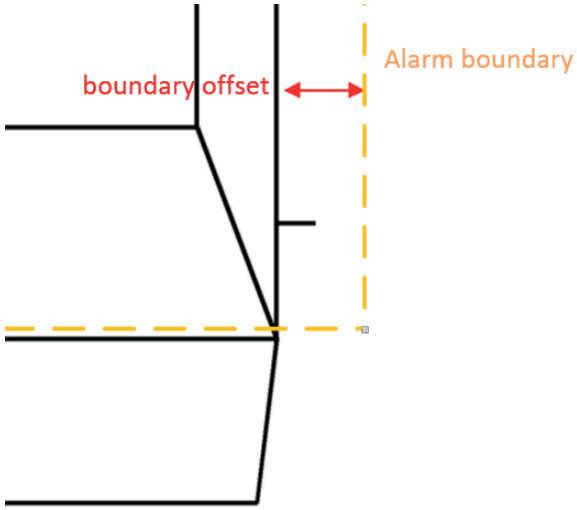

Figure 92: Explanation of boundary offset

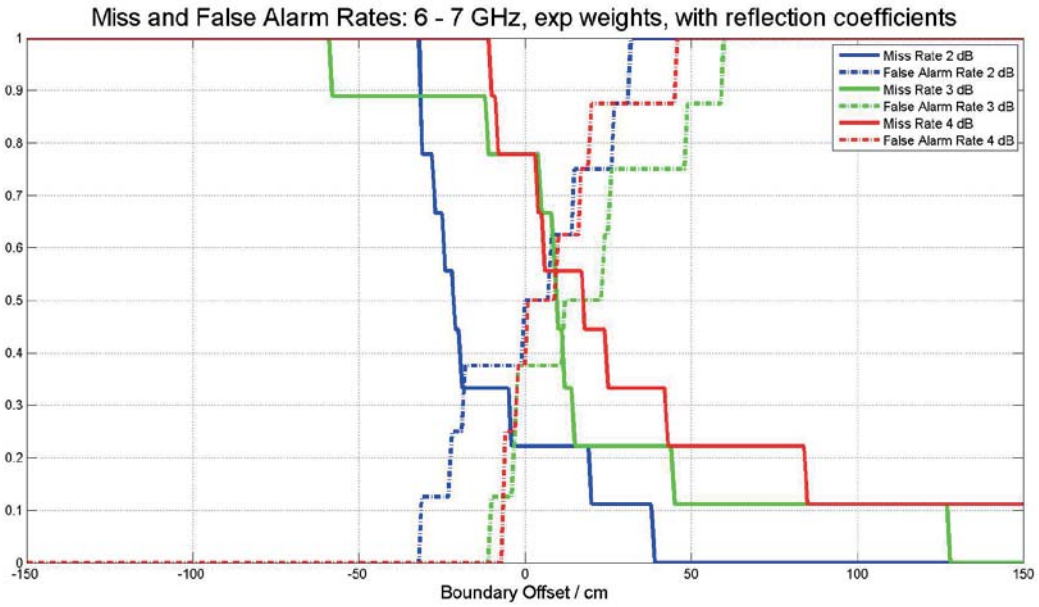

Figure 93: Miss and false alarm rate comparison for different thresholds. Antenna setup 1 at 6 – 7 GHz with reflection coefficients

In Figure 93 it can clearly be seen that for a given miss rate the false alarm rate was higher for a higher threshold. Also the location of the boundary, for a fixed miss rate, for triggering an alarm was shifted towards outside the car for a higher threshold. This result was the same for each of the 3 different setups.

Table 6 shows the impact of different thresholds onto the localization performance. d_x and d_y are the mean distance errors as described in chapter 5.5.1 Equation 5.1.

Table 6: Statistical analysis of different thresholds

	1dB	2dB	3dB
d_x [cm]	34.03	45.03	74.69
d_y [cm]	42.68	67.58	114.83

Table 6 shows clearly that higher thresholds directly impacted localization performance. It has to be said that all setups contributed to this result, even those which did not deliver the best results.

4.5.2 Weights

Choosing the right weights for different S – parameters was very important to achieve the best possible results. Suitable ways to determine these weights had to be found. Furthermore, different weighting methods needed to be compared in terms of performance.

Equal weights

The first and most intuitive step was to use equal weights. Equal weights had proven to deliver good results for nearly any antenna setup tested.

Exponentially decreasing weights

The second method which worked very well with most setups was the method of exponentially decreasing weights. In this method the weight of a parameter was decreased with larger detection distance. This means that detections which occurred closer to the line of sight were weighted more than those farther away.

$$w_i = e^{-\frac{d - \|\vec{z}_0\|}{\gamma}}$$

$$W = \begin{bmatrix} w_1 & 0 & \cdots & 0 \\ 0 & w_2 & & 0 \\ \vdots & & \ddots & \vdots \\ 0 & 0 & \cdots & w_n \end{bmatrix}$$

Equation 4.23

d and $\vec{z}_0$ are the detection distance and line of sight distance as shown in chapter 4.2. To prevent that detections from farther away are down weighted too much, γ was used to lessen the impact of the weighting. A value of $\gamma = 200$ prooved to work very well if d and $\vec{z}_0$ were given in cm.

Comparison of equal and exponential weighting methods

The same analysis done for the threshold was performed for different weighting methods to determine which one works better.

Setup 1

In Figure 94 and Figure 95 a big difference between exponential and equal weights can be seen. This was because with equal weights some detections occurred on totally wrong positions. That was why even for a large boundary offset the miss rate did not go to zero for higher thresholds. Also the false alarm rate should have gone to 1 for high boundary offsets, because of the test case positions mentioned in Figure 85. The equal weighting method had failed in these cases.

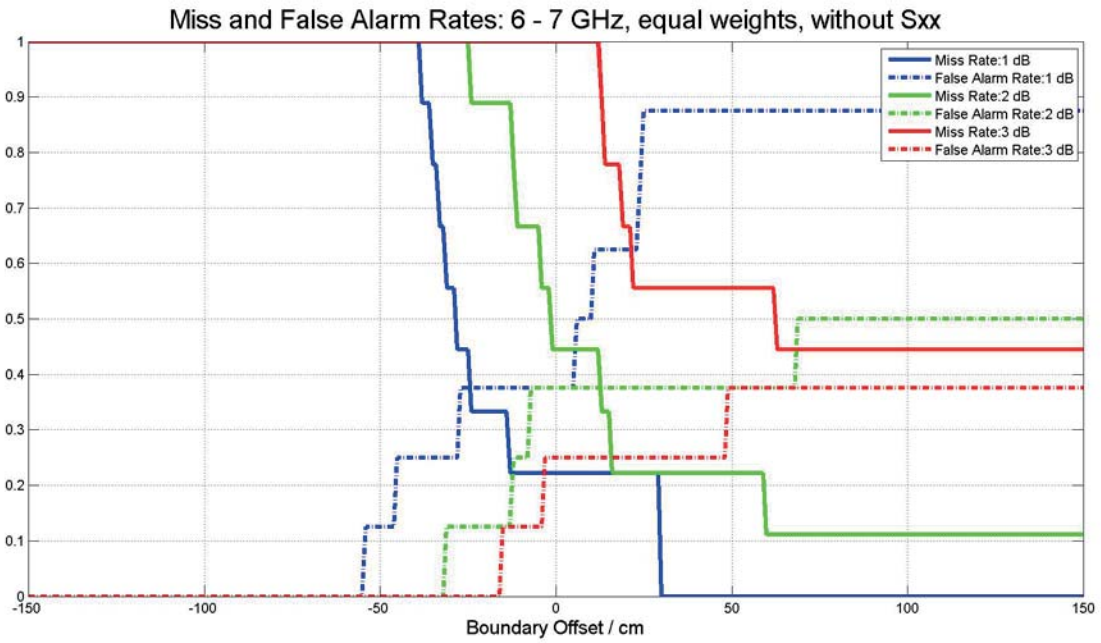

Figure 94: Weighting method comparison – Setup 1: 6 - 7 GHz, equal weights, without reflection coefficients

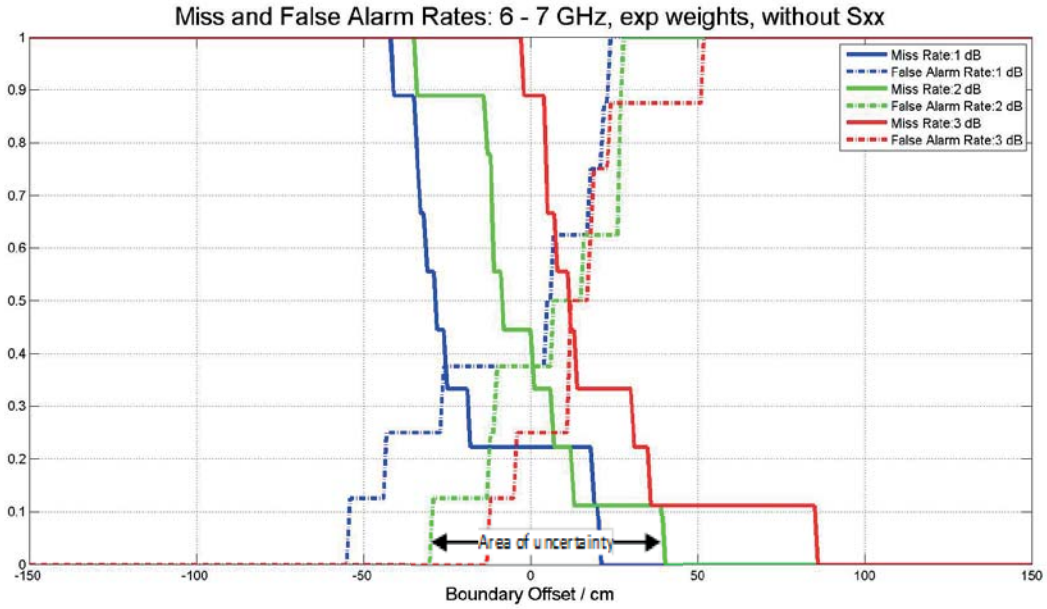

Figure 95: Weighting method comparison - Setup 1: 6 - 7 GHz, exp weights, without reflection coefficients

Setup 2

As shown below in Figure 96 and Figure 97 the exponential weighting method behaved a little better in the marked area. In the remaining areas the results were nearly the same.

In both cases the performance of this setup did not look very good. The same problem of totally wrong detections, as described in setup 1, here arises for both weighting methods.

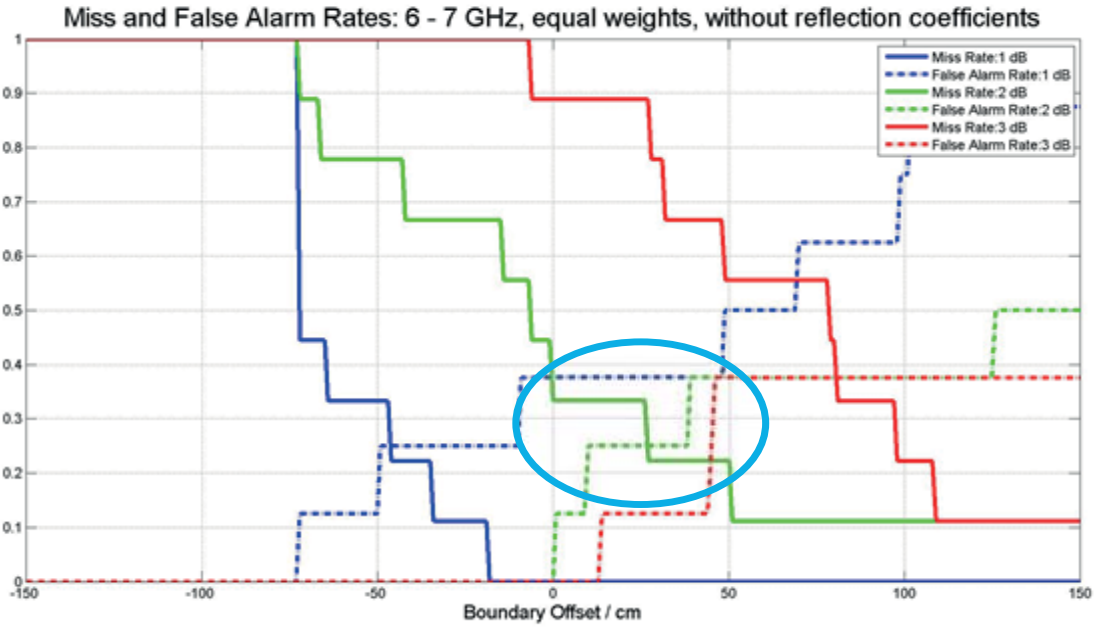

Figure 96: Weighting method comparison – Setup 2: 6 - 7 GHz, equal weights, without reflection coefficients

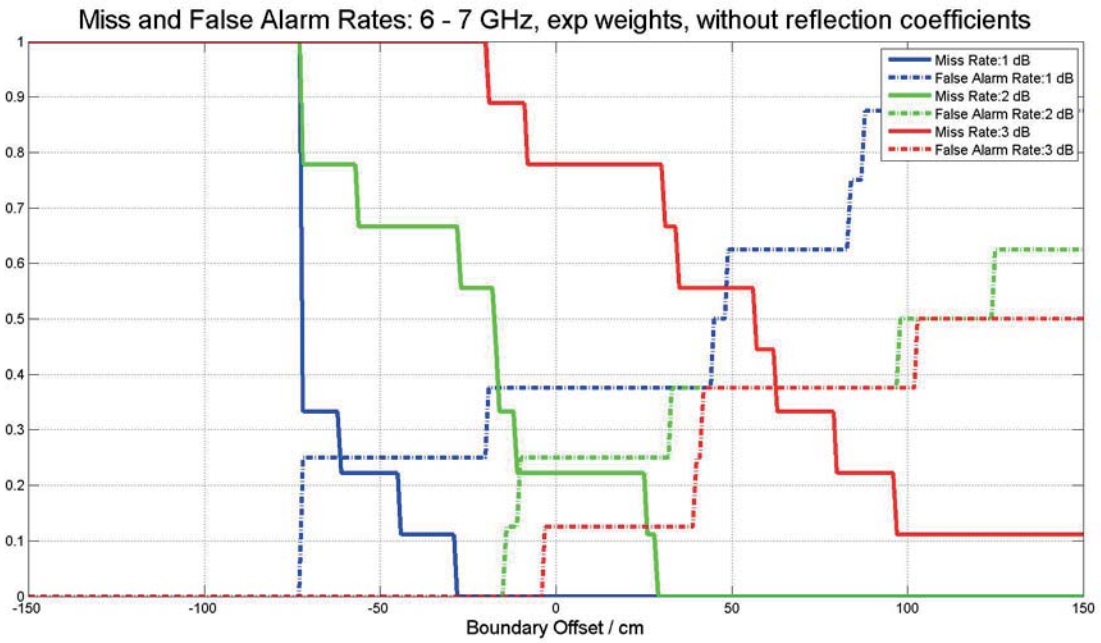

Figure 97: Weighting method comparison - Setup 2: 6 - 7 GHz, exp weights, without reflection coefficients

Setup 3

Here again the method with equal weights produced errors like described in setup 1.

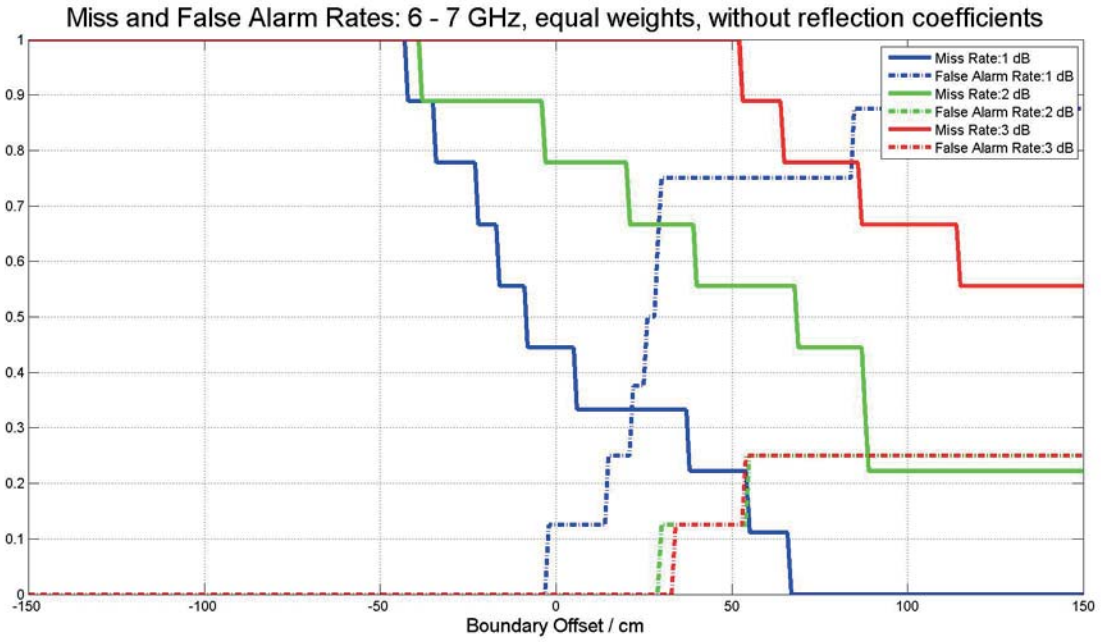

Figure 98: Weighting method comparison - Setup 3: 6 - 7 GHz, equal weights, without reflection coefficients

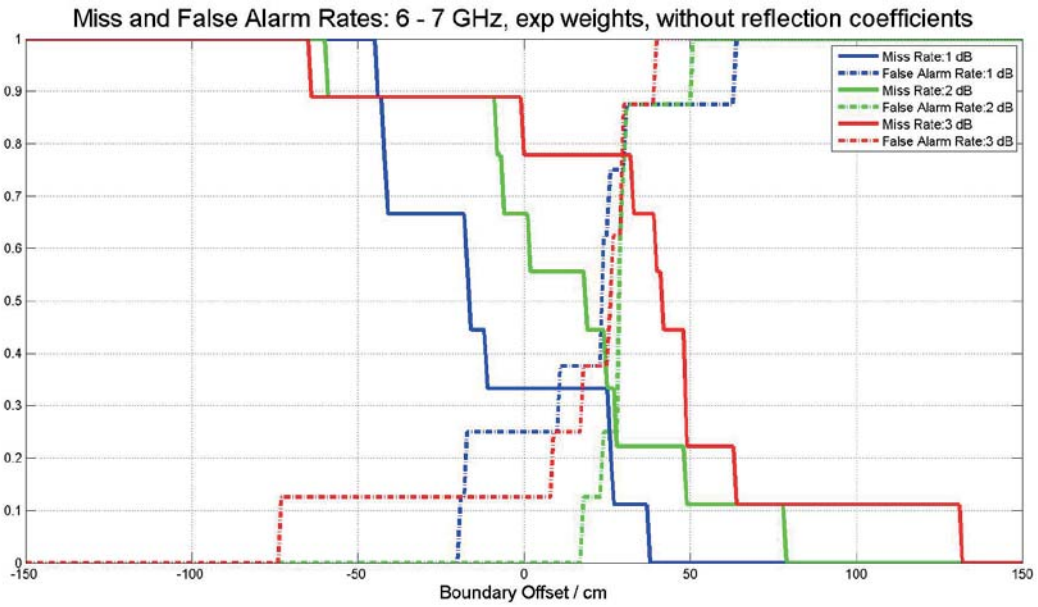

Figure 99: Weighting method comparison - Setup 3: 6 - 7 GHz, exp weights, without reflection coefficients

The same statistical analysis used for different thresholds in Table 6 was also conducted for weighting schemes.

Table 7: Statistical Analysis of different weighting methods

	Equal Weights	Exp. Weights
d_x [cm]	61.40	37.93
d_y [cm]	94.38	47.85

Conclusion about weights

The equal and exponential weighting method only produced similar results for a threshold of 1 dB. For larger thresholds the exponential weighting method worked better most of the time, because the equal weighting method often totally failed.

4.5.3 Frequency range

The frequency range of 3 – 8 GHz used by the network analyser did not match the frequency range of the used transmit pulses. Thus, the spectrum needed to be modified to model the characteristics of the system.

Because the exact spectrum of the transmit pulse was unknown, the spectrum was modified such, that magnitude values outside of the analysed spectrum were dampened to -120 dB with a rectangular window.

Later in chapter 5.5 it was also tried to use a Gaussian window, but the results were worse than the results with a rectangular window.

How the different windows look in time domain is visualized in Figure 100. In can be seen that for the Gaussian windows the main lobe of the pulse in time domain is significantly wider than for the rectangular window. The side lobes of the rectangular window are low enough to not significantly impact the measurement results.

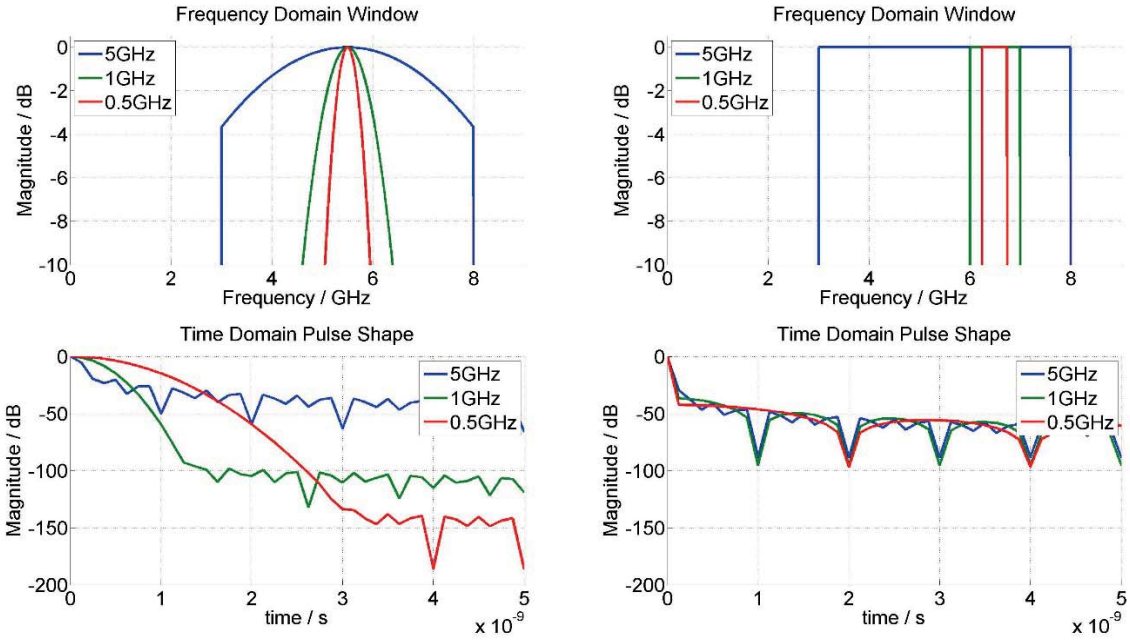

Figure 100: Comparison of different windows for IFFT

These are the different frequency ranges which were analysed.

- 3 – 8 GHz
- 6 – 7 GHz
- 6 – 6.5 GHz

With reduction to bandwidth the results got worse. This can be seen in Figure 101 below.

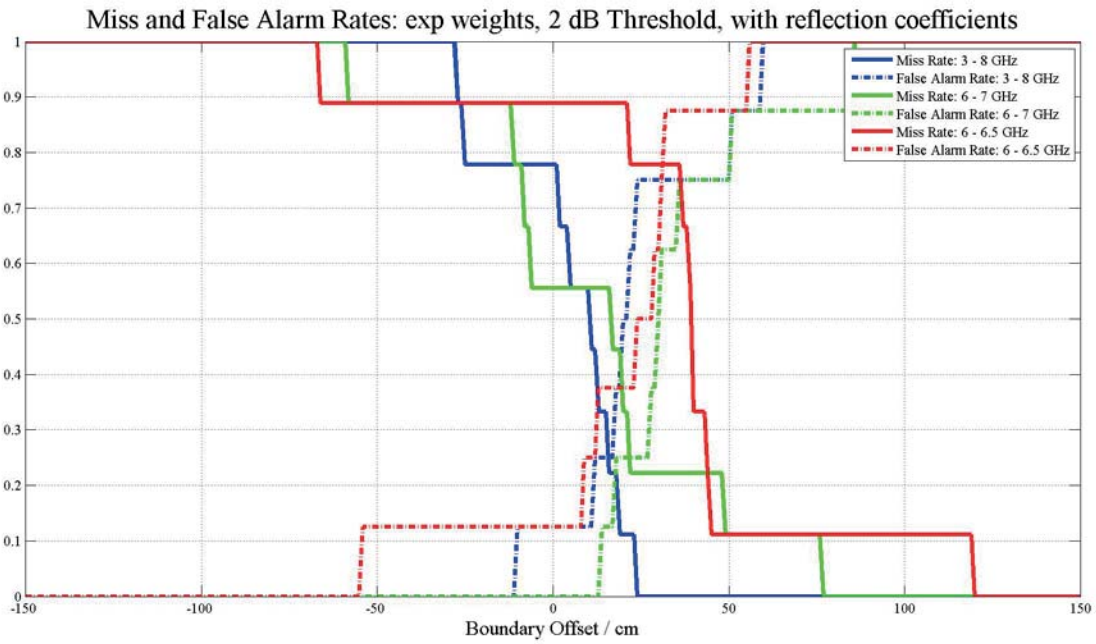

Figure 101: Comparison of different bandwidths at setup 3, exp weights and 2dB

The statistical analysis in Table 8 also shows that localization performance degraded with lower bandwidths.

Table 8: Statistical Analysis of different bandwidths

	5 GHz	1 GHz	0.5 GHz
d_x [cm]	29.69	52.48	66.90
d_y [cm]	37.02	72.23	107.04

4.5.4 Parameters for Particle Filter

The estimation with a Particle Filter needed some additional parameters. In this section it was discussed how these parameters where chosen to achieve optimal results with lowest possible computational effort.

Number of Particles

The best results were achieved with a very high number of particles. However, with the number of particles also the computational effort increased. A good way to find a suitable compromise was to simulate a setup with a high particle number

and then decrease the number systematically. If the results started to differ from one simulation to the other, the number of particles had been chosen to small. The optimal number of particles depended on other parameters of the particle filter and was determined last. For our measurements all particles were spaced on a cubical grid with 20 cm distances.

Exponential factor – α

The exponential factor had to be chosen such, that a given percentage of particles was thrown away after each iteration for a given process noise. Very different percentages from about 10% up to 80% were mentioned in literature. For this task a throw away percentage of about 20% - 30% was chosen. Experimentally this resulted in an exponential factor of $\alpha = 5 \cdot 10^{-4}$.

Variance of process noise – σ_v^2

The process noise was used to model the uncertainty of the process we want to estimate. In our case this was the movement of the test person between two measurements. Because we did not focus on specific measurement intervals, this was chosen such that a movement of about 30 cm between 2 measurements could be tracked. Experimentally a value of $\sigma_v = 2$ had been chosen.

4.5.5 Antenna position accuracy

To determine how big the impact of the not perfectly measured antenna positions was, a simulation had been conducted, where the ideal antenna positions and detection times were known and for estimation the antenna positions were then corrupted by uniformly distributed noise. This simulation had been run 10 times and the mean error resulting from this antenna positioning error had been calculated for a 4 antenna setup. Table 9 shows that for a positioning error of +/- 5 cm the estimation error was only about 2 cm. +/- 5 cm approximately matched the accuracy of the used antenna position measurements. To be on the save side also positioning errors of 10 cm and 20 cm had been simulated. The error

introduced by a uniformly distributed inaccuracy in the bounds of +/- 10 cm was negligible compared to the total error of the estimation.

Table 9: Impact of antenna position accuracy

Positioning Error [cm]	Estimation Error [cm]
+/- 5	2.1
+/- 10	4.3
+/- 20	8.9

5. Results different Setups

Despite the fact that reflection coefficients could not be used in the real system, an analysis was conducted if the use of reflection coefficients would improve detection accuracy. But even with the spectrum analyser, reflection coefficients did not deliver good results because of reflexions from the not ideally matched antennas. These reflexions were the same at the background measurement and the test case measurement, but much stronger than those reflexions which were of interest.

If the miss rate did not go to 0 and the false alarm rate did not go to 1 for high boundary offsets, it indicated that the detection is failing and results started to become random.

5.1 Comparison of different test setups

Figure 102 shows that setups 2 delivered the best results for test cases within the car. Detection of objects outside the car did not work properly as it is indicated by the false alarm rate which does not go to 1 for high boundary offsets. Test case 15 and 11 produced the first misses.

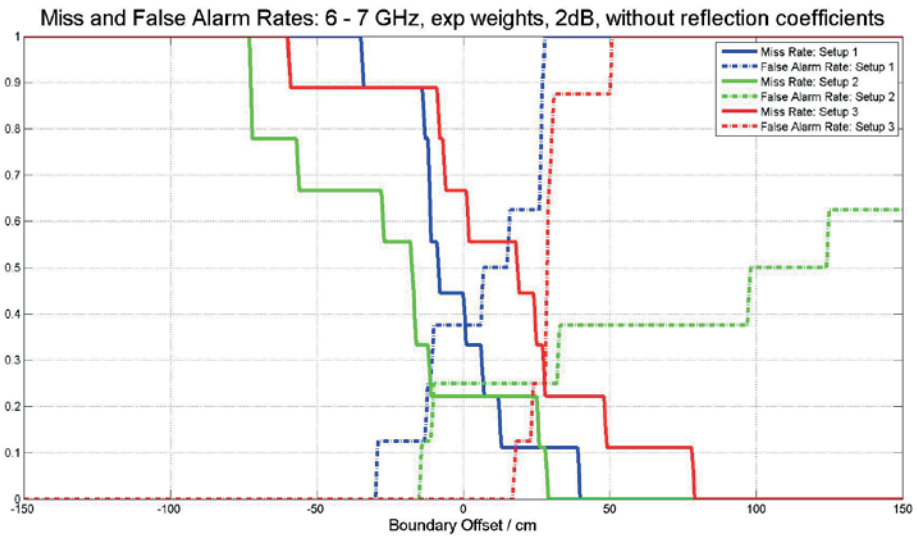

Figure 102: Comparison of setups – miss and false alarm rates: 6 – 7 GHz, exp weights, 2dB, without reflection coefficients

With a threshold of 3 dB, as shown in Figure 103, setup 1 delivered the best performance, while setup 2 started to fail in some cases, as it is indicated by the miss rate not going to 0 and false alarm rate not going to 1. Probably the reason why setup 2 delivered such bad results, was that all antennas were in the middle of the car. Therefore, all test cases were far away from the LOS between the antennas, which resulted in weaker reflections.

Setup 3 also had some outliers, which indicates that these test cases had not been detected properly. Test case 8 delivered the first false alarm and 7 the second one. Where exactly the results of the detection algorithm were can be seen in Figure 104 and Figure 105. For 2 dB the estimated position was a good estimation. The estimation for 3 dB was a very bad estimation of the real position, although the confidence region was very small. Because of the higher threshold the detected distances were wrong. These distances were the foundation of the estimation algorithm. That is why the estimation delivers such a bad result. In general the results degrade with higher thresholds. Outliers indicate that a test case could not be detected at all and the system starts to fail.

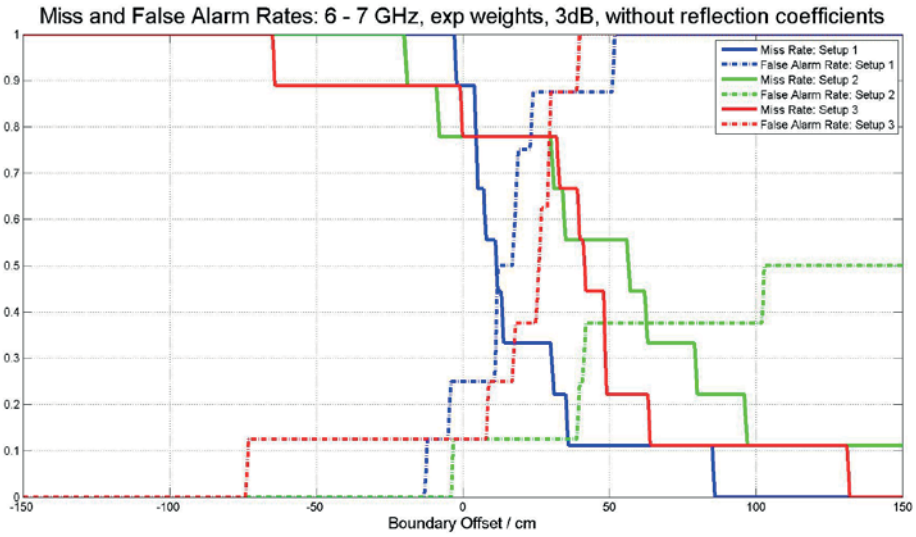

Figure 103: Comparison of setups - miss and false alarm rates: 6 - 7 GHz, exp weights, 3dB, without reflection coefficients

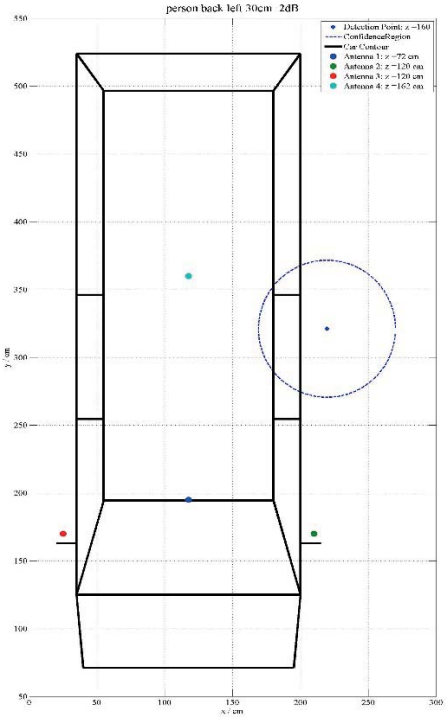

Figure 104: Setup 3, test case 8, 2 dB

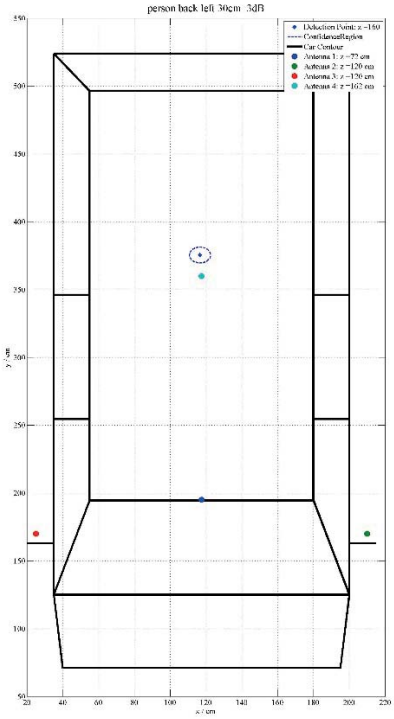

Figure 105: Setup 3, test case 8, 3 dB

5.2 Comparison of different test setups with reflection coefficients

Figure 106 shows again that setup 2 delivered the best results. But in this case the results of setup 3 looked slightly better than the results of setup 1.

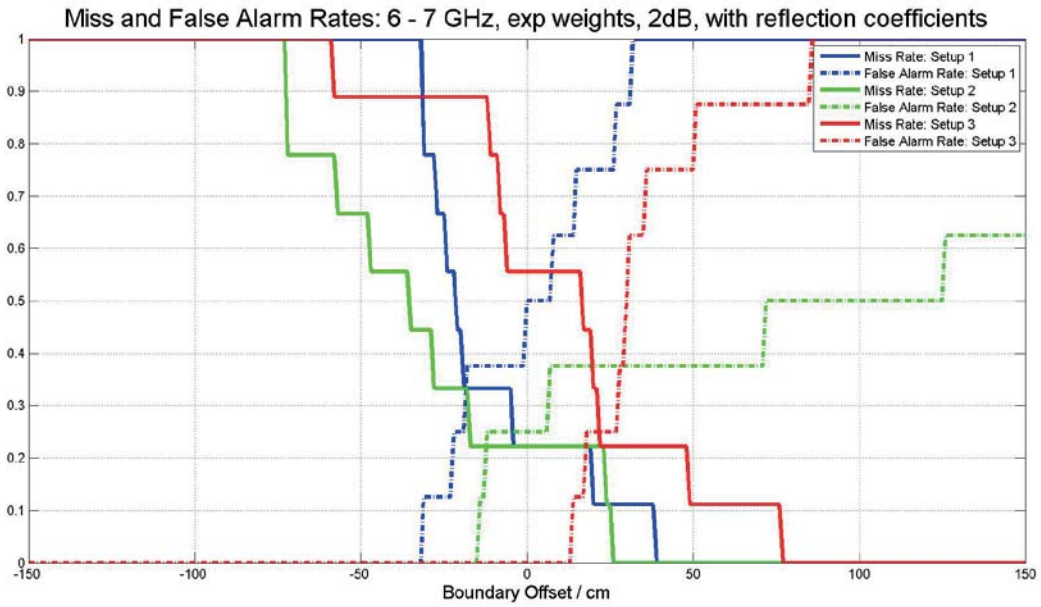

Figure 106: Comparison of setups – miss and false alarm rates: 6 – 7 GHz, exp weights, 2dB, with reflection coefficients

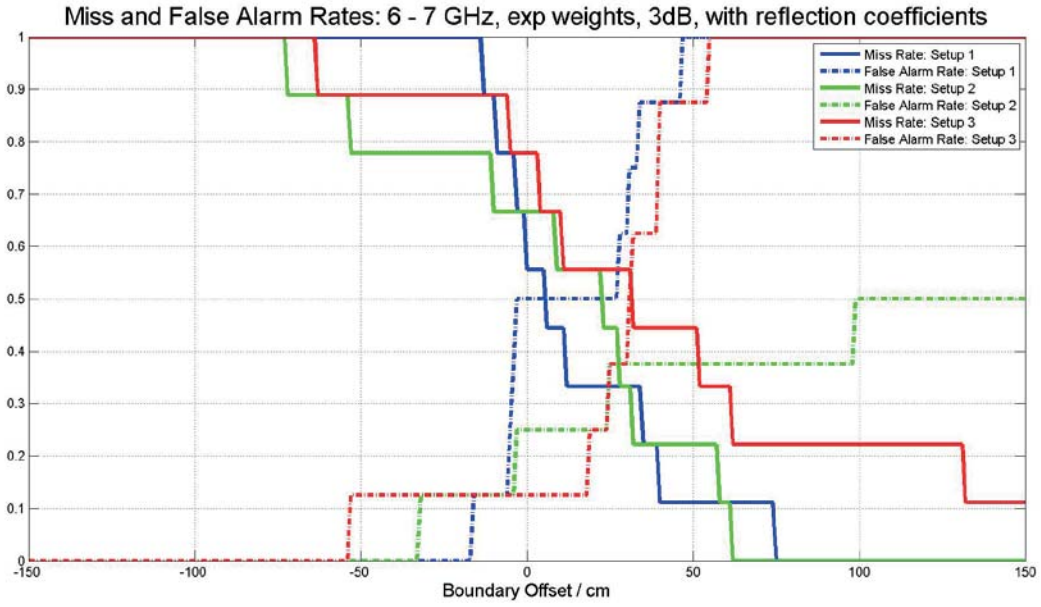

Figure 107: Comparison of setups – miss and false alarm rates: 6 – 7 GHz, exp weights, 3dB, with reflection coefficients

Overall the results with reflection coefficients look very similar to the results without reflection coefficients. That is because most reflection coefficients did not deliver useful information because of the strong reflections from the mismatched

antenna. The difference of the impulse responses calculated of a transmission and a reflection coefficient can be seen in the figures below.

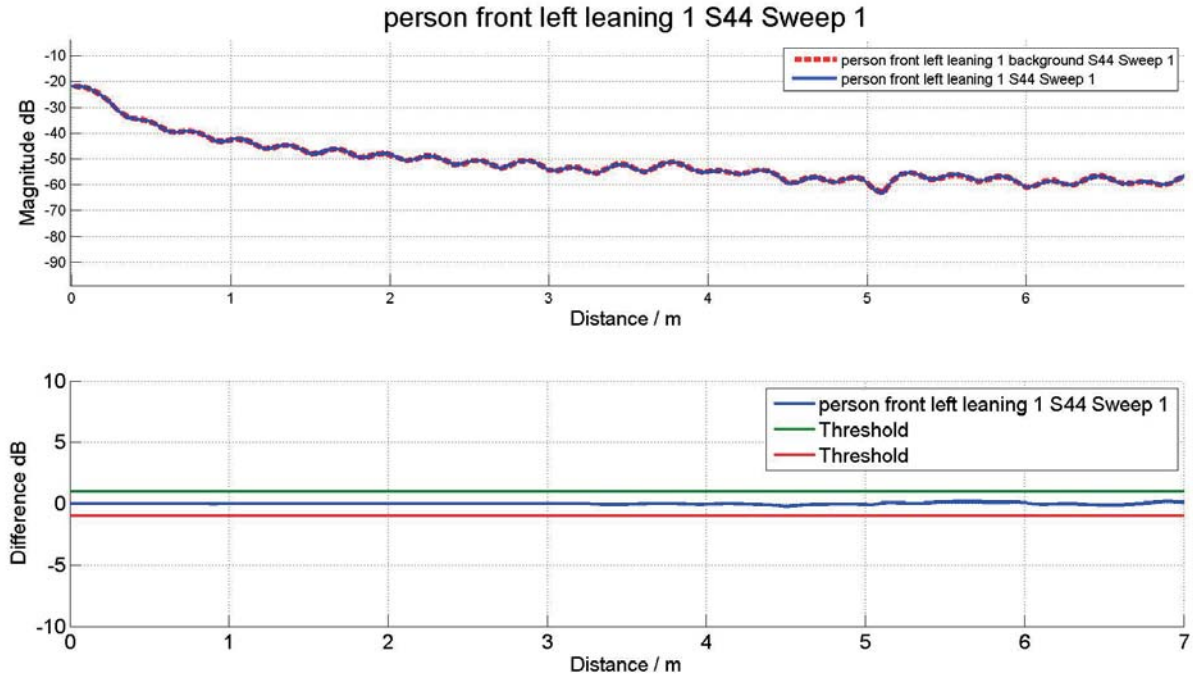

Figure 108: Impulse response - S44 with target at approximately 2.5 m distance

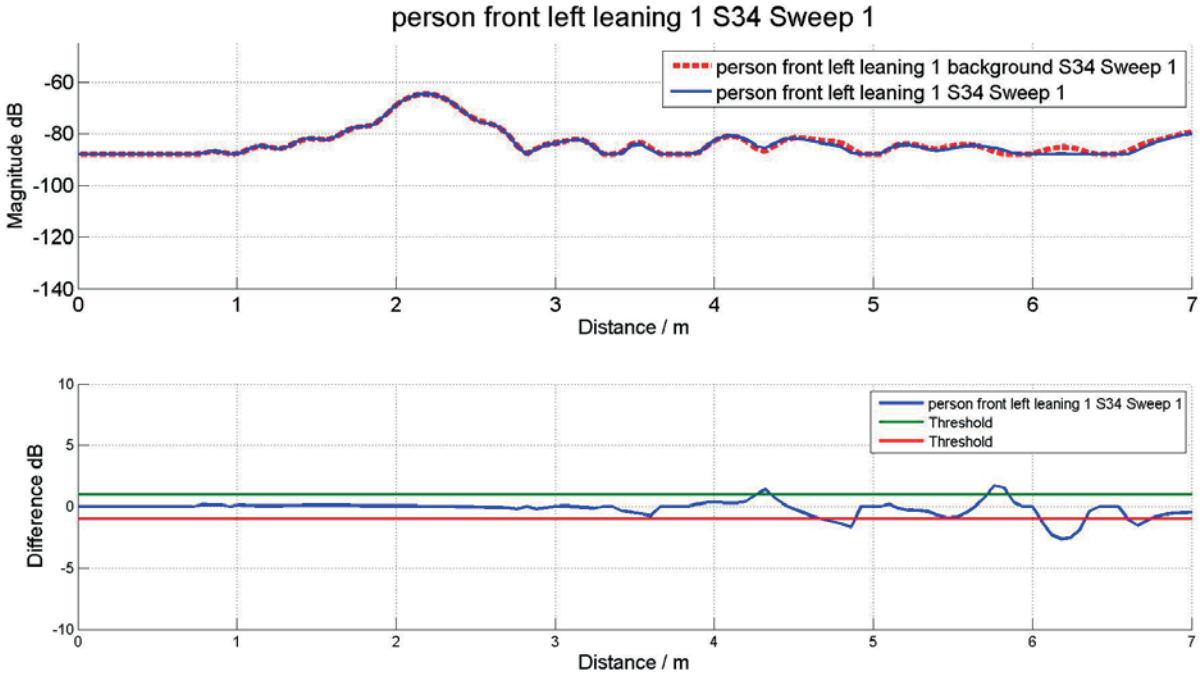

Figure 109: Impulse response – S34

At a bandwidth of 500 MHz the number of outliers for all systems had increased, which indicated that more test cases could not be detected correctly. In Figure 110 it can be observed that many test cases start to fail.

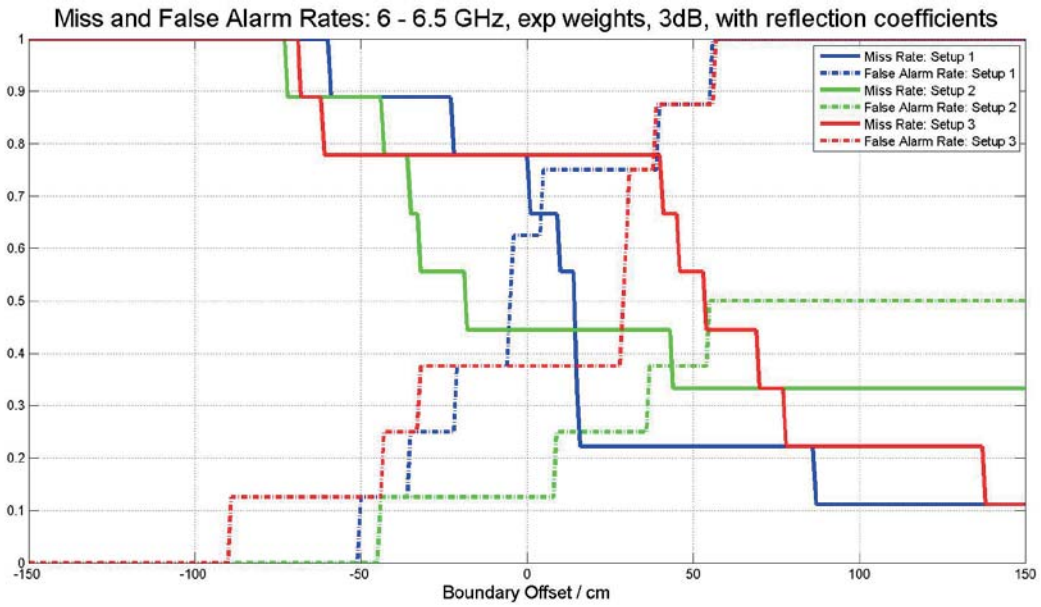

Figure 110: Comparison of systems for 500 MHz bandwidth

5.3 Location specific error analysis

Some specific test locations produced errors more likely than others did. Figure 111, Figure 112 and Figure 113 show the order in which the systems failed to locate a test object. Red marked positions began to fail earlier than green marked positions. The parameter was again the boundary offset of the alarm boundary. The results look very similar for all 3 setups.

Especially the test cases 4, 5, 6 and 14 began to fail early in all 3 setups. Most probably because they were all very close to the alarm boundary. Therefore, already small errors during position estimation could have caused cause misses or false alarms.

1, 2 and 3 behaved better than 4, 5, and 6. Maybe because these cases were positioned more between the antennas, where 4, 5 and 6 were more beside the antennas.

15 was always a very bad test case, because it was close to the alarm boundary and the half-filled bottle was harder to detect than an arm or body. The bottle was also shaded from the outside antennas by the door, as it can be seen in Figure 86.

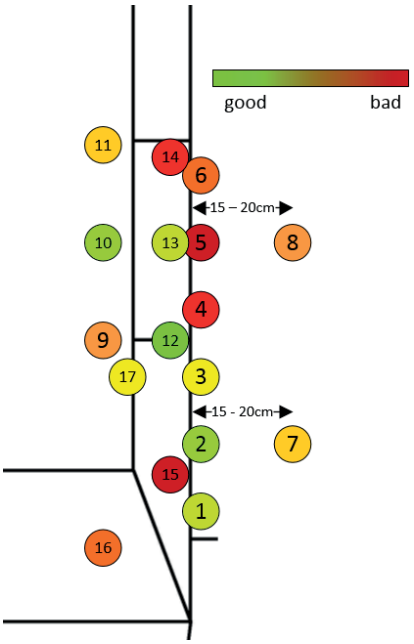

Figure 111: Location specific error analysis - Setup 1, 2 dB, without Sxx

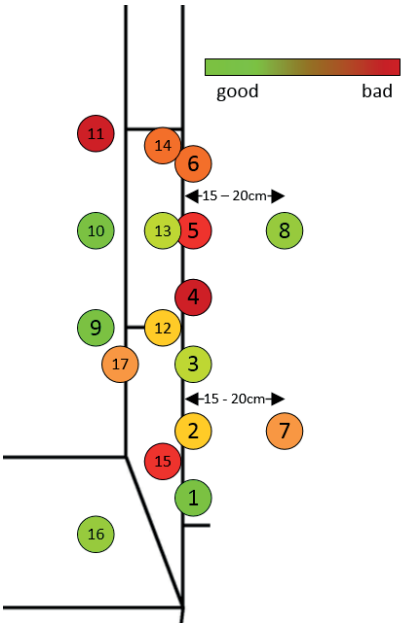

Figure 112: Location specific error analysis - Setup 2, 2 dB, without Sxx

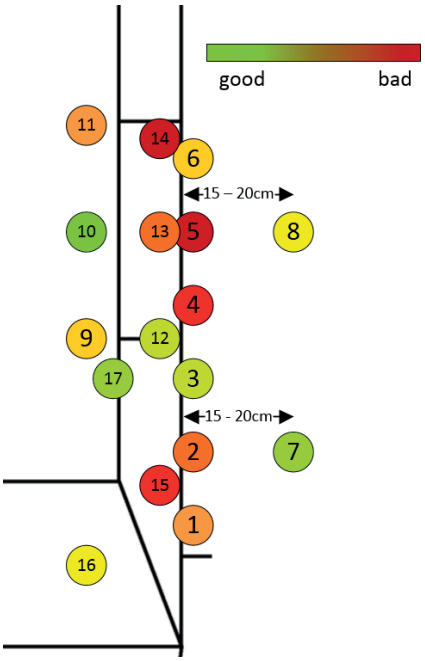

Figure 113: Location specific error analysis - Setup 3, 2dB, without Sxx

5.4 Results with fixed alarm boundary

For the final system a fixed alarm boundary was needed. In this chapter we look at the results for 3 different alarm boundaries. Red circles represent test cases where no correct detection was possible, green test cases represent correctly detected test cases. The fmincon optimization algorithm was used for these tasks. The boundaries were optimized for minimum miss rate, minimum false alarm rate and minimum number of wrong decisions. As shown in the figures below setup 2 had the best performance for a 2 dB threshold. Setup 3 behaved slightly better than setup 1. No setup was found which detected all positions correctly. For a 3 dB threshold the results looked worse than for a 2 dB threshold in all cases, thus they were not plotted in this way.

Figure 114: Setup 1 with fixed alarm boundaries and 1dB, 5GHz for: no false alarms (-15 cm), no misses (25 cm), min. wrong decisions (5 cm)

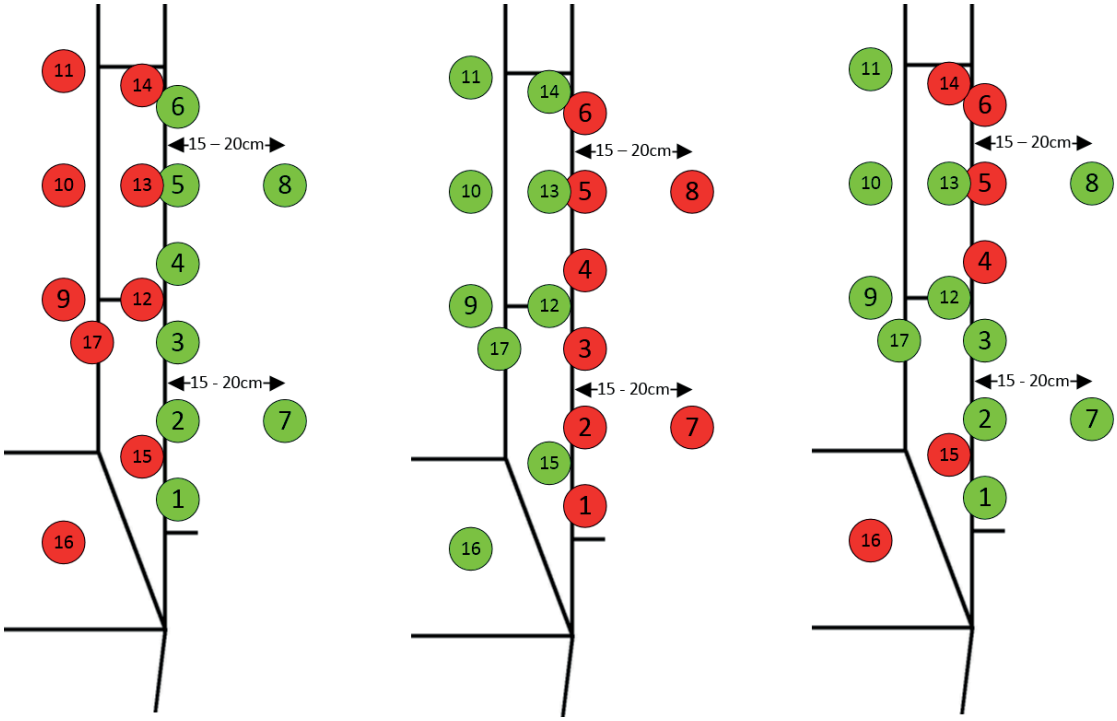

Figure 115: Setup 1 with fixed alarm boundaries and 2dB, 1GHz for: no false alarms (-35 cm), no misses (40 cm), min. wrong decisions (2 cm)

For setup 1 the positions 4, 5, 6, 14, 15 and 16 did not work well for a minimum wrong decision boundary. But the boundary was with an offset of only 2 cm nearly at the true position of the cars door.

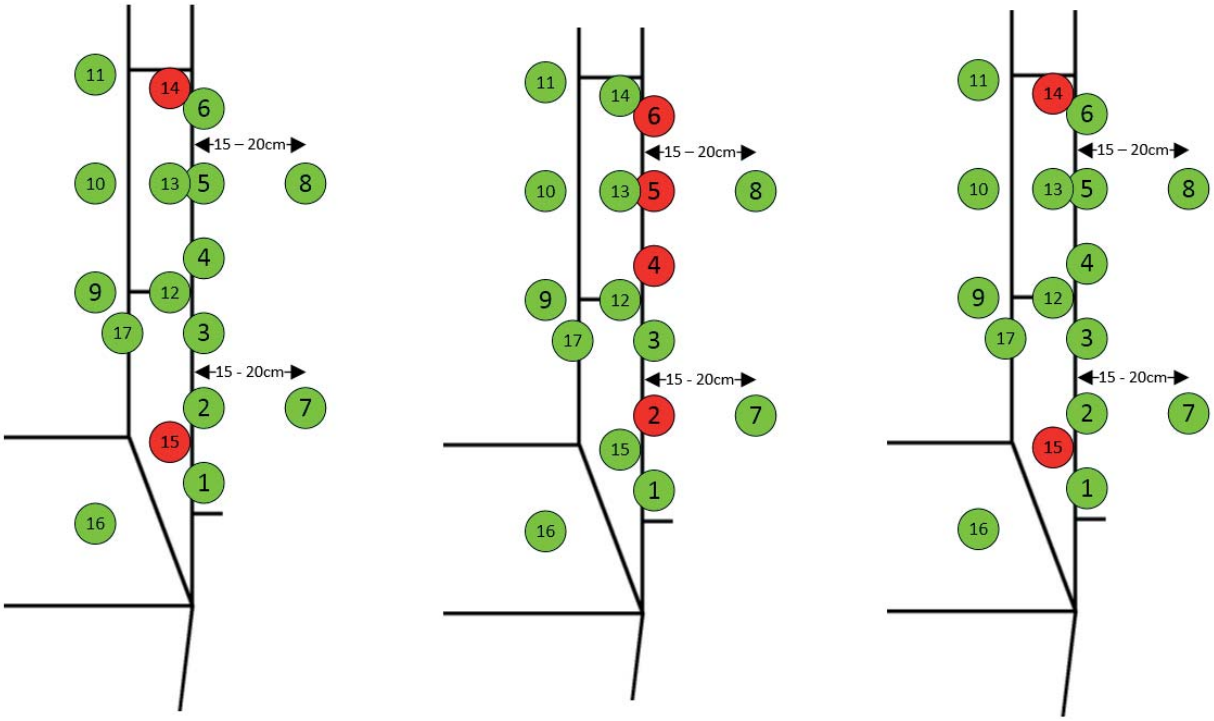

Figure 116: Setup 2 with fixed alarm boundaries and 1dB, 5GHz for: no false alarms (-7 cm), no misses (14 cm), min. wrong decisions (-7 cm)

Figure 117: Setup 2 with fixed alarm boundaries and 2dB, 1GHz for: no false alarms (-15 cm), no misses (29 cm), min. wrong decisions (29 cm)

Setup 2 was the setup with the best results. But here also positions 4, 6, 14, and 15 provided some issues. It can also be seen that the alarm boundary is quite some distance off the true position of the door.

Figure 118: Setup 3 with fixed alarm boundaries and 1dB, 1GHz for: no false alarms (17 cm), no misses (79 cm), min. wrong decision (28 cm)

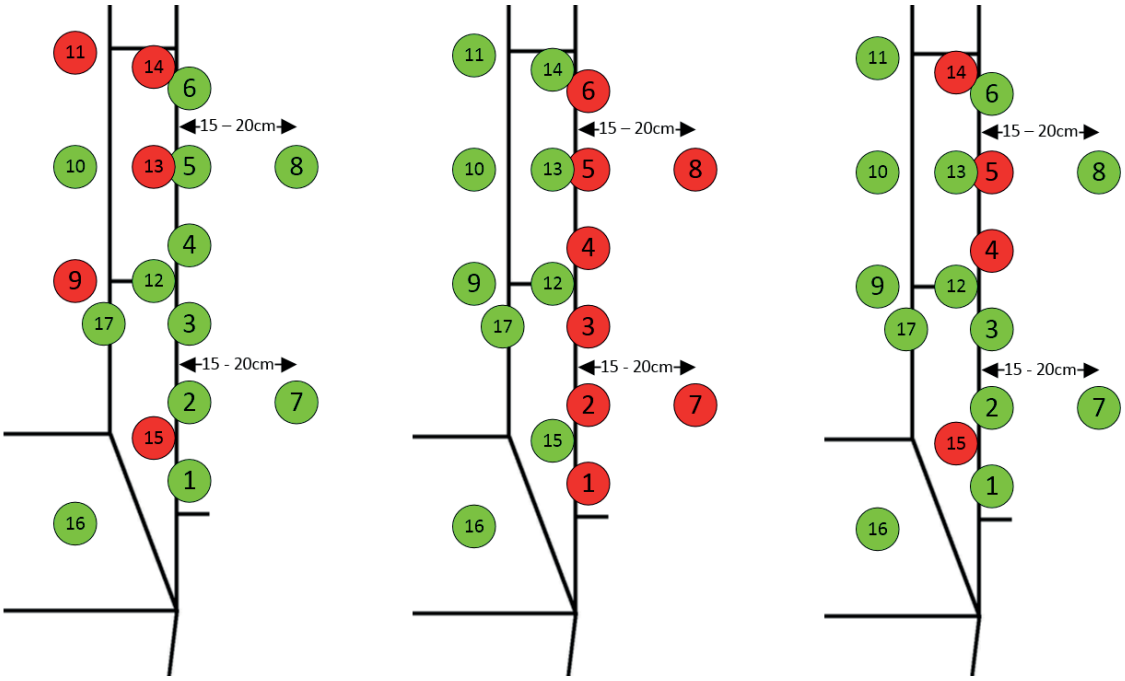

Figure 119: Setup 3 with fixed alarm boundaries and 2dB, 1GHz for: no false alarms (17 cm), no misses (79 cm), min. wrong decision (28 cm)

For setup 3 also the positions at the corners and boundaries provide issues. To have no misses an alarm boundary with an offset of 79 cm from the true position of the door is needed. This indicates that one test case completely failed.

5.5 Combining measurement results for setup simulation

In order to find the best setup, we needed measurement data for each antenna position. However, the measurement work could be reduced by combining already measured S-parameters to build new virtual setups. This would also allow to simulate setups with more than 4 antennas. Until now setups were restricted to 4 antennas because of the number of ports on the network analyser. Furthermore, virtual setups allow the use of a Matlab script to find the best behaving setups.

The following antenna positions were measured and then combined virtually to any combination of antennas, except some for which it was known that they would not work.

1: At the gear leaver
2: Left side mirror
3: Right side mirror
4: Shark fin
5: Middle mirror
6: Back number plate
7: Right back light inside trunk
8: Left back light inside trunk

All S-parameters except S22, S66, S88, S67 and S68 had been measured.

Because the direct measurement of reflection parameters was not possible as it was shown in 5.2, the reflection coefficients were measured with two different antennas at the same position.

5.5.1 Evaluation of simulated setups

During previous analyses it became obvious that the performance of a setup could not only be described by its ability to detect objects on the correct side of the alarm boundary, but also by the error distance between the detected point and the real test location. Therefore the evaluation was split into two parts.

- Finding setups with the least number of detection errors. The “number of errors” is the number of detections on the wrong side of the alarm boundary.
- Finding setups with the least absolute detection error in terms of distance between detected point and optimal detection point. The “mean distance error” is calculated like shown in Equation 5.1.

$$\bar{d}_x = \frac{1}{N} \cdot \sum_{i=1}^{N} \left\| \vec{x} - \vec{x}_{opt} \right\| \qquad \textit{Equation 5.1}$$

d_x … mean distance error in x direction
x … measured position in x direction
N … number of test cases
x_{opt} … true position in x direction

It has to be noted that the median was also calculated, but the final results were the same as for the mean. Also the distance error in y-direction as well as the total distance error were calculated, but the distance error in x-direction showed to be more meaningful, as the alarm boundary is parallel to the y-axis.

A Matlab script sorted over 280 simulated setups corresponding to the points described above.

5.5.2 Least number of detection errors

The ranking of setups with the least number of detection errors is shown in Table 10. If a setup would have had the same number of errors with LSE method and particle filter, then the one with the lower distance error was chosen. To see all results please have a look at chapter C of the appendix.

Table 10: Setup ranking due to number of errors

Antennas	dx[cm]	Errors	Thresh. [dB]	B [GHz]
146	17.8	0	1	5
146	27.8	0	2	5
2356	9.4	2	1	5
1236	13.5	2	1	5
2356	16.5	2	2	5
456	20.4	2	1	5
1456	22.9	2	1	5
2378	23.1	2	2	5
2345	26.3	2	2	5
1234	8.8	3	1	5
2345	10.1	3	1	5
2345	19.8	3	1	1
2356	23.7	3	1	1

For the first and third line the results are also shown in Figure 120 and Figure 121. Note that the figures only show the left side of the car and the red lines show the difference to the optimal detection point. The dashed line in cyan is the alarm boundary. These figures clearly show that the first setup had zero errors, but the detected points were much farther away from the true points than in the second setup. It also has to be noted, that the antennas 1, 4 and 6 came close to the simple solution which was discussed in chapter 4.1 and were also not suitable because of their positions.

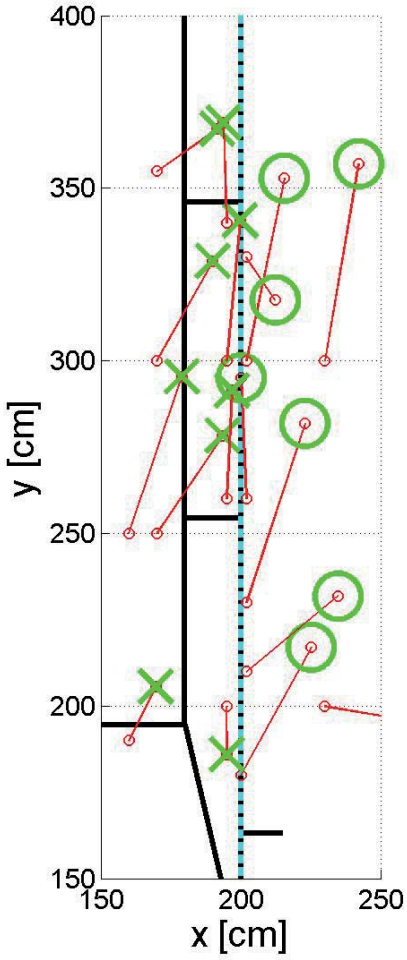

Figure 120: Results for antennas 1, 4 and 6. Corresponding to the first line in Table 10.

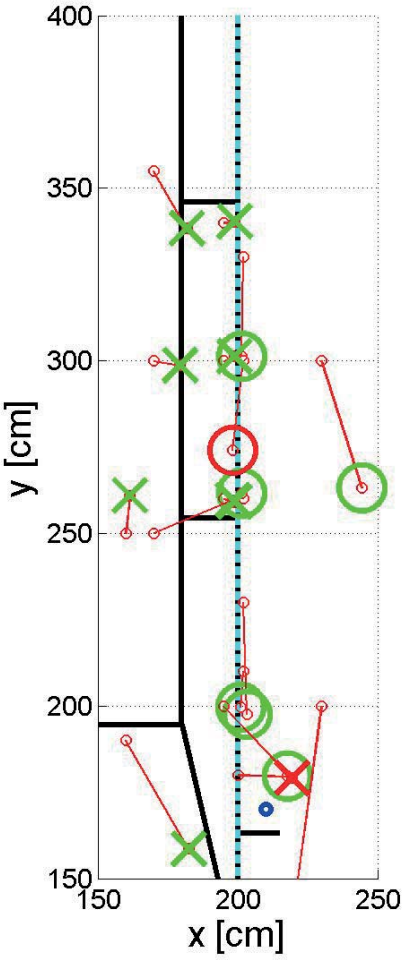

Figure 121: Results for antennas 2,3,5 and 6. Corresponding to the third line in Table 10.

5.5.3 Minimum mean distance error

The setup ranking due to the mean distance error in x direction is shown in Table 11. If a setup would have had two entries in this table from LSE method and particle filter, then only the better result was shown in the table. To see all results please have a look at C

Table 11: Setup ranking due to mean distance error in x direction

Antennas	d_x [cm]	Errors	Thresh. [dB]	B [GHz]
1234	8.8	3	1	5
2346	9.4	6	1	5
2356	9.4	2	1	5
2345	10.1	3	1	5
1236	11.0	3	1	5
2378	11.6	5	1	5
1456	12.0	5	1	5

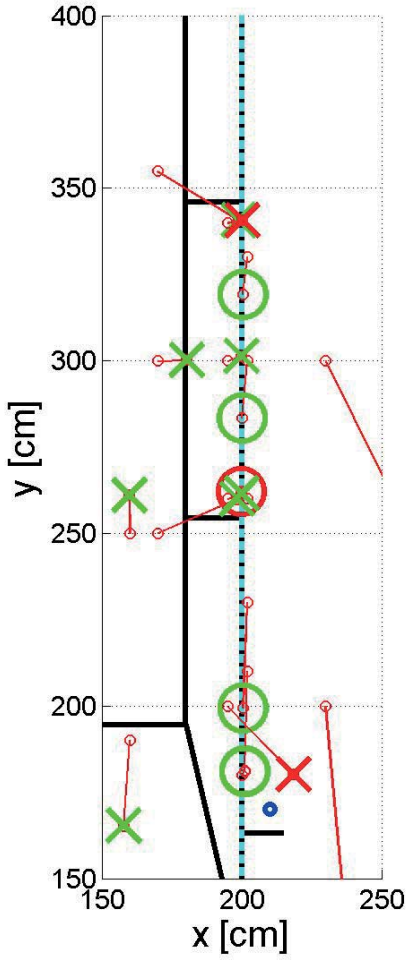

Figure 122: Results for antennas 1, 2, 3 and 4 corresponding to first line in Table 11.

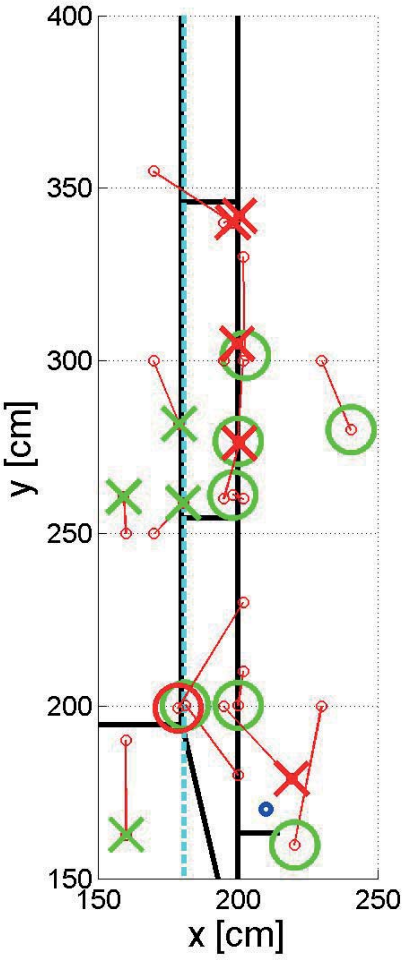

Figure 123: Results for antennas 2, 3, 4 and 6 corresponding to second line in Table 11.

The same evaluation has been conducted for Gaussian windows. This shows that for Gaussian windowing the results get even worse.

Table 12: Setup ranking due to mean distance error in x direction for Gaussian windowing during IFFT

Antennas	d_x[cm]	Errors	Thresh. [dB]	B [GHz]
2356	10.4	5	1	5
1236	12.2	3	1	5
146	14.6	1	1	5
1236	16.5	2	1	5
2356	17.0	5	1	0.5
1236	17.4	5	1	1

5.6 Movement tracking

As shown in the previous chapters, a single measurement was not accurate enough to correctly detect an intrusion. The next step was to continuously measure the movement of a person. For this purpose three scenarios had been measured. For tracking the particle filter was used.

5.6.1 Person approaching the car

In this case a person was approaching the car and leaning against the back door. Then the person reached into the car and then went away. The positions of the person corresponding to the measurements were listed below in Table 13. Setup 1 from chapter 4.4.1 was used for this measurement.

Table 13: Test positions for movement tracking

Measurement	Position
1	Standing - 4 m left of car
2	Standing - 3 m to the left of car
3	Standing – 1.3 m away from door
4	Standing - 75 cm away from door
5	Standing - 30 cm away from door
6	Standing - 15 cm away from door
7	Leaning - front end of back door
8	Hand at inside door latch
9	Hand at backseat headrest
10	Hand at door - back end
11	Hand at door - middle
12	Hand stretched into car - middle of back door
13	Hand stretched into car - 3/4 of back door
14	Hand stretched into car - back of back door
15	Hand stretched into car - middle of back door
16	Hand stretched into car - front of back door
17	Leaning - front end of back door
18	Leaning - middle of back door
19	Standing - 15 cm away from door
20	Standing - 30 cm away from door

The results from the measurements can be seen below in Figure 124 and as zoomed in version in Figure 125. Most test cases except one approximately matched the positions described in Table 13. The test case, which failed was highlighted with a red circle. The approaching person could be located, although accuracy at larger distances was greatly reduced. But it was still not possible to determine if the hand of the person was inside the car, or if the person was just leaning against the door.

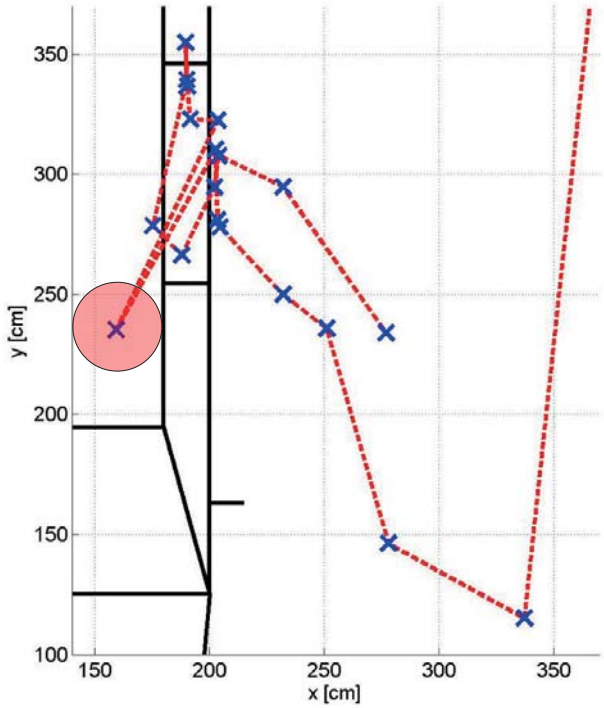

Figure 124: Tracking of approaching person – full view

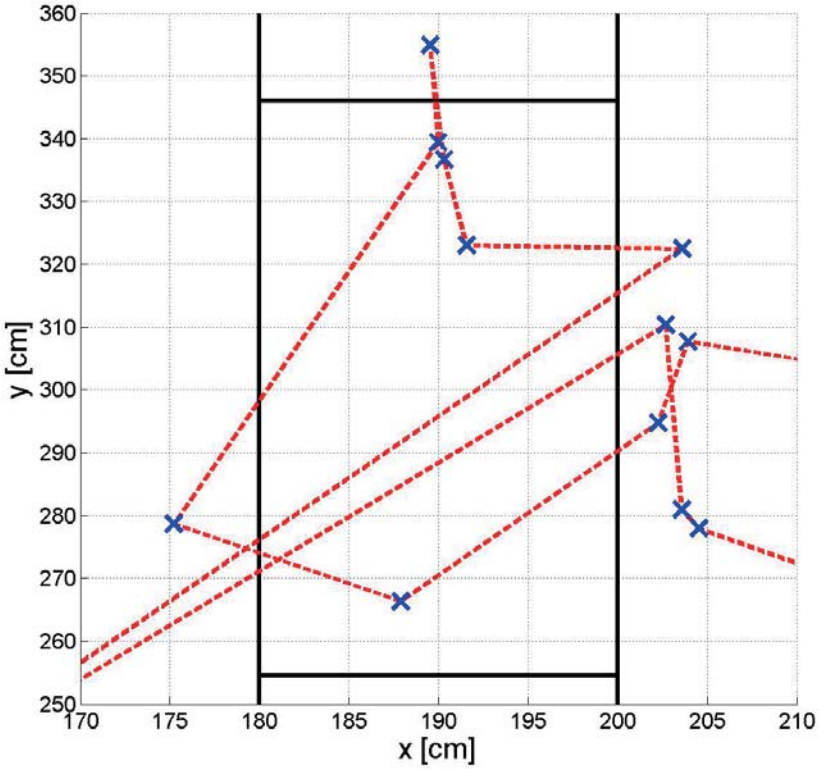

Figure 125: Tracking of approaching person – zoomed view

5.6.2 Person sitting on middle back seat

The second measurement shows a person who was moving around on the back seats and was also stretching an arm to the gear stick for a period of two measurements. The person could be localized correctly on the middle back seat, but it could not be detected that the person was reaching out with one arm to the gear stick.

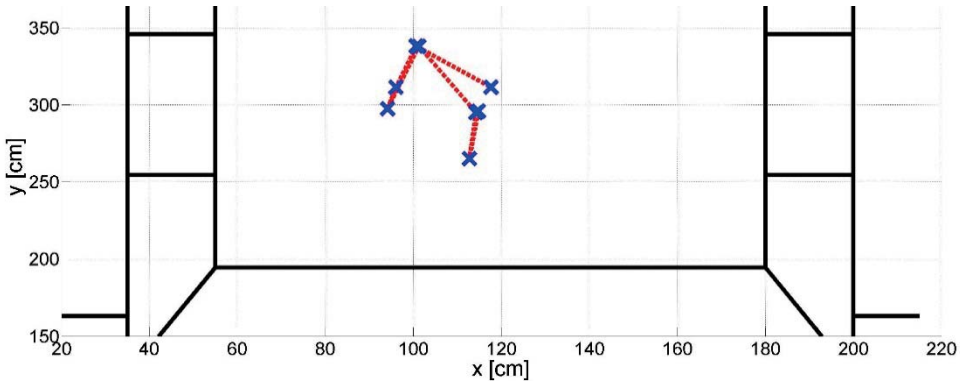

Figure 126: Tracking of person moving around on back seats

5.6.3 Person on driver seat getting out of car

The last measurement of moving persons was to track a person getting out of the car from the driver seat. Although one of the antennas was mounted onto the side mirror, which moved when the door was opened, the movement of the person could be tracked roughly.

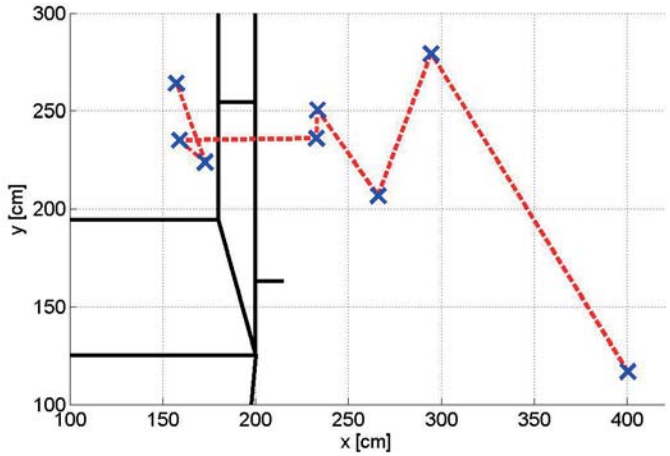

Figure 127: Tracking person leaving the car from driver seat.

5.7 Summarized results for interior surveillance system

Realising an interior surveillance without misses and false alarms was not possible with this system. Each of the tested setups and methods had blind spots where detection of objects would fail more likely and they all reacted very sensible to increased detection thresholds and smaller bandwidths. In addition, the antenna geometry was an issue, because possible positions for antennas which are convenient for the manufacturer are restricted.

Although the simple solution from chapter 4.1 proved to produce no false alarms if tuned correctly, it was not able to provide a location estimate of the intrusion. It also had large blind spots due to antenna positioning and the fact that the alarm boundary always has an elliptical shape as shown in Figure 75. Also the antenna positions were unsuited for final implementation. Therefore, this setup was not a suitable solution for an interior surveillance system.

The more sophisticated solution, which used a localization algorithm to detect intrusions, provided only rough position estimates with an accuracy of approximately 30 cm to 50 cm. None of the tried setups could distinguish between a person leaning against a door and someone reaching into the car close to the door. Also the virtual combination of measurement data to simulate over 280 setups did not help to achieve the hoped results, but helped to study the impact of different parameters. For each of the tested systems a warning area could help to reduce the probability of false alarms. This warning are should have a size of 60 cm to 70 cm to minimize the risk of false alarms.

In chapter 5.6 an experiment was conducted to find out if those problems could be solved by continuous measurement and tracking by means of a particle filter. Also in this case only rough position estimates of the person could be achieved. It was shown that the system was able to distinguish if a person was inside the car or outside the car, but the border case of a person leaning against the car still provided issues.

What can be done to improve the situation? In order to answer this question an analysis was conducted to find out why the system was not working as good as

intended. The first task was to try different weighting methods, so one wrong S-parameter did not affect the final result that much. Although, different weighting as described in chapter 4.5.2, improved results a lot, this was still not enough. The second task was to find out how big the impact of inaccurate antenna positioning was. But in 4.5.5 it was shown that the impact of the measurement error for antenna positions onto the final result was negligible. A last error factor was not analysed because it would have gone beyond the scope of this master thesis. The effect of the simplification that we were looking for a point target. At these distances, persons should have been considered as a spread target, because one reflection might have come from the elbow of the person and another one from the torso. Depending on the antenna geometry this might result in ellipsoids not intersecting in one point, even for optimal conditions. An estimation algorithm should have been designed such, that this is considered.

6. Conclusion

For a parking assistance system antennas with a low directivity were not suitable, because in some cases two objects could not be distinguished from each other. Because of the wide main lobe objects beside the car could interfere with the localization of an object behind the car, and therefore produce wrong results. Also the clutter level from reflections which came from the car itself were very high, which provided issues at close distances. A further problem was that only metallic objects could be detected at all. This means that wooden and plastic poles like they are used at road boundaries, and empty waste containers would not be detected. More detailed information about the results of the parking assistance system can be found in chapter 3.6.

The results for interior surveillance looked more promising, but an accurate localization of an intruder was not always possible. Only rough position estimates could be achieved. In many cases this rough position estimates were not enough to make a reliable decision between triggering an alarm or not. To mitigate this problem a warning zone could be introduced. If an intruder enters the warning zone only some kind of warning would be triggered without triggering an alarm. A different application for this system could be the tracking of movement inside and outside the car. In chapter 5.6 it was shown that the movement of a person inside and outside the car could be tracked roughly. For security reasons the position estimate was not accurate enough, but maybe this could be useful for comfort applications. It has to be considered that if the number of persons around the car increases new problems are introduced. In this thesis it was only tried to track one person at a time. The main problem why the position estmates for one person were so bad, was that the localization algorithm was looking for a point target. But a person is a spread target, which should have been considered by the localization algorithm.

In the future these problems may change, because some car manufacturers start to use infrared reflecting metalized windows. These windows have a high attenuation for electromagnetic waves. This means that a radar system could be used the same way like ultrasonic systems are already today as described in the introduction.

Abbreviations

IFFT … Inverse Fourier Transform

LOS … Line Of Sight

Lidar … Light Detection and Ranging

LRR … Long Range Radar

LSE … Least Square Error

MALSO … Manoeuvring Aids for Low Speed Operations

MRR … Medium Range Radar

PDF … Probability Density Function

SRR … Short Range Radar

Sxx … Reflection coefficients

Sxy … Transmission coefficients

TOSM … Through Open Short Match

UWB … Ultra-Wide Ba

Literature

[1] J. Dickmann, J. Klappstein, H. L. Bloecher, M. Muntzinger and H. Meinel, “Automotive Radar — “quo vadis?””.

[2] ISO, “ISO 17386 - Transport information and control systems -Manoeuvering Aids for Low Speed Operation (MALSO) - Performance requirements and test procedures,” ISO, 2010.

[3] H. Winner, ““'Mit aktiven Sensoren das Kfz-Umfeld erfassen–Funktion und Leistungsfähigkeit von Radar & Co,” De Gruyter, 2007.

[4] Bosch Mobility Sollutions, 1 4 2015. [Online]. Available: http://www.bosch-mobility-solutions.de/de/de/_technik/component/CO_PC_DA_Parking-Aid_CO_PC_Driver-Assistance_4097.html?compId=5440.

[5] N. Martin and R. Peter, “Ultraschallsysteme,” in *Handbuch Fahrassistenzsysteme*, Springer, 2012, pp. 110 - 122.

[6] W. J. Park, B. S. Kim, D. E. Seo, D. S. Kim and K. H. Lee, “Parking Space Detection Using Ultrasonic Sensor,” in *IEEE Intelligent Vehicles Symposium*, 2008.

[7] J. Yongcheng, W. Junfa, G. Yiyuan, X. Fengwei, S. Zhongwei and L. Shukui, “Experimental Investigation on Influencing Factors of the Measuring Accuracy in Ultrasonic Sensors of the Mobile Robot,” in *Third International Conference on Digital Manufacturing & Automation*, 2012.

[8] Sensoparts, “Katalog Ultraschallsensoren,” 2015. [Online]. Available: http://www.sensopart.com/jdownloads/Gesamtkatalog/Ultraschallsensoren.pdf.

[9] GenerationRobots, 1 4 2015. [Online]. Available: http://www.generationrobots.com/de/content/65-ultraschallsensoren-für-kollisionvermeidung.

[10] Wikipedia, 2015. [Online]. Available: www.wikipedia.org.

[11] E. Kommission, *DURCHFÜHRUNGSBESCHLUSS DER KOMMISSION zur Änderung der Entscheidung 2005/50/EG zur Harmonisierung der befristeten Nutzung des Frequenzbands im Bereich um 24 GHz durch Kfz-Kurzstreckenradargeräte in der Gemeinschaft,* Brüssel, 2011.

[12] P. Knoll, “Sensorik für Fahrzeugrundumsicht,” in *Fahrstabilisierungssysteme und Fahrerassistenzsysteme*, 2010, pp. 130 - 145.

[13] I. Gresham, A. Jenkins, R. Egri, C. Eswarappa, N. Kinayman, N. Jain, R. Anderson, F. Kolak, R. Wohlert, P. S. Bawell, J. Bennett and J.-P. Lanteri, “Ultra-Wideband Radar Sensors for Short-Range Vehicular Applications,” in *IEEE TRANSACTIONS ON MICROWAVE THEORY AND TECHNIQUES, VOL. 52, NO. 9*, 2004.

[14] J. Wenger and S. Hahn, “Long Range and Ultra-Wideband Short Range Automotive Radar,” IEEE, 2007.

[15] C. Wolff, 4 2015. [Online]. Available: www.radartutorial.eu.

[16] J. W. Crispin and A. Maffett, “Radar Cross-Section Estimation for Simple Shapes,” IEEE, 1965.

[17] E. V. Lil and J. w. D. Bleser, “On the Efficient Computation of Near-Field Radar Cross Sections,” in *On the Efficient Computation of Near-Field Radar Cross Sections*, The 8th European Conference on Antennas and Propagation (EuCAP 2014), 2014.

[18] C. Bourlier and P. Pouliguen, “Useful Analytical Formulae for Near-Field Monostatic Radar Cross Section Under the Physical Optics: Far-Field Criterion,” *IEEE TRANSACTIONS ON ANTENNAS AND PROPAGATION, VOL. 57, NO. 1,* p. 10, January 2009.

[19] Maxim: Jianwei Wang, “RTM antenna and filter design,” 2015.

[20] M. Neumayer and D. Watzenig, “Lecture Notes on "Statistical Signal Processing Summer Term 2015",” Graz, 2015.

[21] M. Mengelkoch, “Implementieren des FastSLAM Algorithmus zur Karenerstellung in Echtzeit,” Universität Koblenz - Landau, Koblenz, 2007.

[22] Z. Chen, “Bayesian Filtering: From Kalman Filters to Particle Filters, and Beyond”.

[23] Mathworks, “Mathworks.com,” Mathworks, [Online]. Available: http://uk.mathworks.com. [Accessed 2015].

Appendix: Further calculations and measurements

A. Gramschidt Orthogonalization Method

Gramschidt orthogonalization is used to create an orthonormal base of vectors. One vector is needed to start with. The other base vectors can then be calculated out of another given vector or any random vector if the direction of the remaining base vectors is not of importance. The example below shows the method used for a 3 – dimensional space with $\underline{z_0}$ starting vector in direction of $\underline{b_3}$.

$$\vec{b}_3 = \frac{\vec{z}_0}{\|\vec{z}_0\|} \qquad \textit{Equation 0.1}$$

If no other vector is given, a random vector $\underline{x_0}$ is chosen. The next base vector is then calculated as shown in Equation 0.2.

$$\vec{b}_1 = \frac{\vec{x}_0 - \langle \vec{x}_0, \vec{b}_3 \rangle \, \vec{b}_3}{\left\| \vec{x}_0 - \langle \vec{x}_0, \vec{b}_3 \rangle \, \vec{b}_3 \right\|} \qquad \textit{Equation 0.2}$$

The previous step is then repeated with another random vector $\underline{y_0}$.

$$\vec{b}_2 = \frac{\vec{y}_0 - \langle \vec{y}_0, \vec{b}_1 \rangle \, \vec{b}_1 - \langle \vec{y}_0, \vec{b}_3 \rangle \, \vec{b}_3}{\left\| \vec{y}_0 - \langle \vec{y}_0, \vec{b}_1 \rangle \, \vec{b}_1 - \langle \vec{y}_0, \vec{b}_3 \rangle \, \vec{b}_3 \right\|} \qquad \textit{Equation 0.3}$$

B. Further Matlab Scripts

On the attached CD/USB-Stick in folder “Attachments/Matlab Scripts/Antenna Position Accuracy” the script for simulation of the impact of antenna dispositioning can be found.

In the folder “Attachments/Matlab Scripts/Virtual Setup Simulation” the scripts for simulation of virtual setups as well as the raw measurement data can be found. Also the evaluation script (evaluation.m) to create rankings of the simulated setups can be found in this folder.

C. Simulated setups results

A ranking of all simulated setups can be found in the “Attachments” folder on the data storage device added to this master thesis.

- error_sorted.xls
- mean_distance_error_sorted.xls

To find the corresponding plots for the simulation data in the .xls files above please follow the path in the first column of the Excel sheets.

D. Further Measurement Data

On the attached CD/USB-Stick in the folder “Attachments/Outdoor Measurements Lebring” the raw measurement data from the first outdoor radar measurements can be found.